Unsteady aerodynamics and mechanics of force generation in insect free flight

---

A Dissertation

Presented to
the faculty of the School of Engineering and Applied Science
University of Virginia

---

in partial fulfillment
of the requirements for the degree

Doctor of Philosophy

by

Ayodeji Toluwanimi Bode-Oke

August, 2019

Approval Sheet

This Dissertation
is submitted in partial fulfillment of the requirements
for the degree of
Doctor of Philosophy

Author Signature : ______________________

This Dissertation has been read and approved by the examining committee:

Advisor : ______________________

Committee Member : ______________________

Committee Member : ______________________

Committee Member : ______________________

Committee Member : ______________________

Committee Member : ______________________

Accepted for the School of Engineering and Applied Science:

Craig H. Benson, School of Engineering and Applied Science

August, 2019

Acknowledgments

Most importantly, I thank God for allowing me to be alive and for providing me with everything I have. To my dear parents, thank you for your unconditional love, prayers, support, and tremendous investments in me for all these years.

I owe all I know to those that preceded me. In particular, I have been greatly influenced by the works of C.P. Ellington, R. Bomphrey, Z. J. Wang, G.K. Taylor, A.L.R. Thomas, in aerodynamics G. Rüppel for his biomechanics works and field recordings. I thank my advisor, Prof. Haibo Dong, for his tremendous support, guidance, and providing the opportunity to express myself in my work. Under his tutelage, I have been able to approach problems systematically, think outside the box, and become a better scholar.

Many thanks to my committee; Profs. Dan Quinn, Matthew Reidenbach, Gavin Garner, and Rita Schnipke for their guidance, constructive criticism, scientific education and feedback, and willingness to attend to my non-thesis related questions. To all my professors, thank you for imparting your wisdom to me throughout my years as a student. I owe all I know to you, and I hope I made you proud.

To my teammates both past and present; Prof. Chengyu Li, Dr. Yan Ren, Dr. Liu Geng, Pan Han, Qiang Zhong, Junshi Wang, thank you for your support with Picar3d, and discussions. Among my teammates, Dr. Samane Zeyghami deserves a special mention. Her mentorship, friendship, and collaboration on various projects since my undergraduate years have made me a better scholar.

To my friends: Selena Moore, Edem Tetteh, Nick Doolittle, Dr. Kimberly Bassett, Pelumi Bamikole, Joshua Emeter, Sarah Bland, Oluwasefunmi Osinaike, Fritz Bondoa, Femi Suraju, Tochi Eni-Kalu, Ayo Gbenjo and family, Uzo Njoku, OneWay Christian fellowship, Chibueze Nwaiwu, Ralph Ababio, Elizabeth Onyechi, Dawn Nwaebube, and many more, your incredible support outside the lab during this journey kept me sane. Your love and care kept me strong.

This thesis was supported by funding from National Science Foundation [CBET-1313217] and Air Force Office of Scientific Research [FA9550-12-1-007] to PI (Haibo Dong), the University of Virginia distinguished fellowship 2018/19 to Ayodeji Bode-Oke (author).

Abstract

Engineers are interested in designing unmanned aerial vehicles (UAVs) for surveillance, environmental monitoring, assessment, and package delivery, etc. However, as the sizes of these vehicles become smaller, conventional fixed-wing and rotorcraft designs do not scale down well regarding aerodynamics and performance of components needed for propulsion. In the last two decades, bio-inspired flapping flight has offered an approach to bypass the challenges associated with the scalability of rotorcraft. Since the small dimensions and low flight speeds requirements for UAVs are similar to those of most flying insects (nature's most advanced fliers), understanding insect flight serves as a primary source of inspiration. However, our understanding of the flight these agile organisms is still incomplete — the goal of this work to bridge some of the gaps in our understanding of insect flight.

This dissertation describes efforts toward understanding how insects generate forces for flight, in particular, force generation during the upstroke (upstroke effects) which is less known. To transition from hovering to forward flight, a tilt of the path of the wings (stroke plane) is necessary. However, this tilt induces an asymmetry in the half stroke kinematics and aerodynamics so that the downstroke is dominant, being more aerodynamically active, while the upstroke is inactive or less active, playing a supporting role. Using high-speed photogrammetry to capture free-flying insects, high-fidelity three-dimensional surface reconstructions, kinematics quantification, and computational fluid dynamics (CFD) simulations, the coordination between wing and body motion, the techniques of force generation, and use of unsteady aerodynamics, force orientation, and reorientation, and wing half stroke function were unraveled. We elucidated how the upstroke can generate large forces, in particular, lift and even dominate the downstroke forces in free flight. Results indicate that the coordination between wing and body via body postural adjustments leads to stroke plane adjustments, which in turn influences the wing kinematics and aerodynamics. Our investigations also indicate that the upstroke is instrumental in extending the flight envelope of insects in free flight. The aerodynamic activity of the upstroke was found to increase as flight transitioned from positive to negative advance ratios. Flights with negative advance ratios have not been quantitatively characterized in the literature before this work. The mechanisms associated with the upstroke were found to robust among many flying species from complex to simple fliers.

The primary contributions of this dissertation are in the discovery and characterization of a novel flight mode among vastly different species spanning the entire spectrum of Reynolds numbers of small to large-sized insects with varying complexity, quantitative measurement of flight kinematics, discovery of novel upstroke lift and associated unsteady aerodynamics, clarification of the facultative nature of wing half stroke function, elucidation of the importance of body on wing aerodynamics and finally extraction of simple techniques to extend the flight envelope for additional maneuverability.

By enumerating these techniques across diverse species and flight conditions, our fundamental understanding of flapping flight was substantially improved, and the findings from this research are relevant for highly versatile next-generation small-scale flying robots.

To my parents; Olubode and Olusola, and my siblings; Ayomide and Ayotola

Contents

List of Figures

List of Tables

Chapter 1
Introduction

In nature, true flight has only been achieved by three animals: birds, bats, and insects. Among these organisms, insects evolved flight first about 300 million years ago and are the most proficient fliers. There are about 5.5 million documented species of insects [1], of which approximately 1.1 million use flapping wings to fly [2]. These volant organisms are found in all terrestrial ecosystems and possess different morphologies and vast flying abilities, which include forward, hover, turning capabilities, and so on.

To achieve prowess in flight, both body and wing kinematics adjustments are necessary. Two-winged insects, for instance, flies, have a neurosensory system that enables them to execute maneuvers and recover from mid-air perturbations quickly [3, 4]. Likewise, the direct musculature at the wing root allows four-winged predators, such as Odonates, to control each wing independently, and to enhance wingbeat asymmetries useful for generating large flight forces [5, 6]. Auxiliary mechanisms such as wing deformation and airframe morphing have also been shown to influence flight performance and efficiency [7-10]. Nevertheless, our understanding of flapping flight is still incomplete. Since the twentieth century, both biologists and engineers have devoted efforts to understand insect kinematics and aerodynamics, stability and control, evolutionary history and neurobiology. This research has run parallel to advances in aircraft aerodynamics [11], with great strides occurring mainly in the last two to three decades [12].

1.1. Micro-aerial vehicles

Engineers are particularly interested in flapping flight to inspire the design of unmanned aerial vehicles (UAV), popularly known as drones (micro-aerial vehicles (MAV), nano-air vehicles (NAV) and pico-air vehicles (PAV)), for surveillance, environmental monitoring and assessment, package delivery, agriculture, filmmaking, and so on. [13-15]. These vehicles are small, lightweight, and designed to operate at low speeds (Figure 1.1). Flying robots can use fixed, rotary, or flapping wings with each of these configurations having their pros and cons depending on the regime in which the vehicle operates. It is known that both fixed and rotary wings do not scale down well regarding aerodynamics and performance of components needed for propulsion [16]. Bio-inspired flapping flight, thus, offers an approach to bypass the challenges associated with the scalability of rotorcraft [16]. However, there are non-trivial challenges both from manufacturing, control, fluid dynamics, and biomechanics standpoints that affect bio-inspired flight. Since the small dimensions and low flight speeds requirements for flying robots are similar to those of most flying insects, understanding insect flight serves as a primary source of inspiration to solve these challenges. The Delfly Nimble [17] (Figure 1.1(c)) is a prime example of state of the art; a tailless autonomous free-flying robot that can perform rapid turns similar to flies, indicating that findings from research can be translated into design.

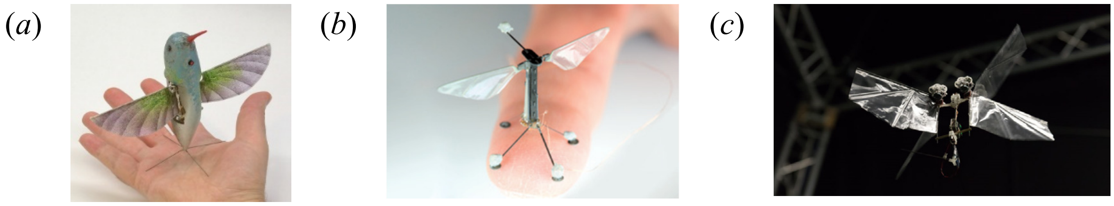

Figure 1.1. State of the art Flapping MAV. (A)Hummingbird Nano [18] developed by AeroVironment Inc. (B) Harvard Robobee [19] developed by Harvard University (C) Delfly Nimble [17] developed by TU Delft.

1.2. Unsteady aerodynamics.

The study of flapping flight is strongly tied to aerodynamic force production. From a fluid dynamics standpoint, the consequence of the low speed and size of flying robots and insects is that they operate in a low Reynolds number (*Re*) regime (10-10^4) where viscous and inertial forces are important [20]. Due to the oscillatory nature of the wings, the flow is highly unsteady, and propulsion is characterized by the manipulation of vortex structures. Two other non-dimensional parameters besides *Re* are essential for quantifying unsteadiness, namely the reduced frequency (*k*) and Strouhal number (*St*). *St* gives the ratio of the fluid convection time scale to the wing motion, while *St* characterizes the behavior of the vortices left behind the flapping wing.

It was thought originally that steady-state aerodynamics with attached flows was sufficient to explain the high-lift generation of insects [21, 22]. However, flow visualizations and force measurements in the last two decades have shown that insects use unsteady aerodynamic mechanisms to generate the high lift required for their flight [23-27]. These high-lift aerodynamic mechanisms include delayed/absence-of stall signified by the presence of a leading edge vortex (LEV), wake-capture, wing-wing, and wing-wake interactions, and rotational effects (see [2, 11, 28] for comprehensive reviews). Insect bodies may also influence the fluid dynamics via 'wing-body interactions' whereby the body generated vortices increase the wing's circulation [29]. The body size may also change LEV characteristics by modifying *Re* and Coriolis accelerations [30]. In low flapping frequency flight, where the time scales of the body and wing can be of the same order of magnitude, body motions also affect both wing kinematics and aerodynamics. There remain, however, phenomena yet to be characterized or understood in the bid to develop an integrated framework for understanding flapping flight, and this remains an active area of research [2].

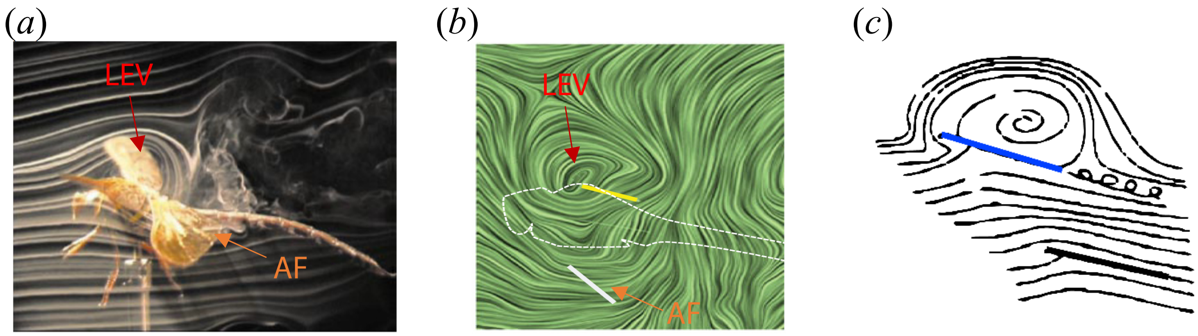

Figure 1.2. Leading edge vortex in dragonfly forward flight. The topology of the LEV is captured at mid-span using (a) smoke visualization [25, 31] and (b) particle image velocimetry (PIV) [27]. (c) Schematic of flow topology. From the images (a-c), an LEV is evident on the forewings, but attached flows (AF) dominate the hindwings in these visualizations. The LEV is dominant in the downstroke phase. In (b), the lift to weight ratio was calculated by the authors, and they concluded that the LEV on the FW alone is sufficient to carry the weight of a dragonfly. All studies listed [25, 27, 31] documented the absence of an LEV on the HW and during the upstroke.

This dissertation is one of the many endeavors to unravel and understand how insects generate forces for flight by kinematics adjustments which influence the aerodynamics.

1.3. References

[1] Stork, N.E. 2018 How Many Species of Insects and Other Terrestrial Arthropods Are There on Earth? *Annual Review of Entomology* **63**, 31-45. (doi:10.1146/annurev-ento-020117-043348).

[2] Chin, D.D. & Lentink, D. 2016 Flapping wing aerodynamics: from insects to vertebrates. *Journal of Experimental Biology* **219**, 920-932.

[3] Ristroph, L., Bergou, A.J., Ristroph, G., Coumes, K., Berman, G.J., Guckenheimer, J., Wang, Z.J. & Cohen, I. 2010 Discovering the flight autostabilizer of fruit flies by inducing aerial stumbles. *Proceedings of the National Academy of Sciences* **107**, 4820-4824. (doi:10.1073/pnas.1000615107).

[4] Dickinson, M.H. & Muijres, F.T. 2016 The aerodynamics and control of free flight manoeuvres in Drosophila. *Phil. Trans. R. Soc. B* **371**, 20150388.

[5] Wakeling, J. & Ellington, C. 1997 Dragonfly flight. II. Velocities, accelerations and kinematics of flapping flight. *Journal of experimental biology* **200**, 557-582.

[6] Rüppell, G. 1989 Kinematic analysis of symmetrical flight manoeuvres of Odonata. *Journal of Experimental Biology* **144**, 13-42.

[7] Bode-Oke, A.T., Zeyghami, S. & Dong, H. 2015 Optimized Body Deformation in Dragonfly Maneuvers. In *American Institute of Aeronautics and Astronautics Student Region I Conference* (Blacksburg, VA.

[8] Zeyghami, S., Bode-Oke, A.T. & Dong, H. 2016 Effect of Body Configuration and Deformation on the dynamic stability of flapping flight. In *AIAA Atmospheric Flight Mechanics Conference* (p. 3540.

[9] Nakata, T. & Liu, H. 2012 Aerodynamic performance of a hovering hawkmoth with flexible wings: a computational approach. *Proceedings of the Royal Society B: Biological Sciences* **279**, 722-731. (doi:10.1098/rspb.2011.1023).

[10] Luu, T., Cheung, A., Ball, D. & Srinivasan, M.V. 2011 Honeybee flight: a novel 'streamlining'response. *Journal of Experimental Biology* **214**, 2215-2225.

[11] Sane, S.P. 2003 The aerodynamics of insect flight. *The journal of experimental Biology* **206**, 4191-4208.

[12] Hedrick, T.L., Combes, S.A. & Miller, L.A. 2014 Recent developments in the study of insect flight. *Canadian Journal of Zoology* **93**, 925-943. (doi:10.1139/cjz-2013-0196).

[13] Wood, R.J., Finio, B., Karpelson, M., Ma, K., Pérez-Arancibia, N.O., Sreetharan, P.S., Tanaka, H. & Whitney, J.P. 2012 Progress on 'pico' air vehicles. *The International Journal of Robotics Research* **31**, 1292-1302. (doi:10.1177/0278364912455073).

[14] Shyy, W., Lian, Y., Tang, J., Viieru, D. & Liu, H. 2007 *Aerodynamics of low Reynolds number flyers*, Cambridge University Press.

[15] James, E.B., Jeremy, A.P., Madhu, K.S., Chang-kwon, K., David Brian, L., Farbod, F. & Hikaru, A. 2018 Achieving bioinspired flapping wing hovering flight solutions on Mars via wing scaling. *Bioinspiration & Biomimetics* **13**, 046010.

[16] Floreano, D. & Wood, R.J. 2015 Science, technology and the future of small autonomous drones. *Nature* **521**, 460. (doi:10.1038/nature14542).

[17] Karásek, M., Muijres, F.T., De Wagter, C., Remes, B.D.W. & de Croon, G.C.H.E. 2018 A tailless aerial robotic flapper reveals that flies use torque coupling in rapid banked turns. *Science* **361**, 1089-1094. (doi:10.1126/science.aat0350).

[18] Keennon, M., Klingebiel, K. & Won, H. Development of the Nano Hummingbird: A Tailless Flapping Wing Micro Air Vehicle. In *50th AIAA Aerospace Sciences Meeting including the New Horizons Forum and Aerospace Exposition* (

[19] Ma, K.Y., Chirarattananon, P., Fuller, S.B. & Wood, R.J. 2013 Controlled Flight of a Biologically Inspired, Insect-Scale Robot. *Science* **340**, 603-607. (doi:10.1126/science.1231806).

[20] Ellington, C.P. 2006 Insects versus birds: the great divide. In *44th AIAA aerospace sciences meeting and exhibit* (pp. 1-6.

[21] Azuma, A., Azuma, S., Watanabe, I. & Furuta, T. 1985 Flight mechanics of a dragonfly. *Journal of experimental biology* **116**, 79-107.

[22] Azuma, A. & Watanabe, T. 1988 Flight performance of a dragonfly. *Journal of Experimental Biology* **137**, 221-252.

[23] Bomphrey, R.J., Taylor, G.K. & Thomas, A.L.R. 2009 Smoke visualization of free-flying bumblebees indicates independent leading-edge vortices on each wing pair. *Experiments in Fluids* **46**, 811-821. (doi:10.1007/s00348-009-0631-8).

[24] Bomphrey, R.J., Lawson, N.J., Harding, N.J., Taylor, G.K. & Thomas, A.L.R. 2005 The aerodynamics of Manduca sexta: digital particle image velocimetry analysis of the leading-edge vortex. *Journal of Experimental Biology* **208**, 1079-1094. (doi:10.1242/jeb.01471).

[25] Thomas, A.L., Taylor, G.K., Srygley, R.B., Nudds, R.L. & Bomphrey, R.J. 2004 Dragonfly flight: free-flight and tethered flow visualizations reveal a diverse array of unsteady lift-generating mechanisms, controlled primarily via angle of attack. *Journal of Experimental Biology* **207**, 4299-4323.

[26] Ellington, C.P., van den Berg, C., Willmott, A.P. & Thomas, A.L.R. 1996 Leading-edge vortices in insect flight. *Nature* **384**, 626-630.

[27] Bomphrey, R.J., Nakata, T., Henningsson, P. & Lin, H.-T. 2016 Flight of the dragonflies and damselflies. *Philosophical Transactions of the Royal Society B: Biological Sciences* **371**. (doi:10.1098/rstb.2015.0389).

[28] Bomphrey, R.J., Nakata, T., Phillips, N. & Walker, S.M. 2017 Smart wing rotation and trailing-edge vortices enable high frequency mosquito flight. *Nature* **544**, 92-95.

[29] Liu, G., Dong, H. & Li, C. 2016 Vortex dynamics and new lift enhancement mechanism of wing–body interaction in insect forward flight. *Journal of Fluid Mechanics* **795**, 634-651.

[30] Bhat, S.S., Zhao, J., Sheridan, J., Hourigan, K. & Thompson, M.C. 2018 The leading-edge vortex on a rotating wing changes markedly beyond a certain central body size. *Royal Society Open Science* **5**. (doi:10.1098/rsos.172197).

[31] Bomphrey, R.J., Srygley, R.B., Taylor, G.K. & Thomas, A.L.R. 2002 Visualizing the Flow around Insect Wings. *Physics of Fluids* **14**, S4-S4. (doi:10.1063/1.4739193).

Chapter 2

Background and research questions.

One of the fundamental questions in insect flight research involves how insects produce and manipulate the forces that enable them to perform aerial maneuvers effectively [1-3]. It has been proposed that specific mechanisms are the keys behind flight performance. Figure 2.1 shows a comprehensive list of the aerodynamic mechanisms used during flapping flight and where gaps lie in our current understanding. Here, we will focus on insects. Filled circles indicate that substantial work has been done to characterize the mechanism while open circles/blank white spaces mean that there is still a need for extensive or new quantitative work to be done. These areas include upstroke effects, wing-wake interactions and body/tail/hindwing contributions/roles in flight (Figure 2.1), and more recently rotational effects when the flapping amplitude is low (<45º) and flapping frequency is high, which applies only to insects such as mosquitos [3].

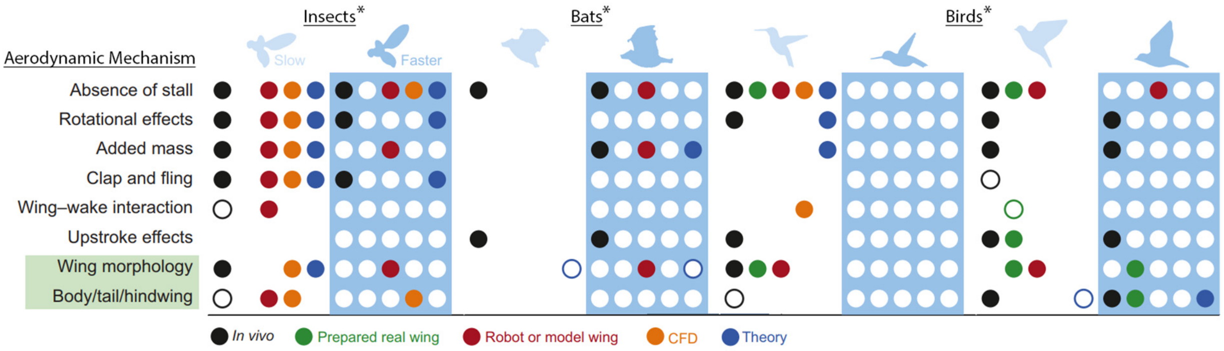

Figure 2.1. Gaps in our current understanding of flapping flight across insects and vertebrates**.** Vertically, seven aerodynamic mechanisms studied so far in the literature for flapping animal flight (the light green shading groups morphological effects as the seventh mechanism) are listed. Horizontally, the studied animals (insects, bats, hummingbirds, and other birds) are listed. White columns represent slow (hover) flight, and light blue columns represent faster (forward) flight. Colored circles indicate the methodology used to study the aerodynamic mechanism. The studies are listed with the color-coding system as follows: **black** – *in vivo*, **green** – prepared real wing, **red** – physical model or robot, **orange** – computational fluid dynamics (CFD), **blue** – theory. Filled circles indicate quantitative studies. Open circles indicate qualitative studies. Figure adapted and modified from Chin and Lentink [4].

2.1. Flight modes and animals studied

Concerning body configuration, the asterisks in Figure 2.1 denote that the majority of the aerodynamics of insect flight has been restricted disproportionally to hovering (slow) flight [4, 5]. There are studies in forward (faster) flight but much less than hovering. Typically, the animal is in a dorso-ventral configuration as indicated by the silhouettes. Altogether, these works inevitably ignore the aerodynamics of other flight configurations which are observed as part of the flight repertoire of insects. Examples include takeoff, sideways, turning maneuvers (of other insects other than flies) and even backward flight. Many unanswered questions exist for some of these interesting flight behaviors simply because they have not been investigated extensively.

Concerning the animals that have been studied, many of the works have focused on two-winged insects like flies (Dipterans) while there are significantly less quantitative studies based on four-winged bimotoric insects and functionally-two-winged/anteromotoric insects. Typically, insects such as dragonflies, hawkmoths and fruit flies, etc., have served as model organisms for research. Nevertheless, insects with simpler wing actuation like cicadas and beetles may provide insights into how complex maneuvers are elicited with simple techniques [6]. Studies on such insects are also needed because most MAVs are often simplified compared to the insects that are said to inspire their designs [7] (Figure 1.1)

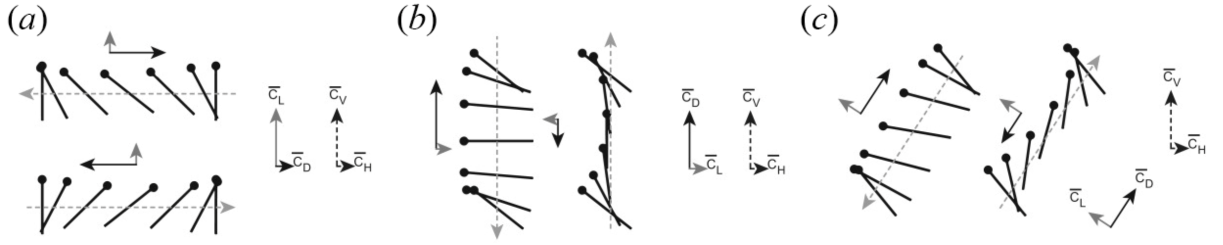

Figure 2.2. Idealized wing motion during hovering. (a) Horizontal stroke plane (HSP) typically used by Diptera. (b) Vertical stroke plane used by butterflies (Lepidoptera). (c) Inclined stroke plane (ISP) used by Odonata. Force partitions are shown in terms of lift ($\overline{C}_L$), drag ($\overline{C}_D$), and vertical ($\overline{C}_V$) and horizontal ($\overline{C}_H$) components. Adapted and modified from Jones et al. [8].

2.2. Wing motion and body configuration

In respect of wing motions, most works have focused on animals which flap in a horizontal stroke plane (HSP) such as fruit flies, bees, and so on. However, there is a need for more understanding of flight with an inclined stroke plane (ISP) [9, 10]. HSP flight is predominant in hovering but rare in forward flight (with an exception, see Ristroph et al.'s work [11]). ISP and HSP flight are drastically different and agile maneuverers like Odonata, who can fly with HSP, actually prefer to beat their wings in an ISP for their rapid, powerful and multi-directional flight since there are maneuverability and stability advantages with ISP [12]. Because the path of the wings is tilted relative to the horizontal in an ISP, the flight forces are partitioned. For example, a combination of lift and drag produces the vertical forces to sustain body weight but drag dominates (Figure 2.2(c)). In 'normal' or HSP hovering, the drag components cancel out in both half strokes and vertical force is dominated by lift with the contributions of the half strokes being nearly symmetric [9] (Figure 2.2(a)).

Another consequence of flapping with an ISP is that asymmetries between the half strokes are evident in both hovering and forward motions. The kinematic asymmetry between the two translational flapping phases, that is, the downstroke (dorsal-to-ventral stroke) and upstroke (ventral-to-dorsal stroke) in an ISP cause a pronounced asymmetry in the force production in each half stroke (Table 2.1). Even for insects that use ‘normal’ hovering, to achieve forward flight, an inclination of the stroke plane is usually a requirement for all insects [13-15] (Figure 2.3) because many insects reorient flight forces by tilting the stroke plane. Stroke plane tilt is achieved indirectly by reducing the body angle in forward flight, which also has the advantage of lowering parasite drag on the body at high speeds [16]. Nevertheless, the tilt angle of the force vector is not exactly the change in body angle. If the force vector and stroke plane are fixed relative to the body, throughout the body configurational changes, then the insect relies on the helicopter model for its flight [17]. As the stroke plane becomes inclined with forward speed, symmetry in kinematics and force production exhibited during HSP hovering is broken, thus rendering one half stroke (the upstroke) less aerodynamically active (or in some cases completely inactive) than the other [18, 19].

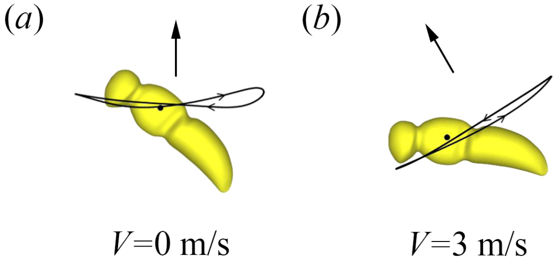

Figure 2.3. Body configuration and motion influence the stroke plane and force vector orientation in the global frame. A qualitative force vector is added to indicate force tilt. Figure modified and adapted from Meng and Sun [20].

2.3. Half stroke force generation and asymmetry

Aerodynamic force production is achieved by controlling both the velocity and circulation of the wings [21-23]. Modulating the velocity and circulation on a half stroke basis thus is also a source of half stroke asymmetries. The wing velocity is a function of the stroke plane and advance ratio (J), which is the ratio of the body velocity to the wing velocity [16]. From a fluid dynamics perspective, $|J|$ is also indicative of the ratio of steady to unsteady effects in flight. When $J>0$ (forward flight), the resultant wing velocity in each half stroke is the vector sum of both the wing and body velocity. The addition of a forward body velocity causes an asymmetry between the half strokes so that the wing net velocity is increased during the downstroke and reduced during the upstroke [18]. If flight with $J<0$, is possible, the reverse will occur. However, we hypothesize that in reality $J<0$ is not the exact reverse of $J>0$. The kinematics and aerodynamics are different.

Insects also control the circulation produced by their wings by regulating the angle of attack (AoA) with wing flexibility and rotation playing auxiliary roles [22]. Because of the wing orientation relative to the stroke plane or the effective wing velocity, the force asymmetry is a function of the wing AoA asymmetry between the half strokes [16]. Experiments on dynamically-scaled robots during ISP hovering have shown that even when the velocity in both half strokes is similar, there is a force asymmetry because of differences in AoA [24, 25]. When a wing flaps at a high AoA, the flow separates at the leading edge and reattaches before the trailing edge, forming an LEV which stays stably attached to the wing due to the balance of centripetal and Coriolis accelerations. The presence of the LEV in insect flight has been associated with enhanced forces on the wing [1, 26]. LEVs are found predominantly in the DS where AoA is high. Attached flows characterize the US, where the AoA is low and little forces are produced during this half stroke. Thus, the US is aerodynamically less active or inactive [2, 19, 27, 28].

Table 2.1. Flight mode, stroke plane type, and half stroke force asymmetry in different flight modes of insects and hummingbirds. The percentage of the contribution to the resultant aerodynamic force in flight is recorded. **-tethered.

insect	flight mode	stroke plane	DS net force (%)	US net force (%)	reference	
cicada	forward	inclined	80	20	Wan et al.	[29]
	forward		90	10	Liu et al.	[30]
damselfly	forward	inclined	75	25	Sato et al.	[31]
	forward		84	16	Bode-Oke et al.	[19]
dragonfly	hovering**	inclined	77	23	Russell	[32]
	forward		80	20	Azuma and Watanabe	[33]
	forward		67	33	Hefler et al.	[34]
fruit fly	forward	inclined	61	39	Meng and Sun	[14]
	hovering	horizontal	37	63	Fry et al.	[35]
	saccade		40	60	Fry et al.	[36]
hawkmoth	forward	inclined	80	20	Willmott et al.	[37]
	hovering		67	33	Aono and Liu	[38]
	hovering		68	32	Zheng et al.	[39]
mosquito	hovering	horizontal	43	57	Bomphrey et al.	[3]
honeybee	hovering	horizontal	43	57	Altshuler et al.	[23]
butterfly	forward	inclined	75	25	Zheng et al.	[40]
hoverfly	hovering	inclined	73	27	Mou et al.	[41]
drone fly	hovering	horizontal	52	48	Liu and Sun	[42]
hummingbird	hovering	horizontal	66	34	Warrick et al.	[43]
	hovering	horizontal	65	35	Song et al.	[44]
	forward	inclined	74	26	Song et al.	[45]
locust	forward	inclined	86	14	Young et al.	[46]

2.4. Upstroke effects

Upstroke (US) effects are concerned with how the upstroke can generate useful forces for flight and typically signified by unique kinematics of the upstroke, and the use of lift-enhancing mechanisms. In vertebrate flight, upstroke lift has been identified in insectivorous birds like hummingbirds [43], and lift is due to an LEV, similar to insects that hover with an HSP since hummingbirds can almost reverse wing camber [47]. For other birds, which are limited by their musculature to reverse the whole wing, the tip reversal upstroke is capable of generating substantial forces [48, 49]. Thus, upstroke lift can also be produced during low-speed turns [49].

In forward flight, however, the tip reversal upstroke contributes to thrust, capitalizing on the 'clap and fling' mechanism to boost flight forces [48]. Studies of upstroke effects are not common in insect flight [4], partly due to the force asymmetry described above and the otherwise rigid function of the half strokes when the insect is in motion.

Inevitably, although the phenomenon of delayed stall is well-known (Figure 2.1, top row), it is coupled with upstroke effects since the LEV is the primary means of lift production in insect flight. The LEV mechanism is primarily associated with the downstroke (DS) as aforementioned. Since aerodynamics depend on morphology and kinematics, understanding the kinematics of upstroke motions and link to consequent aerodynamics will provide insights on upstroke effects in free flight which is currently lacking in the literature, especially with regard to LEV generation. Moreover, since the body configuration/motion can also modify wing kinematics, both body and wing motions may be instrumental in understanding upstroke effects.

Altogether, the background provided leads us to ask the following research questions. What is the aerodynamic function of each half stroke? When $J \geq 0$, the DS produces the vertical (weight-carrying) force, and the upstroke produces the horizontal force [50-52]. Is this trend fixed or could the conventional aerodynamic functions of the DS and US be reversed and under what flight conditions will that occur and what are the implications? The downstrokes are dominated by separated flows (LEV) while attached flows or small vortices characterize the upstroke. It is also possible for the upstroke to contribute nothing to lift generation [19, 28, 30]. So what are the kinematics and aerodynamics that leads to the presence of an active upstroke? Can the upstroke provide substantial weight support or even dominate the net force production in flight (see Table 2.1)? Can a strong LEV be formed in the upstroke if the wings are usually strongly supinated for low AoA? When will this occur and what kinematics changes will be responsible? How do body motion and configuration influence wing performance? If any of these questions can be answered, are the mechanisms identified robust among different fliers? These questions are still unanswered and relatively unexplored in the literature.

Answers to these questions are essential in real-world applications of flying robots where flight will comprise of different maneuvers, and the vehicle will possess different orientations and the kinematics, use of lift-enhancing mechanisms and the function of the half stroke may change. We hypothesize that upstroke effects will be evident if the upstroke can provide weight support. Furthermore, body postural adjustment will be vital since it is a viable way of altering the stroke plane, which determines force partitions as well as the wing aerodynamics.

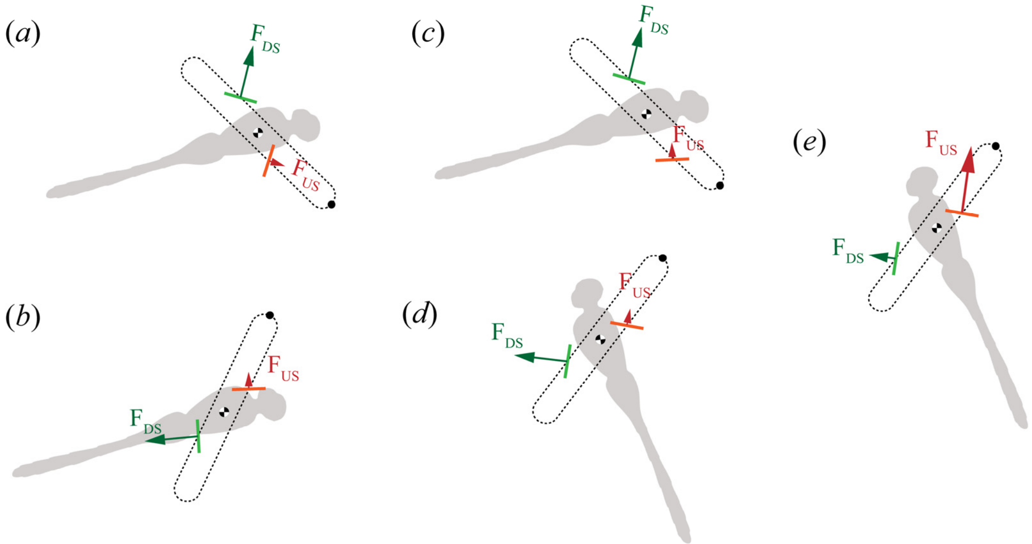

Figure 2.4. Inducing upstroke lift in free flight. Dashed lines denote the stroke plane. The black circle on the stroke plane denotes the stroke plane's front end. Green and red arrow indicate anecdotal flight forces.

In Figure 2.4, we qualitatively evaluated different ways through which an insect may generate substantial upstroke lift while flying ($J \neq 0$). Figure 2.4(a) shows the posture of a dragonfly in forward flight with the force vector orientations and relative magnitude. To generate upstroke lift, the insect may rotate the stroke plane relative to the body but keep the body posture relatively fixed (Figure 2.4(b)). However, to do so, the insect firstly must possess large wing degrees of freedom [53-55] to be able to vary the aerodynamic force relative to the body. Even for insects like damselflies (which we will term a complex insect in this dissertation due to its wing degrees of freedom), the rotation of the stroke plane below the longitudinal axis is restricted to only 5º [53]. Interestingly, if possible, the insect will fly backward ($J<0$) as indicated by the downstroke force orientation.

The insect may also fix the stroke plane and drastically twist the wings (Figure 2.4(c)). Nevertheless, since insect wings are fixed on hinges, it is not viable to completely twist the wings and thus supinate the whole wing area for useful aerodynamic force generation [16, 56]. Another way to look at Figure 2.4(c) is that the downstroke does not supinate at wing reversal. In this case, the upstroke will generate negative lift in slow-speed flight. An exception is a positively loaded upstroke in butterfly forward flight where a vortex from the downstroke rests on the wing in the upstroke, but this is very rare [57]. Another exception occurs in the fast flight of hawkmoths at speeds higher than 5m/s, yet the mechanics of force generation have not been confirmed [58].

The insect may rotate the body without significant changes in wing kinematics. However, weight support is not guaranteed from either half stroke (Figure 2.4(d)), but backward flight will occur. Lastly, the insect may rotate the body and adjust the wing kinematics to ensure that weight support is guaranteed. The kinematics adjustments, however, will induce a new flight mode (reverse/backward/$J<0$ flight). If $J<0$ is the consequence of upstroke effects, then the variation of the kinematics and forces on a half stroke basis, the roles of the half stroke in force generation, and the force control strategy when $J<0$ is unexplored in insects. Therefore, it is from the lens of flight with negative advance ratios that we investigate upstroke effects, in particular, lift generation. The flight physics of the novel flight mode and the utility of the upstroke are intertwined and thus unraveled simultaneously.

2.5. Dissertation outline

Chapter 3 presents the first quantitative study of backward flight in the literature. Experimental and computational work is done on one of nature's most agile species, the dragonfly. We enumerate the kinematics and aerodynamics, confirming our hypothesis and the anecdote in Figure 2.4. The results from chapter 3 formed the basis for the rest of the work in the dissertation.

Chapters 4 and 5 both build on the framework of Chapter 3 by demonstrating that the findings are not restricted to complex fliers like Odonates. We present the first quantitative studies of the backward flight of fliers with restricted wing degrees of freedom (which we term as simple insects in this dissertation) such as cicadas (chapters 4) and butterflies (Chapters 5). The unique kinematics and aerodynamics of each species are discussed. In particular, we test the helicopter model on this simple fliers by comparing the techniques of backward flight with other flight modes.

Chapter 6, investigates the influence of unsteady body motion on backward flight and wing half stroke function. Insects rarely cruise during flight; instead, their body motion is a combination of acceleration, deceleration, and rapid changes in direction. This kind of behavior is exhibited during obstacle avoidance, the transition from one mode to another, station keeping, and environmental assessment ("hesitation behaviors" [59]). However, the kinematics and aerodynamics of this behavior have not been elucidated until now.

Chapter 7 investigates how wing damage influences the wing kinematics and coordination of the wing pairs in backward flight.

Lastly, Chapter 8 summarizes the conclusions and discusses the contribution of this work as well as its limitations. Suggestions for future research directions are made.

2.6. References

[1] Dickinson, M.H., Lehmann, F.-O. & Sane, S.P. 1999 Wing rotation and the aerodynamic basis of insect flight. *Science* **284**, 1954-1960.

[2] Thomas, A.L., Taylor, G.K., Srygley, R.B., Nudds, R.L. & Bomphrey, R.J. 2004 Dragonfly flight: free-flight and tethered flow visualizations reveal a diverse array of unsteady lift-generating mechanisms, controlled primarily via angle of attack. *Journal of Experimental Biology* **207**, 4299-4323.

[3] Bomphrey, R.J., Nakata, T., Phillips, N. & Walker, S.M. 2017 Smart wing rotation and trailing-edge vortices enable high frequency mosquito flight. *Nature* **544**, 92-95.

[4] Chin, D.D. & Lentink, D. 2016 Flapping wing aerodynamics: from insects to vertebrates. *Journal of Experimental Biology* **219**, 920-932.

[5] Hedrick, T.L., Combes, S.A. & Miller, L.A. 2014 Recent developments in the study of insect flight. *Canadian Journal of Zoology* **93**, 925-943. (doi:10.1139/cjz-2013-0196).

[6] Zeyghami, S., Babu, N. & Dong, H. 2016 Cicada (Tibicen linnei) steers by force vectoring. *Theoretical and Applied Mechanics Letters*. (doi:http://dx.doi.org/10.1016/j.taml.2015.12.006).

[7] Zeyghami, S. 2015 Wing in the Loop: Integrating the Wing Into Dynamics of Insect Flight. Charlottesville, VA, University of Virginia, Department of Mechanical and Aerospace Engineering, PHD, 2015.

[8] Jones, S.K., Laurenza, R., Hedrick, T.L., Griffith, B.E. & Miller, L.A. 2015 Lift vs. drag based mechanisms for vertical force production in the smallest flying insects. *Journal of Theoretical Biology* **384**, 105-120. (doi:https://doi.org/10.1016/j.jtbi.2015.07.035).
[9] Wang, Z.J. 2004 The role of drag in insect hovering. *Journal of Experimental Biology* **207**, 4147-4155. (doi:10.1242/jeb.01239).
[10] Sudhakar, Y. & Vengadesan, S. 2010 Flight force production by flapping insect wings in inclined stroke plane kinematics. *Computers & Fluids* **39**, 683-695. (doi:https://doi.org/10.1016/j.compfluid.2009.11.004).
[11] Ristroph, L., Bergou, A.J., Guckenheimer, J., Wang, Z.J. & Cohen, I. 2011 Paddling Mode of Forward Flight in Insects. *Physical Review Letters* **106**, 178103.
[12] ENNOS, A.R. 1989 The Kinematics an Daerodynamics of the Free Flight of some Diptera. *Journal of Experimental Biology* **142**, 49-85.
[13] Ellington, C.P. 1999 The novel aerodynamics of insect flight: applications to micro-air vehicles. *Journal of Experimental Biology* **202**, 3439-3448.
[14] Meng, X. & Sun, M. 2016 Wing Kinematics, Aerodynamic Forces and Vortex-wake Structures in Fruit-flies in Forward Flight. *Journal of Bionic Engineering* **13**, 478-490. (doi:https://doi.org/10.1016/S1672-6529(16)60321-9).
[15] Sane, S.P. 2003 The aerodynamics of insect flight. *The journal of experimental Biology* **206**, 4191-4208.
[16] Dudley, R. 2002 *The biomechanics of insect flight: form, function, evolution*, Princeton University Press.
[17] Taylor, G.K. 2001 Mechanics and aerodynamics of insect flight control. *Biological Reviews* **76**, 449-471.
[18] Ellington, C. 1984 The aerodynamics of hovering insect flight. III. Kinematics. *Philosophical Transactions of the Royal Society of London B: Biological Sciences* **305**, 41-78.
[19] Bode-Oke, A., Zeyghami, S. & Dong, H. 2017 Aerodynamics and flow features of a damselfly in takeoff flight. *Bioinspiration & biomimetics* **12**, 056006.
[20] Meng, X.G. & Sun, M. 2016 Wing and body kinematics of forward flight in drone-flies. *Bioinspiration & Biomimetics* **11**, 056002. (doi:10.1088/1748-3190/11/5/056002).
[21] Dickinson, M.H. & Muijres, F.T. 2016 The aerodynamics and control of free flight manoeuvres in Drosophila. *Phil. Trans. R. Soc. B* **371**, 20150388.
[22] Lehmann, F.O. & Dickinson, M.H. 1998 The control of wing kinematics and flight forces in fruit flies (Drosophila spp.). *The Journal of Experimental Biology* **201**, 385-401.
[23] Altshuler, D.L., Dickson, W.B., Vance, J.T., Roberts, S.P. & Dickinson, M.H. 2005 Short-amplitude high-frequency wing strokes determine the aerodynamics of honeybee flight. *Proceedings of the National Academy of Sciences of the United States of America* **102**, 18213-18218.
[24] Hu, Z. & Deng, X.-Y. 2014 Aerodynamic interaction between forewing and hindwing of a hovering dragonfly. *Acta Mechanica Sinica* **30**, 787-799. (doi:10.1007/s10409-014-0118-6).
[25] Hyungmin, P. & Haecheon, C. 2012 Kinematic control of aerodynamic forces on an inclined flapping wing with asymmetric strokes. *Bioinspiration & Biomimetics* **7**, 016008.
[26] Birch, J.M., Dickson, W.B. & Dickinson, M.H. 2004 Force production and flow structure of the leading edge vortex on flapping wings at high and low Reynolds numbers. *Journal of Experimental Biology* **207**, 1063-1072.
[27] Bomphrey, R.J., Nakata, T., Henningsson, P. & Lin, H.-T. 2016 Flight of the dragonflies and damselflies. *Philosophical Transactions of the Royal Society B: Biological Sciences* **371**. (doi:10.1098/rstb.2015.0389).
[28] Ellington, C.P. 1984 The Aerodynamics of Flapping Animal Flight1. *American Zoologist* **24**, 95-105. (doi:10.1093/icb/24.1.95).
[29] Wan, H., Dong, H. & Gai, K. 2015 Computational investigation of cicada aerodynamics in forward flight. *Journal of The Royal Society Interface* **12**, 20141116.
[30] Liu, G., Dong, H. & Li, C. 2016 Vortex dynamics and new lift enhancement mechanism of wing–body interaction in insect forward flight. *Journal of Fluid Mechanics* **795**, 634-651.
[31] Sato, M. & Azuma, A. 1997 The flight performance of a damselfly Ceriagrion melanurum Selys. *Journal of Experimental Biology* **200**, 1765-1779.
[32] Russell, D.B. 2004 Numerical and experimental investigations into the aerodynamics of dragonfly flight [PhD Dissertation], Cornell University.
[33] Azuma, A. & Watanabe, T. 1988 Flight performance of a dragonfly. *Journal of Experimental Biology* **137**, 221-252.
[34] Hefler, C., Noda, R., Shyy, W. & Qiu, H. 2017 Unsteady Vortex Interactions for Performance Enhancement of a Free Flying Dragonfly. In *ASME 2017 Fluids Engineering Division Summer Meeting* (pp. V01CT21A010-V001CT021A010, American Society of Mechanical Engineers.
[35] Fry, S.N., Sayaman, R. & Dickinson, M.H. 2005 The aerodynamics of hovering flight in Drosophila. *Journal of Experimental Biology* **208**, 2303-2318.

[36] Fry, S.N., Sayaman, R. & Dickinson, M.H. 2003 The aerodynamics of free-flight maneuvers in Drosophila. *Science* **300**, 495-498.

[37] Willmott, A.P., Ellington, C.P. & Thomas, A.L. 1997 Flow visualization and unsteady aerodynamics in the flight of the hawkmoth, Manduca sexta. *Philosophical Transactions of the Royal Society B: Biological Sciences* **352**, 303-316.

[38] Aono, H. & Liu, H. 2006 Vortical Structure and Aerodynamics of Hawkmoth Hovering. *Journal of Biomechanical Science and Engineering* **1**, 234-245. (doi:10.1299/jbse.1.234).

[39] Zheng, L., Hedrick, T.L. & Mittal, R. 2013 A multi-fidelity modelling approach for evaluation and optimization of wing stroke aerodynamics in flapping flight. *Journal of Fluid Mechanics* **721**, 118-154. (doi:10.1017/jfm.2013.46).

[40] Zheng, L., Hedrick, T.L. & Mittal, R. 2013 Time-Varying Wing-Twist Improves Aerodynamic Efficiency of Forward Flight in Butterflies. *PLOS ONE* **8**, e53060. (doi:10.1371/journal.pone.0053060).

[41] Mou, X.L., Liu, Y.P. & Sun, M. 2011 Wing motion measurement and aerodynamics of hovering true hoverflies. *The Journal of Experimental Biology* **214**, 2832-2844. (doi:10.1242/jeb.054874).

[42] Liu, Y. & Sun, M. 2008 Wing kinematics measurement and aerodynamics of hovering droneflies. *Journal of Experimental Biology* **211**, 2014-2025. (doi:10.1242/jeb.016931).

[43] Warrick, D.R., Tobalske, B.W. & Powers, D.R. 2009 Lift production in the hovering hummingbird. *Proceedings of the Royal Society of London B: Biological Sciences* **276**, 3747-3752. (doi:10.1098/rspb.2009.1003).

[44] Song, J., Luo, H. & Hedrick, T.L. 2014 Three-dimensional flow and lift characteristics of a hovering ruby-throated hummingbird. *Journal of The Royal Society Interface* **11**. (doi:10.1098/rsif.2014.0541).

[45] Song, J., Tobalske, B.W., Powers, D.R., Hedrick, T.L. & Luo, H. 2016 Three-dimensional simulation for fast forward flight of a calliope hummingbird. *Royal Society Open Science* **3**. (doi:10.1098/rsos.160230).

[46] Young, J., Walker, S.M., Bomphrey, R.J., Taylor, G.K. & Thomas, A.L.R. 2009 Details of Insect Wing Design and Deformation Enhance Aerodynamic Function and Flight Efficiency. *Science* **325**, 1549-1552. (doi:10.1126/science.1175928).

[47] Warrick, D.R., Tobalske, B.W. & Powers, D.R. 2005 Aerodynamics of the hovering hummingbird. *Nature* **435**, 1094-1097. (doi:10.1038/nature03647).

[48] Crandell, K.E. & Tobalske, B.W. 2015 Kinematics and aerodynamics of avian upstrokes during slow flight. *The Journal of experimental biology* **218**, 2518-2527.

[49] Ros, I.G., Bassman, L.C., Badger, M.A., Pierson, A.N. & Biewener, A.A. 2011 Pigeons steer like helicopters and generate down- and upstroke lift during low speed turns. *Proceedings of the National Academy of Sciences* **108**, 19990-19995. (doi:10.1073/pnas.1107519108).

[50] Azuma, A., Azuma, S., Watanabe, I. & Furuta, T. 1985 Flight mechanics of a dragonfly. *Journal of experimental biology* **116**, 79-107.

[51] Rüppell, G. 1989 Kinematic analysis of symmetrical flight manoeuvres of Odonata. *Journal of Experimental Biology* **144**, 13-42.

[52] Wang, Z.J. & Russell, D. 2007 Effect of forewing and hindwing interactions on aerodynamic forces and power in hovering dragonfly flight. *Physical review letters* **99**, 148101.

[53] Wakeling, J. & Ellington, C. 1997 Dragonfly flight. II. Velocities, accelerations and kinematics of flapping flight. *Journal of experimental biology* **200**, 557-582.

[54] Pfau, H. 1991 Contributions of functional morphology to the phylogenetic systematics of Odonata. *Advances in Odonatology* **5**, 109-141.

[55] Pfau, H.K. 1986 Untersuchungen zur Konstruktion, Funktion und Evolution des Flugapparates der Libellen (Insecta, Odonata). *Tijdschrift voor entomologie.* **129**, 35-123.

[56] Wootton, R.J. 1992 Functional Morphology of Insect Wings. *Annual Review of Entomology* **37**, 113-140. (doi:10.1146/annurev.en.37.010192.000553).

[57] Srygley, R.B. & Thomas, A.L.R. 2002 Unconventional lift-generating mechanisms in free-flying butterflies. *Nature* **420**, 660. (doi:10.1038/nature01223 https://www.nature.com/articles/nature01223#supplementary-information).

[58] Willmott, A.P. & Ellington, C.P. 1997 The mechanics of flight in the hawkmoth Manduca sexta. II. Aerodynamic consequences of kinematic and morphological variation. *The Journal of Experimental Biology* **200**, 2723-2745.

[59] Yokoi, T. & Fujisaki, K. 2009 Hesitation behaviour of hoverflies Sphaerophoria spp. to avoid ambush by crab spiders. *Naturwissenschaften* **96**, 195-200.

Chapter 3

Flying in reverse: kinematics and aerodynamics of a dragonfly in backward free flight

3.1. Abstract

In this study, we investigated the backward free flight of a dragonfly, accelerating in a flight path inclined to the horizontal. The wing and body kinematics were reconstructed from the output of three high-speed cameras using a template-based subdivision surface reconstruction method, and numerical simulations using an immersed boundary flow solver were conducted to compute the forces and visualize the flow features. During backward flight, the dragonfly maintained an upright body posture of approximately 90º relative to the horizon. The upright body posture was used to reorient the stroke plane and the flight force in the global frame; a mechanism known as 'force vectoring' which was previously observed in maneuvers of other flying animals. In addition to force vectoring, we found that while flying backward, the dragonfly flaps its wings with larger angles of attack in the upstroke (US) when compared to forward flight. Also, the backward velocity of the body in the upright position enhances the wings' net velocity in the US. The combined effect of the angle of attack and wing net velocity yields large aerodynamic force generation in the US, with the average magnitude of the force reaching values as high as 2-3 times the body weight. Corresponding to these large forces was the presence of a strong leading edge vortex (LEV) at the onset of US which remained attached up until wing reversal. Finally, wing-wing interaction was found to enhance the aerodynamic performance of the hindwings during backward flight. Vorticity from the forewings' trailing edge fed directly into the hindwings' LEV to increase its circulation and enhance force production.

Keywords: backward flight, downstroke-upstroke reversal, active upstroke, leading edge vortex, dragonfly, force asymmetry.

3.2. Introduction

Insects elicit flight maneuvers by drastically or subtly changing their wing and body kinematics. These changes influence both (i) the production and (ii) orientation and reorientation of aerodynamic forces, consequently determining the type of free flight maneuver that is performed. Examples of such maneuvers include well-studied modes like hovering, forward and turning flight [1-6], which have improved our understanding of flight mechanics and for engineers especially, fostered the design of micro-aerial vehicles (MAVs) [7-9]. However, some flight modes found in nature which may lead to further insights are yet to be explored. A classic example is backward flight. Although just qualitatively characterized in the literature, it has been documented that insects use backward flight for predator evasion, prey capture, flight initiation, station keeping, and load lifting [10-15]. Now, engineers are interested in incorporating retro-flight capabilities into state-of-the-art MAVs for additional maneuverability [9, 16]. To better understand the aerodynamics of backward flight in connection with wing and body kinematics, we studied free-flying dragonflies in this flight mode.

First, to fly, insects need to produce forces by controlling both the velocity of and circulation generated by their wings [5, 17, 18]. Because force production is proportional to wing velocity squared, insects adjust wing speed by altering the stroke amplitude and/or frequency [5, 11, 17]. Honey bees [18], drone flies[19], damselflies[20], and fruit flies [21] all increase stroke amplitude to generate larger flight forces. Insects also modulate the circulation produced by their wings by controlling the angle of attack (AoA) with wing flexibility and rotation speed playing lesser roles [17]. When a wing flaps at a high AoA, the flow separates at the leading edge and reattaches before the trailing edge, forming a vortex which stays stably attached to wing due to the balance of centripetal and Coriolis accelerations [22]. The presence of the leading edge vortex (LEV) in insect flight has been associated with enhanced forces on the wing [10, 23]. Although, there are different views on how the existence and attachment of the LEV contribute to force production in insect flight (absence of stall [24], increasing wing circulation/suction [25], etc.), it is known that a wing with an LEV imparts greater momentum to the fluid, leading to the production of larger forces than under steady-state conditions [26-29]. Bomphrey et al. [30] measured the LEV contribution to weight support during the forward flight of dragonflies and concluded that dragonflies could sustain their weight from the contribution of the LEV on the forewings alone. Since the flight forces are a strong function of wing kinematics, generated flight forces vary drastically during flight because the kinematics of the up and down strokes can be utterly different [3, 20, 31]. In hovering and forward flight, most insects, especially those which flap in an inclined stroke plane, i.e., dragonflies, damselflies, etc., produce larger forces during the downstroke (DS) due to the higher relative wing velocity and the angle of attack in comparison to the upstroke (US) [31, 32]. Conversely, the wing translates at a shallow angle of attack and smaller speed, tracing a shorter path in the US, thus, generating smaller forces [8, 20, 32]. The US is often ‘aerodynamically inactive’ as a result [20]. Currently, the variation of forces on a half-stroke basis and the roles of the US and DS in force generation during backward flight are less understood.

Second, the orientation and reorientation of aerodynamic forces is as essential for successful flight as force production and is vital to positioning the insect in its intended flight direction. Many flying organisms such as cicadas [33], fruit flies [4], dipterans [34], bats [35] and pigeons [36] use force vectoring like a helicopter for force reorientation. Force vectoring involves redirecting flight forces globally by rotating the body while the force vector remains relatively fixed to the body. A helicopter rotates the force vector by inducing a nose-down motion on the fuselage and tilting the tip-path plane (of the blades) forward to induce forward flight. Conversely, to transition to backward flight, a helicopter rotates the force vector by inducing a nose-up motion on the fuselage and tilts the tip-path plane backward. Most of the tilt is accomplished through fuselage rotation since the tilt of the tip-path is limited by the range of motion of the swash plates. Similarly, a tilt of the stroke plane has been reported to precede changes in the flight direction of insects [32]. Dragonflies, which have been reported to have a limited range of variation of the stroke plane with respect to their bodies [37], maintain a pitch-down orientation during forward flight. Like helicopters, flying backward in insects may require a similar strategy where the insect will maintain a pitch-up orientation. Rüppel [11], recorded a dragonfly flying backward with a body angle of 100º from the horizon. Likewise, Mukundarajan et al. [38] reported that a stroke plane tilted backward, and a steep body angle between 50-70º from the horizontal induced backward flight in Waterlily beetles (*Galerucella nymphaeae*). Our observations corroborate these reports as we consistently witnessed an upright body posture during the backward flight of dragonflies in our experiment.

In the present work, our goal is to investigate the kinematics and aerodynamics of a dragonfly in backward flight. More precisely, we aim to identify the role that force vectoring plays in the execution of a backward flight maneuver. Furthermore, we will identify other aerodynamic mechanisms related to backward flight, if any, and quantify their contributions with regard to this unique flight mode. An accurate 3D surface reconstruction technique coupled with a high fidelity Computational Fluid Dynamics (CFD) flow solver [39] is used to quantify the coordination of the wing and body motion and to identify how flight forces are generated during flight. Also, detailed flow features are elucidated and their relations to force generation mechanisms are evaluated and presented.

3.3. Material and methods

3.3.1. Dragonfly, high-speed videography, and three-dimensional surface reconstruction

We captured Dragonflies (*Erythemis simplicicollis*) from the wild and transported them to the lab for motion capture. We dotted the dragonflies' wings for tracking purposes and placed the insects in a filming area. The insects initiated flight voluntarily, and their motion was recorded by three orthogonally arranged high-speed cameras. While many of the flight sequences were of forward motions, we captured ten backward flight videos. These backward sequences included turning and straight backward flight, very short backward flight after take-off and backward flight of individuals with impaired wings. Our aim in this work is to present the best and clearest straight backward flight sequence we captured for analysis in the text. We selected one flight sequence and reconstructed the video in Autodesk Maya (Autodesk Inc.). The morphological parameters of the selected dragonfly are shown in Table 3.1. The reconstruction process captured both the kinematics and deformations. A more detailed study of the 3D reconstruction method is identified elsewhere [40].

Table 3.1. Morphological parameters for the dragonfly in this study. The mass and length measurement uncertainties are ±1 mg and ±1 mm, respectively.

species	flight time (ms)	body weight (mg)	body length (mm)	forewing length (mm)	forewing mean chord (mm)	hindwing length (mm)	hindwing mean chord (mm)	flapping frequency (Hz)
Erythemis simplicicollis	130	130	40	34	8	31	10	27

3.3.2. Wing kinematics and deformation

The wing kinematics are measured with respect to a coordinate system fixed at the wing root. Three Euler angles describe the angular orientation of the wing assuming it is rigid; flap, deviation, and pitch. The effective AoA (α_{eff}) here, is the angle between the chord and the vector sum of the body and wing velocity measured at the leading edge. Previous insect flight studies have measured the AoA at locations between the leading edge and quarter-chord or near the rotation axis of the wing [19, 41]. However, in classical aerodynamics (extended lifting line theory), the three-quarter chord (both for steady and unsteady flow) is the point of choice for calculating the AoA with respect to induced velocities for a wing in curved flow (Pistolesi's theorem) [42, 43]. The geometric AoA (α_{geom}) excludes the body velocity. A least-squares reference plane (LSRP) is generated based on the nodes on the reconstructed wing surface to quantify wing twist (see [40]). The LSRP is a planar fitting to the 3D positions of the wing surface points where the sum of the distances of the wing surface points from this plane is minimized. The twist angle is the relative angle of the deformed wing chord line and the LSRP. These definitions are rendered in Figure 3.1.

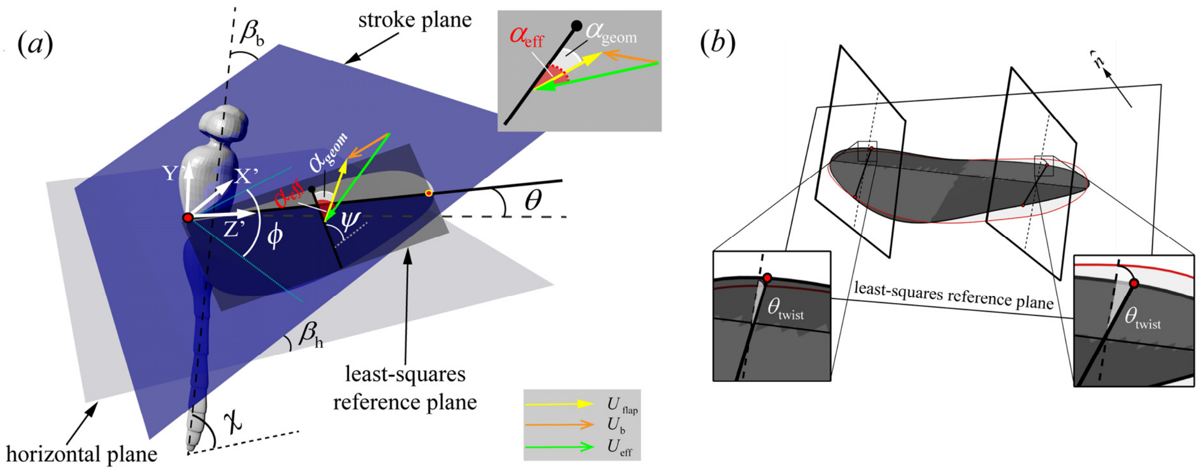

Figure 3.1. Kinematics definitions. (A) β_h and β_b are the stroke plane angles with respect to the horizontal and body longitudinal axis, respectively. ϕ, θ, ψ are the flap, deviation, and pitch angles. U_{eff} is the vector sum of the wing (U_{flap}) and body (U_b) velocity. α_{eff} and α_{geom} are the effective and geometric angles of attack. χ is the body angle. (B) Twist Angle (θ_{twist}). The deformed wing is shown in dark grey, and the least deformed wing is shown in light grey with a red outline. Two dimensional (2D) cross-sections show that the angle between the chord line of the least deformed wing (dashed line) and deformed wing (solid line with red tip) is the twist angle.

3.3.3. Computational fluid dynamics simulation

We used an in-house immersed boundary method flow solver for simulating incompressible flows in this study. We solved the incompressible Navier-Stokes (NS) Equation (Eqn. (1)) using a finite difference method with 2nd order accuracy in space and a 2nd order fractional step method for time stepping. More details of this approach and application can be found in other works [20, 39, 44, 45]. Validations of the flow solver are in the works of Wan et al. [39] and Li & Dong. [46].

$$\nabla \cdot \mathbf{u} = \mathbf{0}; \quad \frac{\partial \mathbf{u}}{\partial t} + \mathbf{u} \cdot \nabla \mathbf{u} = -\frac{1}{\rho} \nabla p + \upsilon \nabla^2 \mathbf{u}, \tag{1}$$

where $\mathbf{u}$ is the velocity vector in Cartesian coordinates, t is time, ρ is density, p is pressure and υ is the kinematic viscosity.

The vortex structures are visualized by the λ_2-criterion [47], which has been used in previous insect flight studies [44, 48]. The λ_2-criterion is based on the observation that a pressure minimum as a detection criterion is insufficient for locating vortex cores. Jeung & Hussein [47] opined that unsteady straining could cause a pressure minimum without vortical motion and viscous effects could also eliminate the pressure minimum in the flow when there is vortical motion. Hence, unsteady straining and viscous effect need to be eliminated to identify a vortex core properly.

The symmetric part of the gradient of Eqn. (1) is expressed as

$$\boldsymbol{S}^2 + \boldsymbol{\Omega}^2 = -\frac{1}{\rho}\nabla(\nabla p) \tag{2}$$

where $\mathbf{S} = 1/2\left[\nabla\mathbf{u} + (\nabla\mathbf{u})^{\mathrm{T}}\right]$ and $\mathbf{\Omega} = 1/2\left[\nabla\mathbf{u} - (\nabla\mathbf{u})^{\mathrm{T}}\right]$ are the strain rate and vorticity tensors respectively after the unsteady straining ($D\boldsymbol{S}/Dt$ term) and viscous effects (υ term) have been discarded. A vortex core is then defined as a region connected by real negative eigenvalues ($\lambda_2 < 0$) of equation (2).

We ran the simulations on a non-uniform Cartesian grid. The domain size was $50\bar{c}$ x $50\bar{c}$ x $50\bar{c}$ totaling 14 million grids. High-resolution uniform grids surround the insect in a volume of $13\bar{c}$ x $15\bar{c}$ x $23\bar{c}$ with a spacing of about $0.06\bar{c}$ with stretching grids extending from the fine region to the outer boundaries. The pressure and velocity boundary conditions at the domain's boundaries are homogeneous Neumann conditions set to zero. The Reynolds number defined by $\mathrm{Re} = \bar{U}_{tip}\bar{c}/\upsilon$ is about 1840, based on the average effective wing tip speed of the wing pair ($\overline{U}_{\text{tip}} = \overline{\left|\boldsymbol{u}_{\text{tip}} + \boldsymbol{u}_{\text{body}}\right|} = \frac{1}{T}\int_0^T \sqrt{(\dot{x}_{\text{tip}} + \dot{x}_{\text{body}})^2 + (\dot{y}_{\text{tip}} + \dot{y}_{\text{body}})^2 + (\dot{z}_{\text{tip}} + \dot{z}_{\text{body}})^2}\,dt = 3.44\, m/s$, where $\boldsymbol{u} = \langle \dot{x}, \dot{y}, \dot{z} \rangle$ is the time derivative of the displacement vector and T is the flapping duration), mean-chord length ($\bar{c} = 0.008m$), kinematic viscosity of air at room temperature ($\upsilon = 1.5\times10^{-5}\, m^2 s^{-1}$). Figure 3.2 shows the comparison of forces during the second stroke from three grid setups (coarse, medium, and fine). The difference of both the mean and peak values between the medium-grid (adopted in this paper) and the fine-grid is about 2% (Table 3.2) which indicates grid convergence following Liu et al.'s work [44].

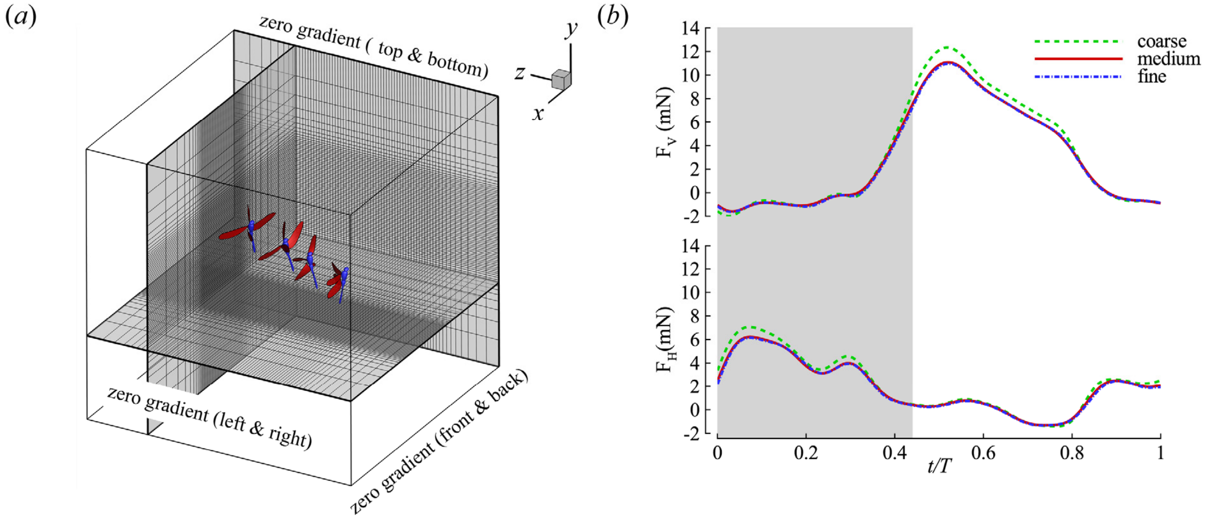

Figure 3.2. Computational setup. (A) Computational mesh employed in the study. For display, the meshes coarsened four times. (B) Grid Independent Study. The sum of the FW and HW forces is shown during the second stroke (F_V: Vertical Force, F_H: Horizontal Force). Grey shading indicates the forewing DS. Medium grids are shown in (A).

Table 3.2. Forces from three different grids set-up.

	grids	mean vertical force (mN)	max vertical force (mN)	mean horizontal force (mN)	max horizontal force (mN)
Coarse	214x214x214	3.40	12.35	2.17	7.06
Medium	240x240x240	3.08	11.08	1.93	6.22
Fine	252x252x252	3.02	10.95	1.88	6.14

3.4. Results

3.4.1. Kinematics

3.4.1.1. Body kinematics

The body kinematics are documented in Figure 3.3. At the onset of flight, the dragonfly rested on a platform posing at an initial body angle of ~87º. There was a preparatory stage (t=-20 ms to 0s). However, obvious body translation did not occur until the successive DS during which the wing generated enough propulsive force. This time instant (t=0s) is the start of the flight. The insect left the platform smoothly while increasingly leaning backward. Both the body velocity and angle increased for the next 2.5 flapping cycles slightly attenuating in the last half wingbeat. The center of mass of the body was elevated by about $5\overline{c}$ during the last two flapping cycles with most of the body motion occurring in the horizontal direction ($12\overline{c}$).

The average body angle during the entire flight duration was approximately 90º. The wings propelled the body backward with an average velocity of -1 m/s. The advance ratio (*J*), defined as the ratio of the average body to wingtip velocity is -0.31±0.12. Because the dragonfly is accelerating, the advance ratio changes on a half stroke basis and is larger in the second and third flapping strokes. In addition to body motion, we observed some tail movement typical of dragonfly flight. The tail motion trailed the body's by about half a wingbeat, although the profile of the time histories was similar. At the beginning of the third US, the insect slowed down and reduced its body and tail angle (Figure 3.3(e,f)).

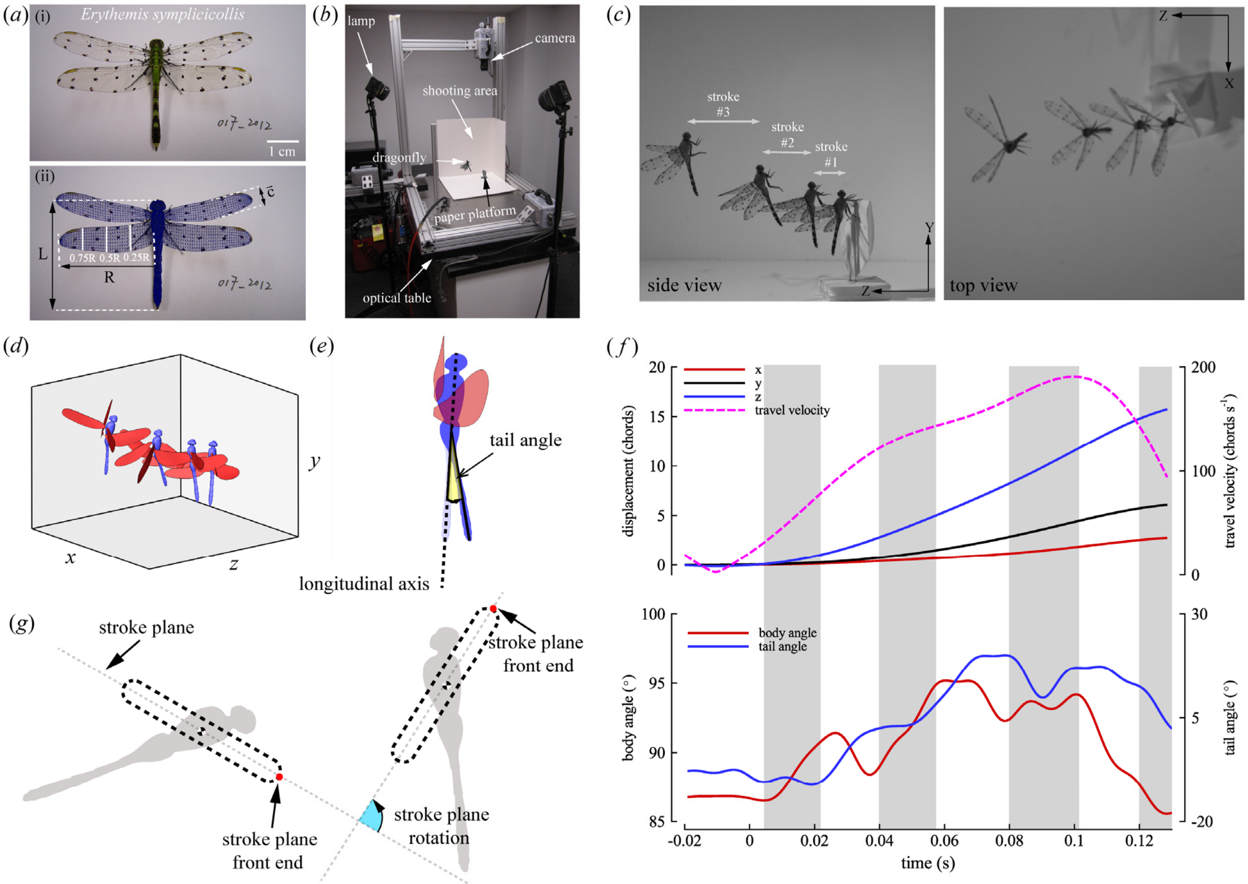

Figure 3.3. Body motion during backward flight. (A) Reconstructed dragonfly (ii) overlapped on a real image (i). L- body length, R- wing length from root to tip, $\bar{c}$ - mean chord length (B) Experimental Setup (C) Snapshots of the dragonfly in backward flight. (D) Montage of 3D model of dragonfly used in CFD simulation. (E) Tail angle definition. The tail angle is the angle between the thorax and the tail. (F) Body kinematics. Grey shading denotes the forewing DS. (G) Stroke plane reorientation (blue shading) due to change in body angle from forward to backward flight.

3.4.1.2. Wing kinematics and deformations

Both wing pairs swept through a stroke plane (β_b) that maintained an orientation of 35±4° measured relative to the straight line that connects the head to the tail in the absence of body deformation (body longitudinal axis, Figure 3.3(e)). This β_b is slightly less than the stroke plane angle measured in forward flight (relative to the longitudinal axis), which is about 50-60° [37, 49]. Nevertheless, in the global frame, the stroke plane in backward flight is almost perpendicular to that in forward flight due to the change in the body angle in backward flight (Figure 3.3(g)). The mean stroke plane angle relative to the horizon (β_h) is 46.8±5.5° for the forewings (FW) and hindwings (HW).

Figure 3.4 shows the measured wing kinematics. The HW led the FW typical of dragonfly flight [49, 50]. The phase difference increased from one stroke to another; ~37°, 51°, 94° for the three strokes, respectively. The phasing of the fore and hindwing may help reduce oscillations in the body posture during flight [31]. The DS-to-US duration ratio changed on a stroke-by-stroke basis from 0.9 (first stroke) to 0.7 (second stroke) to 1 (third stroke) for the FW and from 0.9 (first stroke) to 0.8 (second and third strokes) for the HW.

The wings flapped at high AoAs while deforming considerably. We report the AoAs at four spanwise locations ~0.25, 0.5, 0.75, and 0.9R, where R is the distance from the wing root to tip (Figure 3.4). The AoA decreased from root to tip. In the text, the mid-span (0.5R) AoA is reported. Averaged across all strokes, the DS α_{geom} was 39.0±2.2° and 47.0±3.7°, and that for the US was 52.4±7.8° and 55.8±2.2° for FW and HW, respectively. Taking into account the body motion, we found that α_{geom} was significantly reduced. Hence, the DS α_{eff} was 22.5±2.1° and 26.1±9.3°, and that for the US was 25.3±5.6° and 31.2±6.6° for the FW and HW respectively. At these intermediate AoAs insect wings usually carry a stable LEV [1, 51]. We also tracked the velocity of the leading edge at the spanwise locations where we calculated the AoAs. Overall, the resultant wing velocities squared were higher during the US than the DS by 20% and 15% for the FW and HW at mid-span.

In addition to the rigid wing kinematics, the wing twist is reported in Figure 3.4. The twist angle, which is the relative angle of the deformed wing chord line and the LSRP (see Figure 3.1(b)), increased from mid-span to tip and is greater for the HW and during the US. The twist was as much as 40°, twice higher than previous measurements on dragonflies [40].

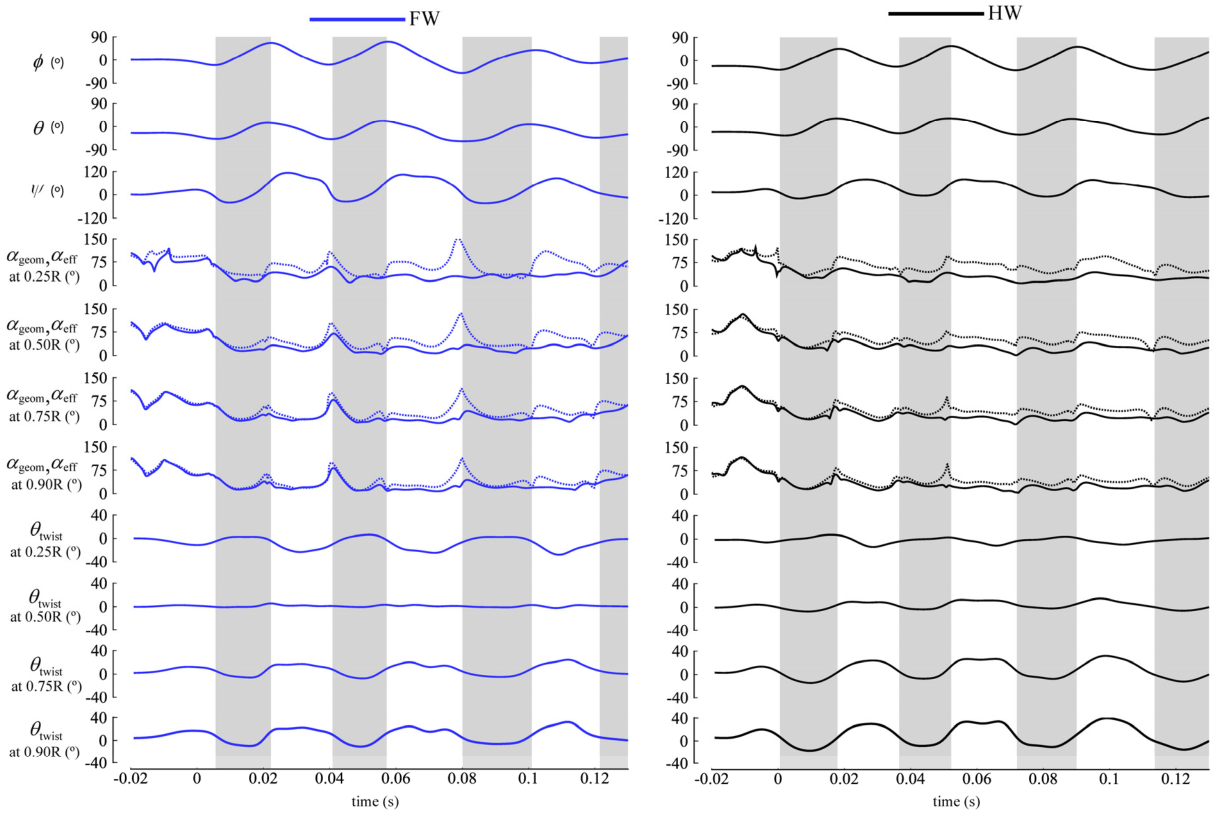

Figure 3.4. Wing kinematics and twist. The average Euler angles are shown. The geometric (dashed lines) and effective AoAs (solid lines) and twist angles at four spanwise location are reported. Grey shading denotes the DS phase.

3.4.2. Force generation: aerodynamic force and power

The flight forces were computed by the integration of the wing surface pressure and shear stress. The aerodynamic power is defined as $p_{aero} = -\iint (\vec{\sigma} \cdot \vec{n})\vec{u}\, ds$ where $\vec{\sigma}$ is the stress tensor, $\vec{u}$ is the velocity of the fluid adjacent to the wing surface, $\vec{n}$ and ds are the unit normal direction and the area of each element, respectively. The forces and muscle-mass specific power consumption ($p^*_{aero} = \frac{p_{aero}}{M_m}$) are displayed in Figure 3.5. The muscle mass (M_m) is 49% of the body mass based on previous measurements [52, 53].

Consistent with the phase difference between the wing pairs, the peak forces produced by HW led the FW. The magnitudes of peak vertical force generated by the FW (all USs) and HW (first DS) are similar (~4mN), while the peak vertical force of the hindwings is about twice FW's in the 2nd and 3rd strokes as the insect ascends (see § 3.4.1.1). The peak horizontal forces for the wing pairs are also comparable, although on average, the hindwings generate greater horizontal forces.

Most of the vertical force is generated during the US, while horizontal force is generated in the DS. Both wing pairs generate larger forces in US compared to DS. Greater forces are produced by HW compared to FW. The peak vertical and horizontal forces during the flight are about 9 and 5.5 times the body weight, respectively. The dragonfly generates an average vertical force 2.5-3 times the body weight to sustain flight and ascend while propelling backward with an average force of 1.5 times the body weight.

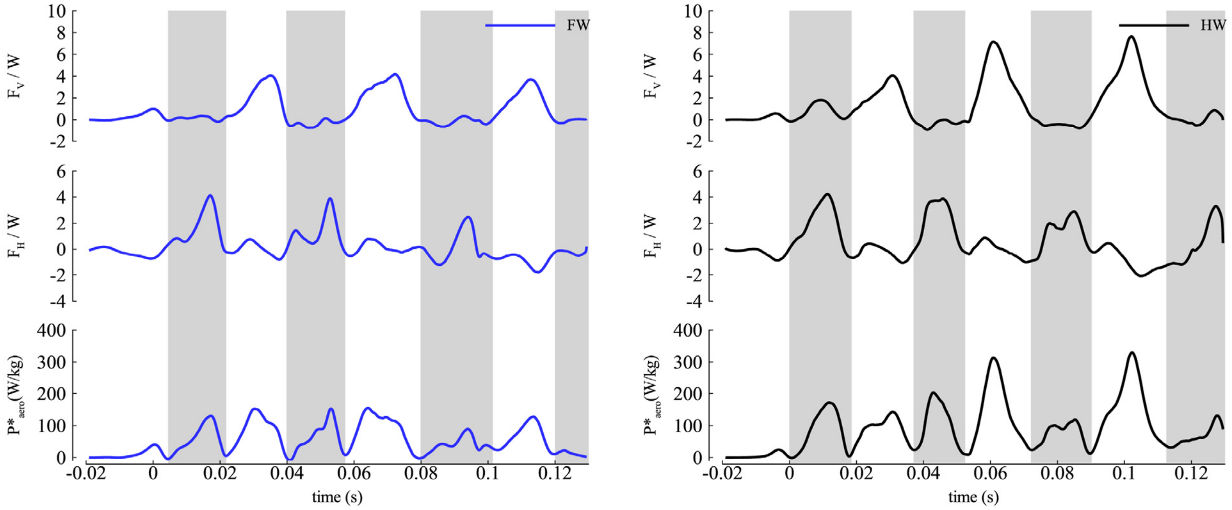

Figure 3.5. Force generation and muscle-specific power consumption. Time history of forces (F_V: vertical force, F_H: horizontal force, W: Weight=1.275mN) and muscle-mass specific power (P^*_{aero}) consumption. Grey shading denotes the DS phase.

The average muscle-mass specific power consumed by the dragonfly was 146W/kg (FW: 54W/kg; HW: 92W/kg). This was in the same range (76-156 W/kg and 160 W/kg) measured by Wakeling and Ellington [52], and Azuma et al. [50], respectively for forward flight.

3.4.3. Force vectoring

Force vectoring is a mechanism commonly used by insects and birds to change flight direction. Using this strategy, body rotation is used to redirect the flight forces, especially if the forces are directionally constrained within the animal's body frame [33, 36]. By rotating the body relative to the ground, the insect changes the global orientation of the aerodynamic force to perform the desired maneuver.

To investigate how the dragonfly's body posture affects the orientation of aerodynamic force vector, we visualized the half stroke-averaged force vectors in Figure 3.6 in the Y-Z plane which coincides with the mid-sagittal plane of the dragonfly. In Figure 3.6(c), the green and red arrows represent the DS-averaged ($\overline{F}_{DS}$) and US-averaged force vectors ($\overline{F}_{US}$) respectively. Although the magnitude of both US and DS forces change from cycle to cycle, $\overline{F}_{DS}$ and $\overline{F}_{US}$ were produced in a somewhat uniform direction with respect to the longitudinal axis of the body. The angle between the force vector and longitudinal axis is obtained from the dot product of the force vector and a unit vector parallel to the longitudinal axis. The angle between $\overline{F}_{US}$ and the longitudinal axis was 12±8° (FW) and 10±5° (HW). $\overline{F}_{DS}$ was oriented at 107±15° (FW) and 96±18° (HW). The body posture tilted the DS force backward and the US force upward for generation of propulsive and lifting force, respectively. However, the change in magnitude of the force, as well as production of large aerodynamic forces in US cannot be explained by force vectoring alone.

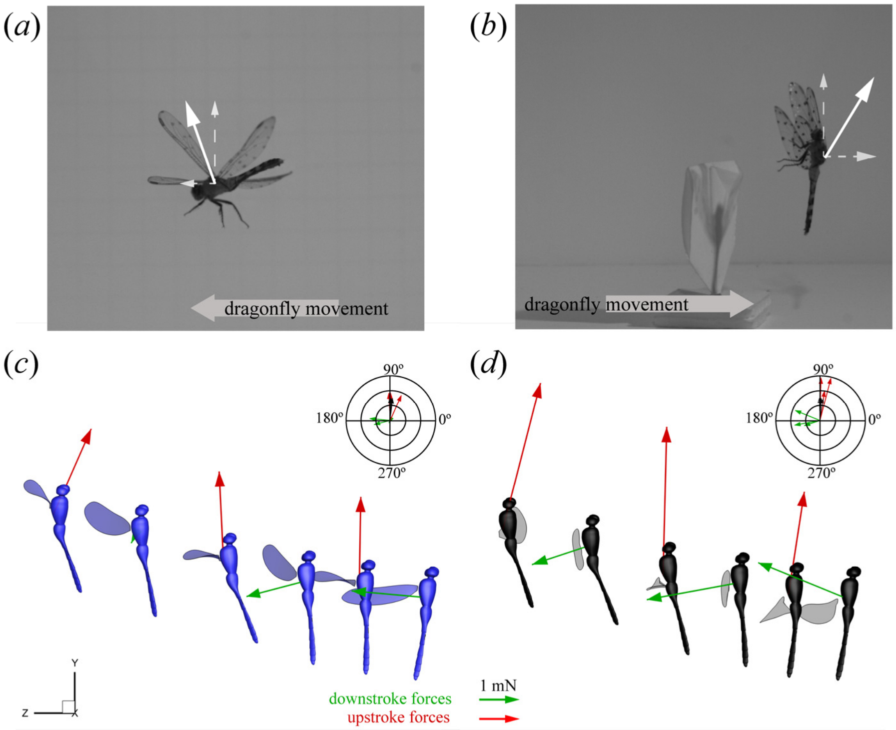

Figure 3.6. Force vectors in the mid-sagittal plane. (a, b) show anecdotally using real footage, how dragonflies may appropriate the force vectoring for forward and backward flight. Solid and dashed arrows show resultant force and its components, respectively. (c, d) Measured flight forces. The dragonflies are colored based on FW (Blue) and HW (Black) timing. Red and green force vectors represent $\overline{F}_{US}$ and $\overline{F}_{DS}$, respectively. In the polar plot, black vectors clustered around 90º indicate the body longitudinal axis.

3.4.4. Vortical structures during backward flight: three-dimensional flow structures and leading edge vortex circulation.

We plotted the iso-surface of the λ_2-criterion at two different values ($|\lambda_2| = 10, 15$) to visualize the flow structures. In Figure 3.7, we present the evolution of the wake structures during the second stroke based on the hindwings' timing. Whereas in Figure 3.8, the flow structures are shown during maximum force production. The flow features on the right wings are reported although the flow phenomena are similar on both sides of the wings.

An LEV forms as the wings translate during the DS. For most of the stroke (Figure 3.7), the LEV grows in size and strength while being stably attached. During the DS, an LEV and TV are observed, and the vorticity in the LEV feeds into a tip vortex (TV). As reversal approaches, the LEV deteriorates and sheds from the trailing edge. Concurrently, another vortex forms on the upper surface of the wing during reversal because of the rapid increase in AoA during wing rotation (Figure 3.7(d)).

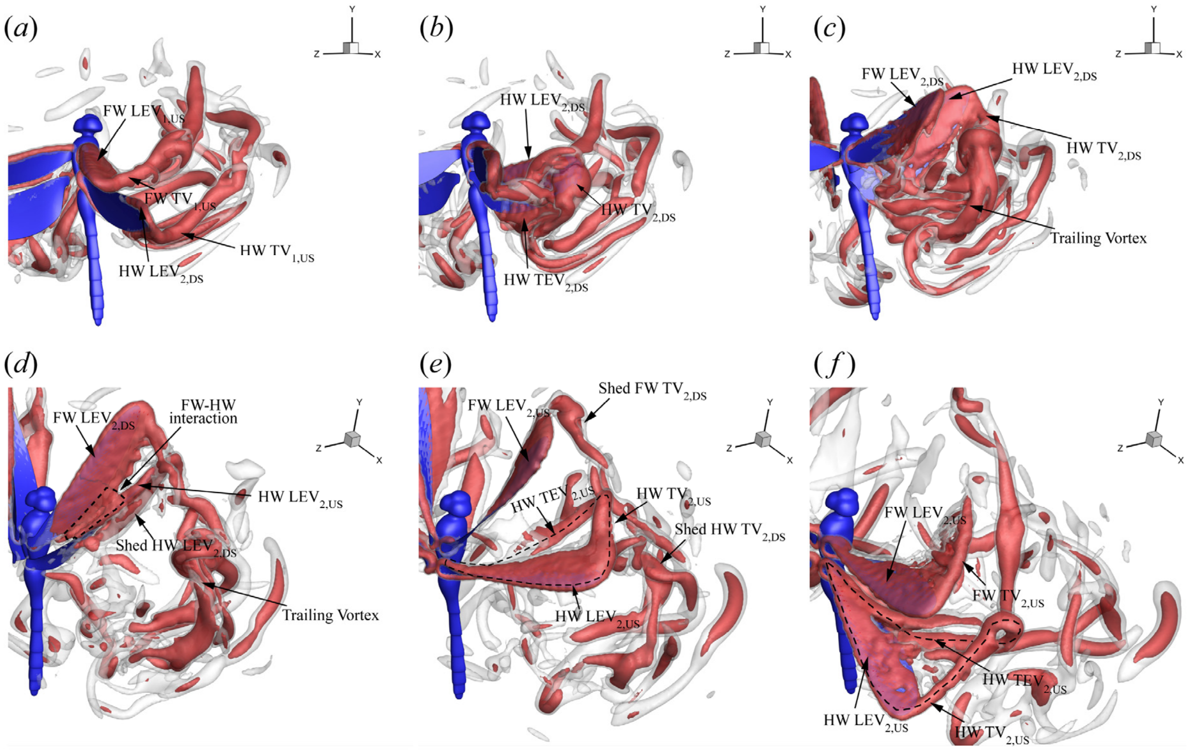

Figure 3.7. Vortex development in backward flight. The flow features visualized by the λ_2-criterion during the 2nd flapping stroke. TEV=Trailing Edge Vortex. TV=Tip Vortex. Subscripts 1, 2 denote vortices created by flapping strokes 1 and 2. Top row (a - c) represents snapshots during HW DS at t/T=0.07, 0.19 and 0.34, respectively. The bottom row (d-f) represents snapshots during HW US at t/T=0.52, 0.70 and 0.87, respectively.

In the US, the LEV formed covers the entirety of the wing surface (Figures 3.7(e, f), and (b, d)). The LEV in the US is larger than that formed in the DS. The TV is also more pronounced and suggests that the strength of the LEV feeding it may be greater than the DS's. Also, both the FW and HW have LEVs on them. During the mid-US and at maximum force production, the HW flow consists of an LEV, TV and a trailing edge vortex (TEV) connected to form a vortex loop (Figures 3.7(e) and (d)). The loop creates a downward jet which boosts vertical force production.

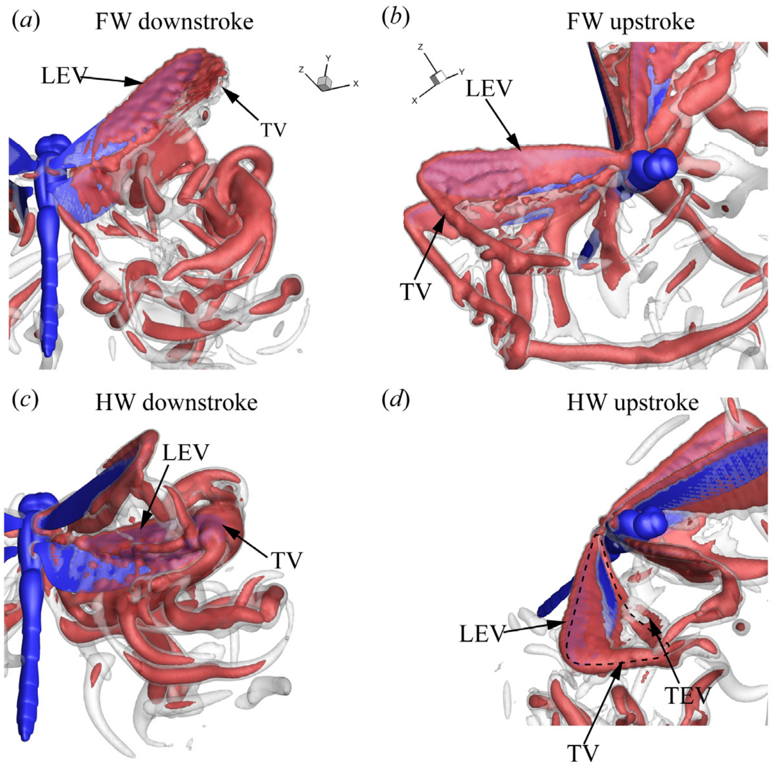

Figure 3.8. Flow features at maximum force production during 2nd stroke for each wing pair. (A) FW DS t/T=0.35, (B) FW US t/T=0.82 (C) HW DS t/T=0.25 (D) HW US t/T=0.70.

We also quantified the strength (circulation) of the LEV throughout the second and third stroke. At every time step, a 2D plane normal to the axis of LEV was constructed (Figure 3.9(a)). A vorticity threshold was set to capture the vortex. The circulation is the flux of the vorticity and is non-dimensionalized by the product of a reference velocity, U_{ref} and length, l (Eqn. (3)).

$$\Gamma^{*}_{\mathrm{LEV}} = \frac{1}{lU_{\mathrm{ref}}}\iint_{S} \omega \cdot dS, \tag{3}$$

where ω is the vorticity. The area of integration (dS) is bound by the vorticity threshold. $\overline{\mathrm{U}}_{\mathrm{tip}}$ and $\overline{c}$ were chosen for the non-dimensionalization. The instantaneous LEV circulation at mid-span (0.5R) is displayed in Figure 3.9(c). There is a discontinuity at reversal due to the deterioration of the LEV and the emergence of another LEV on the opposite surface of the wing. The circulation slightly lags behind the kinematics due to the delay of growth of circulation in the vortex formation process during wing excursion.

The peak circulation (Figure 3.9(c)) occurs in the same region where maximum force is generated for each wing pair (Figure 3.5). The HWs have higher LEV circulation than the fws. Also, the LEV circulation in the US is greater than the DS's. All the DS-to-US LEV circulation ratios are less than unity (Table 3.3). The spanwise distribution of circulation on the wing surface at the instant of maximum force production in the 2nd and 3rd stroke are reported in Figure 3.9(d, e). The circulation increases along the span and tapers toward the tip. The US circulation, shown in dashed lines, is higher than the DS circulation, consistent with greater flight force generated in the US.

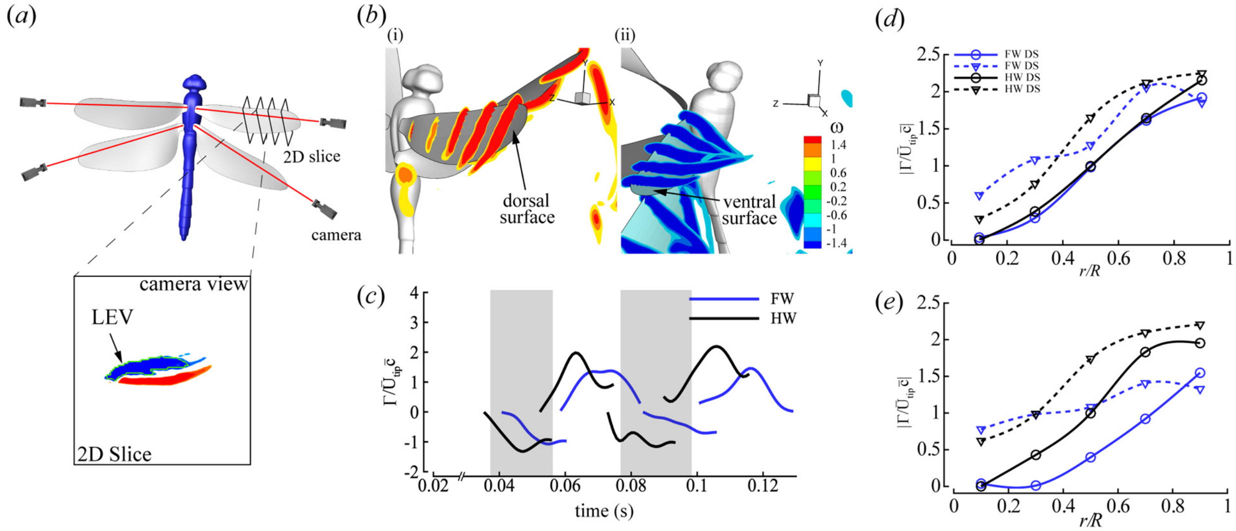

Figure 3.9. LEV circulation. (a) Schematic of a dragonfly with 2D slices on the wings with the virtual camera looking through a line passing through the LEV core. (b) Spanwise vorticity on FW during the (i) DS (dorsal surface shaded in grey) and (ii) US in the 3rd stroke (ventral surface shaded in blue). (c) LEV circulation during the 2nd and 3rd stroke. Grey shading denotes FW DS. (d,e) Spanwise distribution of LEV circulation at maximum force production during the 2nd and 3rd Stroke, respectively.

Table 3.3. Quantification of LEV circulation. $\bar{\Gamma}^*$ represents the time half stroke averaged values. $\bar{\Gamma}^*_{max}$ represents the maximum circulation per half stroke. All values are measured at 0.50R.

flapping stroke			$\bar{\Gamma}^*$	$\bar{\Gamma}^*_{max}$	$\left\lvert\bar{\Gamma}^*_{DS}/\bar{\Gamma}^*_{US}\right\rvert$	$\left\lvert\Gamma^*_{max_{DS}}/\Gamma^*_{max_{US}}\right\rvert$
2nd	FW	DS	-0.67	-1.08	0.64	0.81
		US	1.05	1.34		
	HW	DS	-0.96	-1.32	0.83	0.67
		US	1.16	1.98		
3rd	FW	DS	-0.35	-0.71	0.40	0.49
		US	0.88	1.45		
	HW	DS	-0.89	-1.16	0.59	0.53
		US	1.50	2.19		

3.4.5. Wing-wing interaction

We observed some interaction between the wings during backward flight (Figure 3.7(d)). Previous studies have indicated that the FW experience in-wash due to the HW and the HW are affected by the downwash from the FW with benefits being dependent on the phase difference between wing pairs [31, 54-57]. Experiments on hovering kinematics showed that both wing pairs generate maximum lift when the HW lead by a quarter of the cycle and the distance between the wings is closest [54]. By leading the FW, the HW avoids the FW's downwash. Simulations of dragonfly-like wings at different advance ratios and phase differences indicated that total forces of the fore and hindwings are influenced by WWI when the HW lead the FW [56]. Lehmann [58], reported that a hindwing leading by 90° could achieve the same mean lift as an isolated wing due to wake capture. The FW could also benefit from interaction due to the distortion of the FWs wakes by the HWs via the "wall effect" [20, 58, 59].

We compared three simulation cases; (i) with all four wings (ALL; shown in Figures 3.8 and), (ii) the FWs only (FO) and (iii) HWs only (HO), to elucidate wing-wing interaction during flight (Table 3.4).

Table 3.4. Effect of wing-wing interaction during flight (all strokes combined).

force (10^{-3} N)	forewings		hindwings	
	FO	ALL	HO	ALL
vertical force during entire duration	1.26	1.37 (8.7% ↑)	2.17	2.27 (4.6% ↑)
horizontal force during entire duration	0.63	0.52 (17.5% ↓)	0.68	0.77 (13.2% ↑)
vertical force during US	2.49	2.75 (10.4% ↑)	3.98	4.13 (3.77% ↑)
Horizontal Force during DS	1.28	1.21 (5.5% ↓)	2.16	2.18 (0.9% ↑)

On average, both wing pairs benefitted from WWI for vertical force production. The fore and hind wing vertical forces were boosted by 8.7% and 4.6% respectively. For thrust production, the interaction was detrimental for the FW leading to a 17.5% decrease in force while benefitting the HW by as much as 13.2%. During the US, both pairs of wings profited from WWI; 10.4% and 3.7% for the FW and HW respectively. During the DS, horizontal forces for the FW are attenuated by 5.5%.

The mechanism of WWI, which led to increased force production during the 2nd stroke, is shown in Figures 3.10 and . In Figure 3.10, the vortical structures are projected on a 2D slice cut at mid-span, similar to Figure 3.9(a). At the onset of interaction, vorticity emanating from the FW's trailing edge feeds into an already stronger LEV on the HW, boosting its circulation (Figure 3.10(a(i)). As the wings separate from each other during the excursion, the initial increase in HW LEV circulation is maintained in addition to the new vorticity influx formed as the LEV grows during translation (Figure 3.10(b-d)). Comparing this finding to the HW only case, there is no vorticity transfer from the FW and the LEV is smaller.

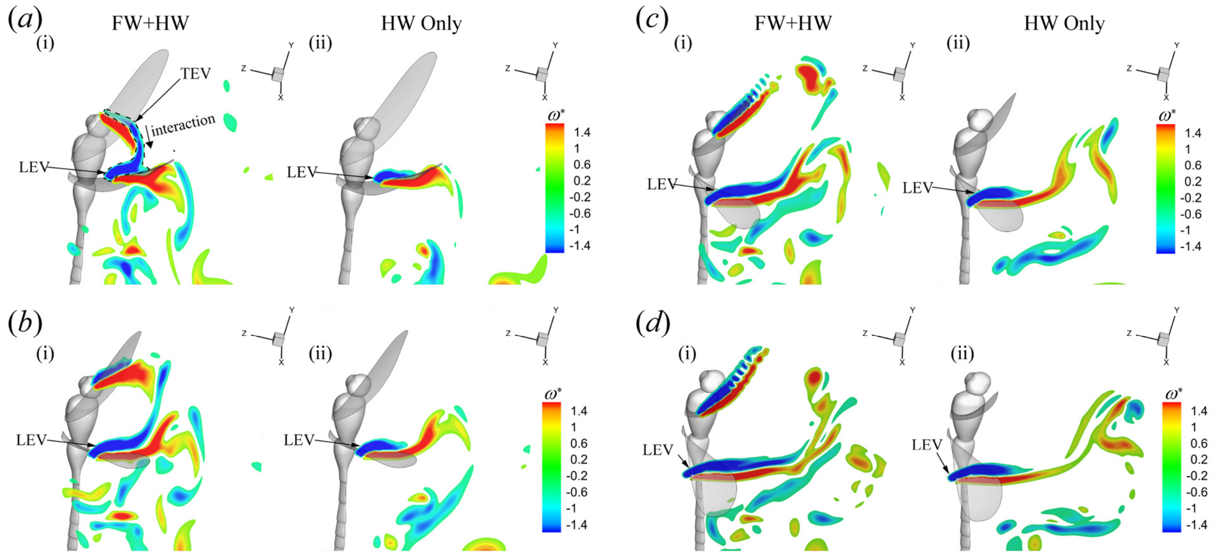

Figure 3.10. Visualization of vortical structures at mid-span during wing-wing interaction. Slices similar to Figure 3.9(a, b) are shown here to elucidate WWI. A-D represent snapshots, where wing-wing interaction occurred as labeled in Figure 3.12. The region of interaction is shown in dashed lines with an arrow indicating the direction of vorticity transfer (a(i)). Contours represent non-dimensional vorticity.

In Figure 3.11, the velocity field is superimposed on the vorticity contours in a zoomed-in snapshot of Figure 3.10(a). The FW TEV and HW LEV are linked together due to interaction (Figure 3.11(a)). The presence of the FW induces an additional inflow into the LEV, which is favorable in this case. This influx is absent in the HW only case, leading to the formation of a weaker LEV and consequently, a weaker jet below the wing (Figure 3.11(b)).

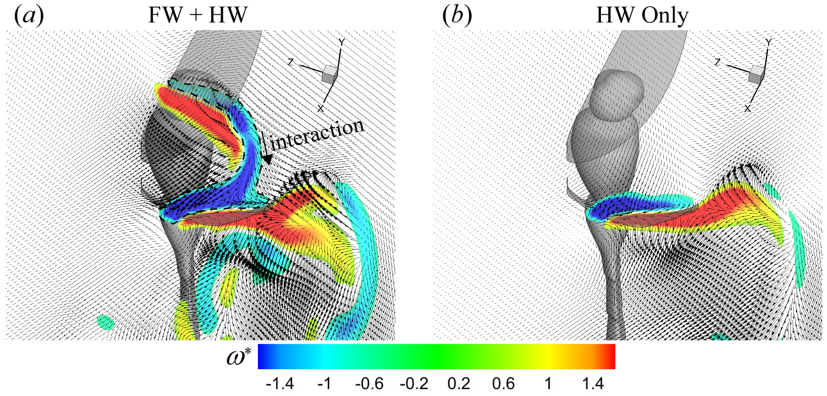

Figure 3.11. Mechanism of Wing-wing interaction. This figure shows the mechanism of vorticity transfer from the fore to hindwings during backward flight.

3.5. Discussion and conclusion

Alterations in kinematics and aerodynamic features which are different from hovering and forward flight characterize backward flight of dragonflies. Our study shows that dragonflies can use backward flight as an alternative to forward flight voluntarily. Backward flight is not merely a transient behavior but is sustainable for a relatively extended period, which may have implications for biology (prey capture or predator evasion) as well as MAV design. To fly backward, dragonflies tilt their stroke plane toward their bodies, but the primary reorientation of the stroke plane and force vector is because of the steep body posture that is maintained. In addition to redirecting the force, we found that the force magnitude is significantly increased in the US (when compared to forward flight). In contrast to forward flight, during which dragonflies generates little force in US [49], the magnitude of the half-stroke-averaged force generated in US during backward flight is 2-4 times the body weight. In addition, we showed that a strong and stable LEV in the US was responsible for greater force production (Figure 3.9 and Table 3.3). The flow visualizations corroborated these findings in Figures 3.7 and . The mechanism of wing-wing interaction was also illustrated (Figures 3.10 and). Vorticity from the FW trailing edge enhanced the HW's LEV.

Here, we compare our findings; kinematics, aerodynamics and flow features, with hovering and forward flights which have been documented in the literature. Tables 3.5 and 3.6 show a summary of previous research on different flight modes. The high body angles (χ) during dragonfly backward flight parallels similar observations of hummingbird [13] and insect backward flight [11] and could be a mechanism of convergent evolution [13]. However, χ was significantly larger than those of hummingbirds (50-75º) which utilize a horizontal stroke plane and waterlily beetles (50-70º), which use an inclined stroke plane [13, 38]. Our χ corroborated previous observation in dragonfly backward flight (100º) [11]. A state-of-the-art MAV, the Delfly-II, has also been shown to induce backward flight by increasing its body angle to about 100º from its stable flight configuration [16].

Although a steep body posture during backward flight has been thought to generate higher drag due to a higher projected area, Sapir and Dudley [13], showed that drag forces only differed by 3.6% between backward and forward flight in hummingbirds. It is not certain whether by maintaining a high body angle, dragonflies will drastically increase body drag because they possess slender bodies. While body drag is present, we measured it to be eleven times smaller than the horizontal forces being generated by the wings during flight. The steep body angle is in contrast to forward and hovering flight during which the dragonfly keeps its body slightly inclined from the horizontal (~2-40º) [31, 37, 49]. We define the parasite drag (pressure drag + viscous drag on the body) coefficient as $C_D = \frac{\bar{F}_H}{0.5\rho \bar{U}_b^2 S_{frontal}}$ where $\bar{F}_H$ is the mean horizontal force and $\bar{U}_b$ is the average translation velocity of the body and $S_{frontal}$ is the frontal area presented to the flow. Comparing the C_D measured from our simulation (Reynolds number based on body length, Re_b ~ 3860) with results for forward flight of dragonflies of similar Re_b ~2460-7790 in literature, the results were comparable indicating that an upright body posture did not substantially influence body drag production. Our measured C_D was 0.57 and within the range (0.31-0.84) found in the literature [53, 60].

Table 3.5. Kinematic parameters of several organisms in flight.

	flight mode	Re	J	phase shift (°)	stroke plane (°)		body angle (°)	angle of attack (°)			
					β_{FW}	β_{HW}	χ	$\alpha_{\mathrm{FW}}^{\mathrm{down}}$	$\alpha_{\mathrm{FW}}^{\mathrm{up}}$	$\alpha_{\mathrm{HW}}^{\mathrm{down}}$	$\alpha_{\mathrm{HW}}^{\mathrm{up}}$
dragonfly	hovering* [31]	4232	0	22	53	44	14	83	10	87	15
	hovering [61, 62]	1350	0	180	52	52	--	--	--	--	--
	forward [63]	3100	0.30	60	52	52	--	50	15	50	15
	forward* [51, 64]	1100	0.75	--	--	25	--	--	--	25	15
	forward ascending[50]	3200	0.13	77	37	40	10	24.1	11.8	27	22.9
	forward [37]	--	0.21–0.47	47–110	9–28	7–29	23–36	--	--	--	--
	backward (current)	1840	-0.30	37–94	47	47	85–95	21	32	37	55
hummingbird	backward [13]	--	-0.30	--	0–6		50–75	--	--	--	--
waterlily beetle	backward [38]	--	--	--	0–30		50–70	--	--	--	--
delfly II	backward [16]	--	--	--	--		70–100	--	--	--	--

α is the instantaneous geometric angle of attack at midstroke. *-tethered.

Table 3.6. Force asymmetry: DS versus US. This table reports the contribution of each half stroke to the total aerodynamic force during a flapping cycle in different flight modes of insects.

insect	flight Mode	DS force (%)	US force (%)	Reference
cicada	forward	80	20	Wan et al. [39]
damselfly	forward	75	25	Sato et al. [6]
		84	16	Bode-Oke et al. [20]
	take-off	50	50	
dragonfly	backward	33	67	Current Study
	forward	80	20	Azuma and Watanabe [49]
bumble bee	forward	50-100		Dudley. [65]
fruit fly	hovering	37	63	Fry et al. [3]
	saccade	40	60	Fry et al. [2]
	forward	61	39	Meng and Sun [66]
hawkmoth	forward	80	20	Willmott et al. [67]
mosquito	hovering	43	57	Bomphrey et al. [68]
honey bee	hovering	43	57	Altshuler et al. [18]

During backward flight, the dragonfly wings swept through a stoke plane (β_{b}) inclined at 35±5°; an angle shallower than β_{b} of dragonflies of similar mass and morphology in forward flight by 15° [37, 50]. The stroke plane with respect to the horizon (β_{h}) during backward flight was reported as 46.8±5.5° for both wing pairs which also was about 20-40° greater. Compared to hovering [62], β_{h} in backward flight was about 15° less.

For force production, a strong LEV was present on both wing pairs. Contrary to previous works on dragonfly forward flight [1, 30, 63], the presence of the LEV was not limited to the FW but was evident on the HW as well [51]. The LEV was also present in both half strokes with the US LEV being stronger. We verified this finding by calculating the LEV circulation of the wing and found DS-to-US LEV circulation ratios as low as 0.4 and 0.59 for the fore and hind wings, respectively. In previous works, the LEV circulation was significantly larger in DS compared to US where the LEV may be completely absent [20, 67, 69-71]. Willmott et al. [67] noted that the US tip vortex was relatively weak in comparison to the DS's. Hence, the LEV circulation should be much smaller than that measured in the DS. From their smoke visualization and analysis, there was no hint of an LEV to enhance lift in the US. Thomas et al. [1] also arrived at a similar conclusion with smoke visualizations on dragonflies in tethered and free forward light. Wang and Sun [63], using CFD, verified the absence of the LEV in the US in hovering as well as forward flight of dragonflies. The reason for LEV absence during the US was attributed to very low AoAs as the wing slices through the air, hence, no flow separation. Higher AoAs were recorded in our study (Figure 3.4), and we observed the formation of a stable LEV on the wing surface (Figures 3.7 and).

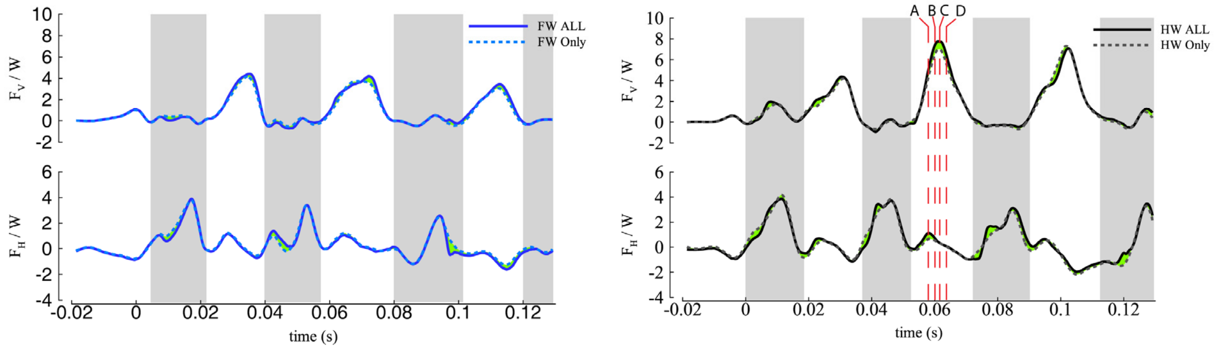

Figure 3.12. Wing-wing interaction. The solid lines and dashed lines indicate the ALL case and where the wings are isolated, respectively. The difference is shaded in green. A, B, C, and D represent snapshots, where the flow field is evaluated in Figure 3.10.

The higher LEV circulation and forces in the US shows that during backward flight, dragonflies utilize an aerodynamically active US (Figures 3.5, and). This is achieved by inducing large AoAs plus an enhancement in the velocity of the wing, resulting from the body's backward motion, in the US. Due to their relatively low flapping frequency, the magnitude of body velocity of a dragonfly is comparable to its wing velocity. Thus, the motion of the body can yield significant effects on the net wing velocity. In contrast to backward flight, during forward and hovering flight, most of the flight force is produced in the DS [20, 31, 72]. In these flight modes, the DS is conventionally regarded as vertical force producing and the US, thrust (horizontal force) producing [11, 31, 50]. Also, the forces generated in the US are significantly less (inactive) and account for about 10-20% of the body weight [8, 20, 67]. Current literature, summarized in Table 3.6, indicates that, during forward flight, the DS generates 80% of the total force created by Cicadas [39], 80% for dragonflies [49], 75-84% for damselflies [6], and 80% of body weight in Hawkmoths [67]. As flight speed increases, the relative contribution of the US in force production diminishes [8, 20]. During backward flight, the US must become active because of its weight supporting role. Previously, there has been some evidence of the US producing larger forces than the DS such as hovering and saccadic flight of Drosophila (60-63%) [2, 3], hovering flight of mosquitos (57%) [68] and honey bees (57%) [18]. However, in contrast to dragonflies, these insects use a horizontal stroke plane in the flight scenarios listed.

3.6. References

[1] Thomas, A.L., Taylor, G.K., Srygley, R.B., Nudds, R.L. & Bomphrey, R.J. 2004 Dragonfly flight: free-flight and tethered flow visualizations reveal a diverse array of unsteady lift-generating mechanisms, controlled primarily via angle of attack. *Journal of Experimental Biology* **207**, 4299-4323.

[2] Fry, S.N., Sayaman, R. & Dickinson, M.H. 2003 The aerodynamics of free-flight maneuvers in Drosophila. *Science* **300**, 495-498.

[3] Fry, S.N., Sayaman, R. & Dickinson, M.H. 2005 The aerodynamics of hovering flight in Drosophila. *Journal of Experimental Biology* **208**, 2303-2318.

[4] Muijres, F.T., Elzinga, M.J., Melis, J.M. & Dickinson, M.H. 2014 Flies Evade Looming Targets by Executing Rapid Visually Directed Banked Turns. *Science* **344**, 172-177. (doi:10.1126/science.1248955).

[5] Dickinson, M.H. & Muijres, F.T. 2016 The aerodynamics and control of free flight manoeuvres in Drosophila. *Phil. Trans. R. Soc. B* **371**, 20150388.

[6] Sato, M. & Azuma, A. 1997 The flight performance of a damselfly Ceriagrion melanurum Selys. *Journal of Experimental Biology* **200**, 1765-1779.

[7] Phan, H.V., Nguyen, Q.V., Truong, Q.T., Van Truong, T., Park, H.C., Goo, N.S., Byun, D. & Kim, M.J. 2012 Stable vertical takeoff of an insect-mimicking flapping-wing system without guide implementing inherent pitching stability. *Journal of Bionic Engineering* **9**, 391-401.

[8] Ellington, C.P. 1999 The novel aerodynamics of insect flight: applications to micro-air vehicles. *Journal of Experimental Biology* **202**, 3439-3448.

[9] De Croon, G.C.H.E., Perçin, M. & Remes, B. 2016 *The DelFly Design, Aerodynamics, and Artificial Intelligence of a Flapping Wing Robot*. 1st ed. 2016 ed, Springer Netherlands.

[10] Dickinson, M.H., Lehmann, F.-O. & Sane, S.P. 1999 Wing rotation and the aerodynamic basis of insect flight. *Science* **284**, 1954-1960.

[11] Rüppell, G. 1989 Kinematic analysis of symmetrical flight manoeuvres of Odonata. *Journal of Experimental Biology* **144**, 13-42.

[12] Rüppell, G. & Hilfert, D. 1993 The flight of the relict dragonfly Epiophlebia superstes (Selys) in comparison with that of the modern Odonata (Anisozygoptera: Epiophlebiidae). *Odonatologica* **22**, 295-309.

[13] Sapir, N. & Dudley, R. 2012 Backward flight in hummingbirds employs unique kinematic adjustments and entails low metabolic cost. *The Journal of experimental biology* **215**, 3603-3611.

[14] Yokoi, T. & Fujisaki, K. 2009 Hesitation behaviour of hoverflies Sphaerophoria spp. to avoid ambush by crab spiders. *Naturwissenschaften* **96**, 195-200.

[15] Zeil, J. & Wittmann, D. 1989 Visually controlled station-keeping by hovering guard bees ofTrigona (Tetragonisca) angustula (Apidae, Meliponinae). *Journal of Comparative Physiology A* **165**, 711-718.

[16] Caetano, J.V., de Visser, C.C., Remes, B.D., De Wagter, C., Van Kampen, E.-J. & Mulder, M. 2013 Controlled flight maneuvers of a Flapping Wing Micro Air Vehicle: a step towards the DelFly II Identification. In *AIAA Atmospheric Flight Mechanics (AFM) Conference* (p. 4843.

[17] Lehmann, F.O. & Dickinson, M.H. 1998 The control of wing kinematics and flight forces in fruit flies (Drosophila spp.). *The Journal of Experimental Biology* **201**, 385-401.

[18] Altshuler, D.L., Dickson, W.B., Vance, J.T., Roberts, S.P. & Dickinson, M.H. 2005 Short-amplitude high-frequency wing strokes determine the aerodynamics of honeybee flight. *Proceedings of the National Academy of Sciences of the United States of America* **102**, 18213-18218.

[19] Chen, M.W., Zhang, Y.L. & Sun, M. 2013 Wing and body motion and aerodynamic and leg forces during take-off in droneflies. *Journal of The Royal Society Interface* **10**, 20130808.

[20] Bode-Oke, A., Zeyghami, S. & Dong, H. 2017 Aerodynamics and flow features of a damselfly in takeoff flight. *Bioinspiration & biomimetics* **12**, 056006.

[21] Lehmann, F.O. & Dickinson, M.H. 1997 The changes in power requirements and muscle efficiency during elevated force production in the fruit fly Drosophila melanogaster. *The Journal of Experimental Biology* **200**, 1133-1143.

[22] Lentink, D. & Dickinson, M.H. 2009 Rotational accelerations stabilize leading edge vortices on revolving fly wings. *Journal of Experimental Biology* **212**, 2705-2719.

[23] Birch, J.M., Dickson, W.B. & Dickinson, M.H. 2004 Force production and flow structure of the leading edge vortex on flapping wings at high and low Reynolds numbers. *Journal of Experimental Biology* **207**, 1063-1072.
[24] Nabawy, M.R.A. & Crowther, W.J. 2017 The role of the leading edge vortex in lift augmentation of steadily revolving wings: a change in perspective. *Journal of The Royal Society Interface* **14**.
[25] Shyy, W. & Liu, H. 2007 Flapping Wings and Aerodynamic Lift: The Role of Leading-Edge Vortices. *AIAA Journal* **45**, 2817-2819. (doi:10.2514/1.33205).
[26] Muijres, F., Johansson, L., Barfield, R., Wolf, M., Spedding, G. & Hedenström, A. 2008 Leading-edge vortex improves lift in slow-flying bats. *Science* **319**, 1250-1253.
[27] Ristroph, L., Bergou, A.J., Guckenheimer, J., Wang, Z.J. & Cohen, I. 2011 Paddling Mode of Forward Flight in Insects. *Physical Review Letters* **106**, 178103.
[28] Sane, S.P. 2003 The aerodynamics of insect flight. *The journal of experimental Biology* **206**, 4191-4208.
[29] Chin, D.D. & Lentink, D. 2016 Flapping wing aerodynamics: from insects to vertebrates. *Journal of Experimental Biology* **219**, 920-932.
[30] Bomphrey, R.J., Nakata, T., Henningsson, P. & Lin, H.-T. 2016 Flight of the dragonflies and damselflies. *Philosophical Transactions of the Royal Society B: Biological Sciences* **371**. (doi:10.1098/rstb.2015.0389).
[31] Wang, Z.J. & Russell, D. 2007 Effect of forewing and hindwing interactions on aerodynamic forces and power in hovering dragonfly flight. *Physical review letters* **99**, 148101.
[32] Ellington, C. 1984 The aerodynamics of hovering insect flight. III. Kinematics. *Philosophical Transactions of the Royal Society of London B: Biological Sciences* **305**, 41-78.
[33] Zeyghami, S., Babu, N. & Dong, H. 2016 Cicada (Tibicen linnei) steers by force vectoring. *Theoretical and Applied Mechanics Letters*. (doi:http://dx.doi.org/10.1016/j.taml.2015.12.006).
[34] ENNOS, A.R. 1989 The Kinematics an Daerodynamics of the Free Flight of some Diptera. *Journal of Experimental Biology* **142**, 49-85.
[35] Iriarte-Díaz, J. & Swartz, S.M. 2008 Kinematics of slow turn maneuvering in the fruit bat Cynopterus brachyotis. *Journal of Experimental Biology* **211**, 3478-3489. (doi:10.1242/jeb.017590).
[36] Ros, I.G., Bassman, L.C., Badger, M.A., Pierson, A.N. & Biewener, A.A. 2011 Pigeons steer like helicopters and generate down- and upstroke lift during low speed turns. *Proceedings of the National Academy of Sciences* **108**, 19990-19995. (doi:10.1073/pnas.1107519108).
[37] Wakeling, J. & Ellington, C. 1997 Dragonfly flight. II. Velocities, accelerations and kinematics of flapping flight. *Journal of experimental biology* **200**, 557-582.
[38] Mukundarajan, H., Bardon, T.C., Kim, D.H. & Prakash, M. 2016 Surface tension dominates insect flight on fluid interfaces. *Journal of Experimental Biology* **219**, 752-766. (doi:10.1242/jeb.127829).
[39] Wan, H., Dong, H. & Gai, K. 2015 Computational investigation of cicada aerodynamics in forward flight. *Journal of The Royal Society Interface* **12**, 20141116.
[40] Koehler, C., Liang, Z., Gaston, Z., Wan, H. & Dong, H. 2012 3D reconstruction and analysis of wing deformation in free-flying dragonflies. *The Journal of experimental biology* **215**, 3018-3027.
[41] Kang, C.-k. & Shyy, W. 2013 Scaling law and enhancement of lift generation of an insect-size hovering flexible wing. *Journal of The Royal Society Interface* **10**, 20130361.
[42] Schlichting, H.T. & Truckenbrodt, E.A. 1979 *Aerodynamics of the Airplane*, McGraw-Hill Companies.
[43] Taha, H.E., Hajj, M.R. & Beran, P.S. 2014 State-space representation of the unsteady aerodynamics of flapping flight. *Aerospace Science and Technology* **34**, 1-11.
[44] Liu, G., Dong, H. & Li, C. 2016 Vortex dynamics and new lift enhancement mechanism of wing–body interaction in insect forward flight. *Journal of Fluid Mechanics* **795**, 634-651.
[45] Mittal, R., Dong, H., Bozkurttas, M., Najjar, F., Vargas, A. & von Loebbecke, A. 2008 A versatile sharp interface immersed boundary method for incompressible flows with complex boundaries. *Journal of computational physics* **227**, 4825-4852.
[46] Chengyu, L. & Haibo, D. 2017 Wing kinematics measurement and aerodynamics of a dragonfly in turning flight. *Bioinspiration & Biomimetics* **12**, 026001.
[47] Jeong, J. & Hussain, F. 1995 On the identification of a vortex. *Journal of fluid mechanics* **285**, 69-94.
[48] Lu, Y. & Shen, G.X. 2008 Three-dimensional flow structures and evolution of the leading-edge vortices on a flapping wing. *Journal of Experimental Biology* **211**, 1221-1230.
[49] Azuma, A. & Watanabe, T. 1988 Flight performance of a dragonfly. *Journal of Experimental Biology* **137**, 221-252.
[50] Azuma, A., Azuma, S., Watanabe, I. & Furuta, T. 1985 Flight mechanics of a dragonfly. *Journal of experimental biology* **116**, 79-107.

[51] Chen, Y.H. & Skote, M. 2015 Study of lift enhancing mechanisms via comparison of two distinct flapping patterns in the dragonfly Sympetrum flaveolum. *Physics of Fluids* **27**, 033604. (doi:10.1063/1.4916204).

[52] Wakeling, J. & Ellington, C. 1997 Dragonfly flight. III. Lift and power requirements. *Journal of Experimental Biology* **200**, 583-600.

[53] MAY, M.L. 1991 Dragonfly flight: power requirements at high speed and acceleration. *Journal of Experimental Biology* **158**, 325-342.

[54] Lehmann, F.-O. 2009 Wing–wake interaction reduces power consumption in insect tandem wings. *Experiments in fluids* **46**, 765-775.

[55] Usherwood, J.R. & Lehmann, F.-O. 2008 Phasing of dragonfly wings can improve aerodynamic efficiency by removing swirl. *Journal of The Royal Society Interface* **5**, 1303-1307.

[56] Sun, M. & Huang, H. 2007 Dragonfly forewing-hindwing interaction at various flight speeds and wing phasing. *AIAA journal* **45**, 508-511.

[57] Alexander, D.E. 1984 Unusual phase relationships between the forewings and hindwings in flying dragonflies. *Journal of Experimental Biology* **109**, 379-383.

[58] Lehmann, F.-O. 2008 When wings touch wakes: understanding locomotor force control by wake–wing interference in insect wings. *Journal of Experimental Biology* **211**, 224-233.

[59] Rayner, J.M. 1991 On the aerodynamics of animal flight in ground effect. *Philosophical Transactions of the Royal Society of London B: Biological Sciences* **334**, 119-128.

[60] Wakeling, J. & Ellington, C. 1997 Dragonfly flight. I. Gliding flight and steady-state aerodynamic forces. *Journal of Experimental Biology* **200**, 543-556.

[61] Sun, M. & Lan, S.L. 2004 A computational study of the aerodynamic forces and power requirements of dragonfly (Aeschna juncea) hovering. *Journal of Experimental Biology* **207**, 1887-1901.

[62] Norberg, R.Å. 1975 Hovering flight of the dragonfly Aeschna juncea L., kinematics and aerodynamics. In *Swimming and flying in nature* (pp. 763-781, Springer.

[63] Wang, J.K. & Sun, M. 2005 A computational study of the aerodynamics and forewing-hindwing interaction of a model dragonfly in forward flight. *Journal of Experimental Biology* **208**, 3785-3804. (doi:10.1242/jeb.01852).

[64] Chen, Y.H., Skote, M., Zhao, Y. & Huang, W.M. 2013 Dragonfly (Sympetrum flaveolum) flight: Kinematic measurement and modelling. *Journal of Fluids and Structures* **40**, 115-126. (doi:https://doi.org/10.1016/j.jfluidstructs.2013.04.003).

[65] Dudley, R. & Ellington, C.P. 1990 Mechanics of Forward Flight in Bumblebees: II. Quasi-Steady Lift and Power Requirements. *Journal of Experimental Biology* **148**, 53-88.

[66] Meng, X. & Sun, M. 2016 Wing Kinematics, Aerodynamic Forces and Vortex-wake Structures in Fruit-flies in Forward Flight. *Journal of Bionic Engineering* **13**, 478-490. (doi:https://doi.org/10.1016/S1672-6529(16)60321-9).

[67] Willmott, A.P., Ellington, C.P. & Thomas, A.L. 1997 Flow visualization and unsteady aerodynamics in the flight of the hawkmoth, Manduca sexta. *Philosophical Transactions of the Royal Society B: Biological Sciences* **352**, 303-316.

[68] Bomphrey, R.J., Nakata, T., Phillips, N. & Walker, S.M. 2017 Smart wing rotation and trailing-edge vortices enable high frequency mosquito flight. *Nature* **544**, 92-95.

[69] Ellington, C.P., van den Berg, C., Willmott, A.P. & Thomas, A.L.R. 1996 Leading-edge vortices in insect flight. *Nature* **384**, 626-630.

[70] Song, J., Luo, H. & Hedrick, T.L. 2014 Three-dimensional flow and lift characteristics of a hovering ruby-throated hummingbird. *Journal of The Royal Society Interface* **11**. (doi:10.1098/rsif.2014.0541).

[71] Warrick, D.R., Tobalske, B.W. & Powers, D.R. 2009 Lift production in the hovering hummingbird. *Proceedings of the Royal Society of London B: Biological Sciences* **276**, 3747-3752. (doi:10.1098/rspb.2009.1003).

[72] Wang, Z.J. 2005 Dissecting insect flight. *Annu. Rev. Fluid Mech.* **37**, 183-210.

Chapter 4

On the mechanics and aerodynamics of the backward flight of the annual cicada (*Tibicen Linnei*)

4.1. Abstract

Cicadas are heavy fliers well-known for their life cycles and sound production; however, their flight capabilities have not been extensively investigated. Here, we show for the first time that cicadas appropriate backward flight for additional maneuverability. We studied this unique flight mode using computational fluid dynamics (CFD) simulations based on three-dimensional reconstructions of high-speed videos captured in the laboratory. Backward flight was characterized by steep body angles, high angles of attack, and high wing upstroke velocity. Wing motion occurred in an inclined stroke plane that was fixed relative to the body. Likewise, the directions of the halfstroke-average aerodynamic forces relative to the body (local frame) were constrained in a narrow range (<20º). Despite the drastic difference, approximately 90º, in body posture between backward and forward flight in the global frame, the aerodynamic forces in both flight scenarios were maintained in a similar direction relative to the body. The forces relative to the body were also oriented in a similar direction as observed during climbs and turns, although the body orientation and motions are different. Hence, the steep posture appropriated during backward flight was primarily for reorienting both the stroke plane and aerodynamic force in the global frame. A consequence of this reorientation was the reversal of aerodynamic functions of the half strokes in backward flight when compared to forward flight. The downstroke generated the propulsive force, while the upstroke generated the vertical force. For weight support, the upstroke which typically generates lesser forces due to its non-weight supporting role in forward flight became aerodynamically active in backward flight. A leading edge vortex (LEV) was observed on the forewings during both half strokes. The LEV's effect, together with the high upstroke velocity increased the upstroke's force contribution from 10% of the net forces in forward flight to 50% in backward flight.

Keywords: cicada, backward flight, downstroke-upstroke reversal, active upstroke, force control, maneuverability.

4.2. Introduction

Over millions of years, insects have developed techniques to generate forces and enhance maneuverability in flight. A combination of a robust neuro-sensory system, kinematics control, and the use of different aerodynamic mechanisms makes their flight possible [1, 2]. While previous works have focused mainly on hovering and forward flight to understand the aerodynamics and mechanics of insect flight, some insects extend their flight envelope to include backward or reverse flight [3-7]. Examples include hovering specialists, pollinators, as well as hematophagous insects

[7]. For maneuverability and other biological purposes [8-12], backward locomotion is also expressed widely in nature among fish, birds, humans, and ants, etc. In insect flight particularly, backward locomotion is appropriated for prey capture, flight initiation from vertical surfaces, obstacle avoidance and may render immediate turning after an activity such as hematophagy or pollination unnecessary [3, 6, 10, 13]. Our understanding of this flight mode (backward flight), which is an alternative to forward flight as an extra avenue for maneuverability is still incomplete. Before now, insect backward flight had only been quantitatively documented by a few studies [14, 15] and further investigations may provide insights and inspire micro-aerial vehicle (MAV) design.

Highly maneuverable insects such as Odonates and Dipterans have typically served as candidates for studying complex flight behaviors [2, 15]. However, in this study, we investigated the backward free flight of the annual cicada, which, like other Homopterans is not characteristically associated with excellence in maneuverability [16]. Thus, prior works on cicadas have often focused on other aspects such as sound production [17], life cycle [18], energetics and thermoregulation [19], wing surface topography [20], etc. More recent studies ([21-24]), however, have pointed to new insights regarding cicada flight. Our lab observations during video capture for this study also revealed that cicadas display diverse flight modes similar to those exhibited by highly maneuverable insects, for example, Odonates, although cicadas are more massive and slower [25]. Because of the ability to carry a heavy payload (in terms of body mass), force control technique [23], and wing design [26], cicadas can inspire micro-aerial vehicle (MAV) design [21]. After emergence from the developmental stages underground, maneuverability is essential to their survival in the aerial world above. To escape from predators, to navigate their arboreal environment and for food, cicadas perform controlled maneuvers. These include forward flight, takeoff and more exotic maneuvers like banked turns and Immelmann turns, as well as backward flight which hitherto was an undocumented flight mode of this animal.

To perform maneuvers, Zeyghami et al. [23] reported that despite having different body orientations and motions in forward flight, turns and climbing flights, cicadas used a similar force control strategy. The cicadas did not vary the stroke plane relative to their bodies considerably, and the local orientation of flight forces was similar among the flight modes. Less stroke plane variation point to fewer degrees of freedom of the wing, and hints at simpler wing actuation apparatus [23, 27-29]. To induce maneuvers when the stroke plane is constrained relative to the body, flying animals use changes in body posture to reorient the stroke plane in the global frame [7, 15, 30]. Considering the limited range of stroke plane motion relative to the body in other flight modes, we opine that Cicadas will primarily rely on body postural changes for backward flight. Nevertheless, we do not know whether or how the Cicadas will vary the orientation of flight forces relative to the body during backward flight in comparison to other previously identified flight modes. A common force control strategy both in forward, turning and backward flight is exciting for designing simple but versatile MAVs without complex wing actuation.

Vis-à-vis aerodynamics, Wan et al. [21] and Liu et al. [22] both studied the forward flight of a cicada. Wan et al. [21] identified body generated vortices, while Liu et al. [22], quantified the interaction of the wing with these body generated vortices. Lift enhancement on the body occurred due to wing-body interactions (WBI) while body lift was negligible when isolated from the wings. The overall lift enhancement due to WBI was about 19% [22]. Despite the lift increase due to WBI, the wings remained the dominant source of force generation. By controlling the wing kinematics asymmetrically on a half stroke basis, typical of insects which flap in an inclined stroke plane, cicadas produce 80-90% of the net aerodynamic forces during the downstroke (dorsoventral stroke) while the upstroke (ventrodorsal stroke) plays an auxiliary role contributing 10-20% of the net force in forward flight [21, 22]. The downstroke (DS) forces provide weight support, similar to other insects in forward flight due to the combination of higher effective wing velocity (body + wing velocity) and angle of attack (AoA) in comparison to the upstroke (US) [7, 31]. The US is aerodynamically inactive for weight support but provides some thrust in forward flight [22]. The smaller forces produced in the US are generally due to both lower effective AoA and wing velocities [32, 33].

To understand the kinematics and aerodynamics trends of backward flight, we used a combination of high-speed photogrammetry and three-dimensional reconstruction to capture the flight kinematics. A computational fluids dynamics (CFD) solver was then employed to calculate flight forces and visualize the flow features. The cicadas we observed were either engaged in free flight shortly after takeoff before switching the flight mode to backward flight or initiated backward flight directly from takeoff. All flights were self-motivated. The exact roles of the upstroke (ventrodorsal stroke) and downstroke (dorsoventral stroke) in force production in the local and global frame, the force control strategy, and the aerodynamics during the backward flight of cicadas have not been elucidated before now. Some aspect of backward flight may not be direct extrapolations of forward flight.

4.3. Material and methods

4.3.1. Insects, data acquisition and three-dimensional (3-D) surface reconstruction

The methods used in this work have been documented in previous works [21, 22] and briefly outlined here. Cicadas (both *Tibicen linnei* (annual species) and *Magicicada septendecim* (seventeen-year periodical species)), were captured in the wild and transported to the lab for experiments. Afterward, we dotted their wings for tracking purposes using a felt-tip marker. The insects were then placed on a platform where their voluntary flight was captured by three synchronized orthogonally arranged high-speed cameras (Photron FASTCAM SA3, Photron USA, Inc., San Diego, CA) recording at 1000 frames per second (Figure 4.1(a)). Of the captured footage, which included similar flights as observed by previous works [21-23], we obtained six backward flight sequences, which were substantial in flight duration. By way of example, we selected two flight sequences from the *T. linnei* species for analysis in the text. These cicadas either transitioned into backward flight after a few wingbeats (CCD #1) or initiated backward flight directly from takeoff (CCD #2). Using a template based reconstruction technique [34] (Figure 4.1(b,c)), we obtained a 3-D model of the cicada, with the motion of the body and wings, which was used for kinematics analysis and CFD simulations. The morphological parameters of the two selected cicadas are documented in Table 4.1.

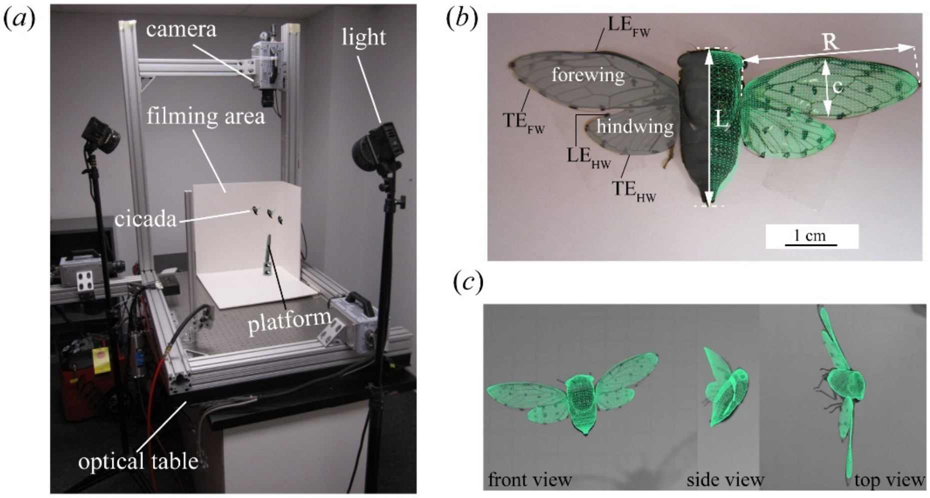

Figure 4.1. Cicada in free flight (a) Experimental set-up showing filming arena with high-speed cameras (b) Cicada (*Tibicen linnei*) image and template (shown in green) with relevant labels. LE- leading edge, TE- trailing edge, FW- forewing, HW- hindwing, c is the mid-span chord, L is the body length, R is the wing length. (c) Reconstructed cicada template overlapped on the cicada in free flight.

Table 4.1. Morphological parameters of the selected cicadas. The uncertainty in mass and length measurements are ±1mg and ±0.5 mm, respectively.

species	ID	body weight (mg)	L (mm)	FW/HW length (mm)	FW/HW chord (mm)	FW/HW area (mm^2)	flapping frequency (Hz)
Tibicen linnei	CCD #1	1174	30	38/22	14/11	352/171	47.6
	CCD #2	1514	30	39/22	14/11	359/175	52.2

4.3.2. Wing kinematics definitions

From the reconstruction, we quantified the wing kinematics. A coordinate system was fixed at the wing root, and the kinematics were measured with respect to the mean stroke plane. The stroke plane was defined as the least-squares reference plane that passed through the centroid of the points of the wing root and tip coordinates. We averaged the stroke plane for all complete wings beats to obtain the mean stroke plane. The Euler angles, flap (ϕ), deviation (θ), and pitch (ψ), define the rigid wing orientation relative to the stroke plane (Figure 4.2(a)). ϕ refers to the forward and backward motion of the wing projected on the stroke plane. The up and down rotation with respect to the mean stroke plane is expressed by θ . ψ is the angle between the wing chord and the mean stroke plane. ψ_{DS} is less than 90º while ψ_{US} is greater than 90º in our definition. The geometric AoA (α_{geom}) is the angle between the wing chord and flapping velocity while the effective AoA (α_{eff}) is the angle between the wing chord and the vector sum of the body and wing velocities, (Figure 4.2(b)).

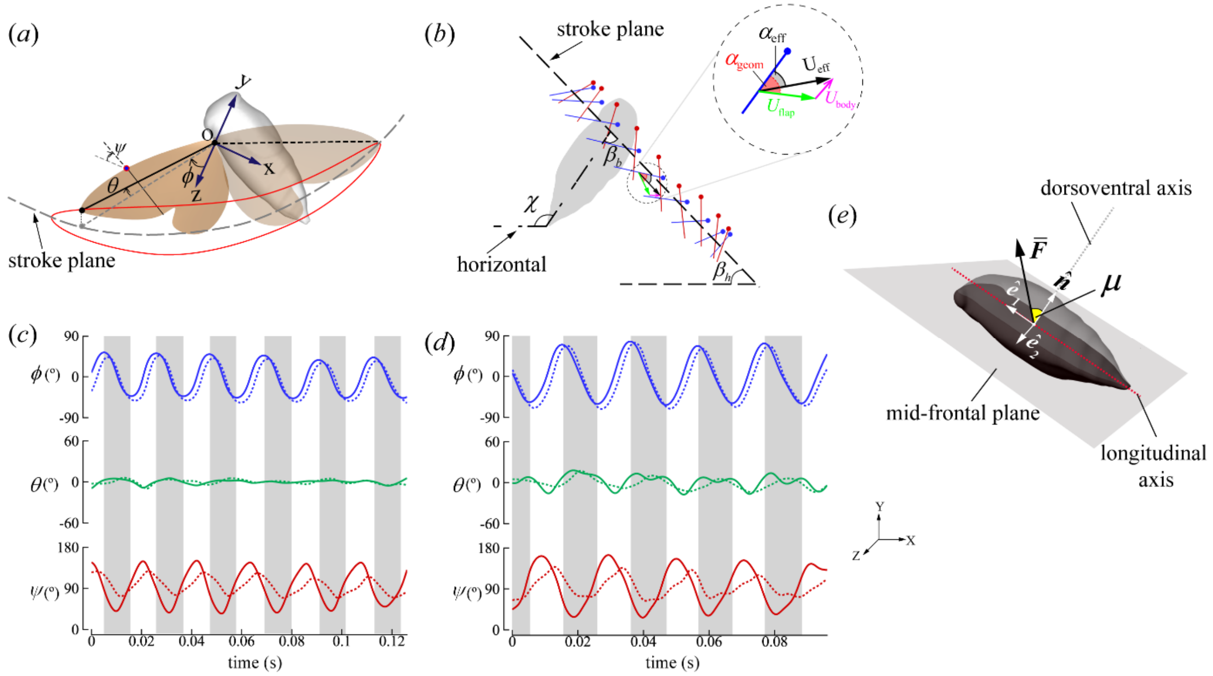

Figure 4.2. Relevant definitions. (a) Wing Euler angle definitions. (b) Wing chord at 0.75R. US-blue, DS-red. Measured wing kinematics of (c) CCD#1 and (d) CCD#2 based on the definitions in (a). The solid and dashed lines represent the fore and hindwing measurements, respectively. (e) $\hat{e}_1$, $\hat{e}_2$ and $\hat{n}$ are orthonormal and form the basis for the local/body coordinate frame. The angle between the halfstroke-average aerodynamic force ($\overline{\mathrm{F}}$) and body normal ($\hat{n}$) is denoted as μ. X, Y, and Z form the basis for the global coordinate frame.

4.3.3. Computational fluid dynamics (CFD) simulation

The CFD simulation was based on a sharp-interface immersed boundary flow solver for simulating incompressible flows around 3-D objects [35]. Validations can be found in previous works [21, 36]. The methods are concisely outlined here. The time-dependent incompressible viscous Navier-Stokes (N-S) equation (Eqn.(1)),

$$\nabla \cdot \mathbf{u} = 0; \quad \frac{\partial \mathbf{u}}{\partial t} + \mathbf{u} \cdot \nabla \mathbf{u} = -\frac{1}{\rho} \nabla p + \upsilon \nabla^2 \mathbf{u}, \tag{4}$$

where $\mathbf{u}$ is the velocity vector, ρ is the density, υ is the kinematic viscosity and p is the pressure, was solved using a finite difference method with 2nd order accuracy in space and a fractional step method for time-stepping. A second-order Adams-Bashforth scheme and implicit Crank-Nicolson scheme were used to discretize the convection and diffusion terms of the momentum equation, respectively. The N–S equation was discretized on cartesian grids, and boundary conditions on the immersed boundary were imposed using a ghost-cell procedure. The domain boundary conditions (BC) of both the pressure and velocity are zero gradients. The size of the computational domain was 50c x 50c x 50c (Figure 4.2). The Reynolds number defined as $Re = \frac{\overline{\mathrm{U}}_{\mathrm{eff}}\, c}{\upsilon}$, is measured based on FW mid-span chord length (c = 0.014m), kinematic viscosity of air at room temperature (υ =$1.5\text{x}10^{-5}$ m^2/s) and the average effective wing tip speed (

$\overline{\mathrm{U}}_{\mathrm{eff}} = \frac{1}{T}\int_0^T \sqrt{(\dot{x}_{\mathrm{tip}} + \dot{x}_{\mathrm{body}})^2 + (\dot{y}_{\mathrm{tip}} + \dot{y}_{\mathrm{body}})^2 + (\dot{z}_{\mathrm{tip}} + \dot{z}_{\mathrm{body}})^2}\,dt$, where $\langle \dot{x}, \dot{y}, \dot{z} \rangle$ is the time derivative of the displacement vector and T is the flapping duration), and ranged between 5400 and 9300 for both cicadas. The *Re* is in the range for large insects. The vortex structures were visualized by positive values of the Q-criterion [37] (Eqn.(5)),

$$Q = \frac{1}{2}\left[|\mathbf{\Omega}|^2 - |\mathbf{S}|^2\right] > 0 \tag{5}$$

where $\mathbf{S} = \frac{1}{2}\left[\nabla\mathbf{u} + (\nabla\mathbf{u})^{\mathrm{T}}\right]$ and $\mathbf{\Omega} = \frac{1}{2}\left[\nabla\mathbf{u} - (\nabla\mathbf{u})^{\mathrm{T}}\right]$ are the strain rate and vorticity tensors, respectively. A grids convergence study was set up based on different mesh sizes (Figure 4.3(b) and Table 3.2). The simulation results presented are based on the ‘fine’ grid results. The difference between mean as well as the maximum values of the fine and finer grids was about 2% (Table 3.2) and deemed sufficient following Liu et al.’s work [22].

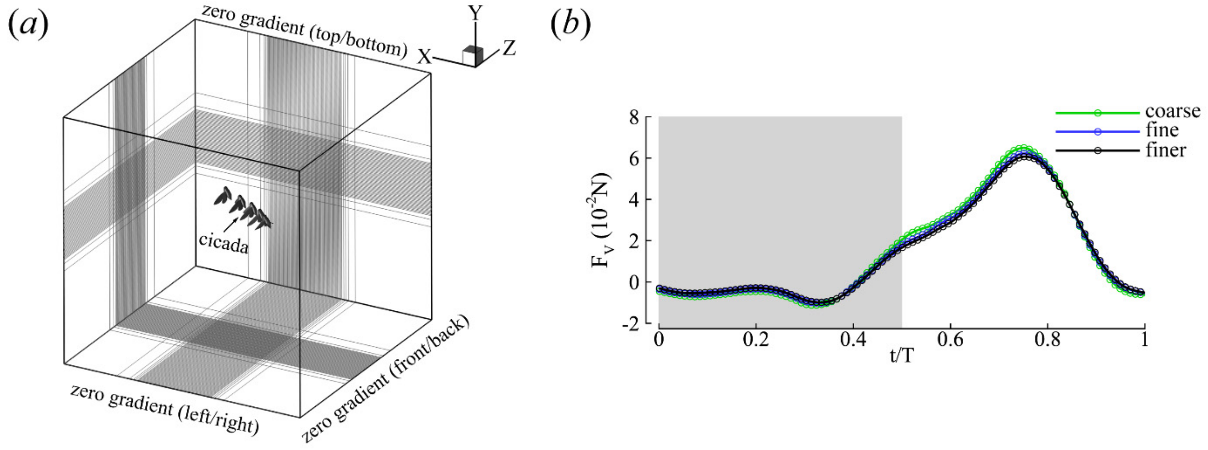

Figure 4.3. CFD simulation setup. (a). Computational domain with boundary conditions. For display, the meshes are coarsened 9, 6, and 3 in the x,y, and z directions, respectively. (b) Grid refinement. The vertical force during the second flapping stroke of CCD #1 is shown. Grey shading denotes the DS. Medium grids are shown in (a).

Table 4.2. Forces for three different grids setup. Values are listed for the 2nd flapping stroke of CCD #1.

	grid size	$\overline{F}_V$ (10^{-2} N)	$F_{V,max}$ (10^{-2} N)
coarse	336x216x192	1.48	6.50
fine	480x320x216	1.45	6.22
finer	600x392x336	1.42	6.08

4.4. Results

4.4.1. Kinematics

4.4.1.1. Body kinematics

The body kinematics of the selected cicadas are shown in Figure 4.4. CCD #1 initiated flight voluntarily and flew upward and forward during the preparatory phase, as indicated by the transparent images in Figure 4.4(a,i). Afterward, the cicada pitched its body to a steep angle, slowed down and initiated backward flight. The cicada flew for approximately six flapping strokes in a relatively straight path with a mean body angle ($\bar{\chi}$) of 122° before leaving the view of one the cameras (Figure 4.4(b,i)). The average backward velocity ($\bar{U}_b$) was -1 m/s as the insect flew in a flight angle of about 15° relative the horizontal (Figure 4.4(c)). CCD #2 also initiated flight voluntarily, albeit via a jumping takeoff. Its initial body angle was 86°, and it increased to 130° by the end of the flight (Figure 4.4(d)). This cicada flew for approximately four flapping strokes with $\bar{U}_b$ of -0.94 m/s and increased its altitude in an angle of about 50° relative to the horizontal (Figure 4.4(e)). The advance ratio (*J*), which is defined here as the ratio of the average resultant body velocity to wingtip velocity was about -0.2 for both cicadas.

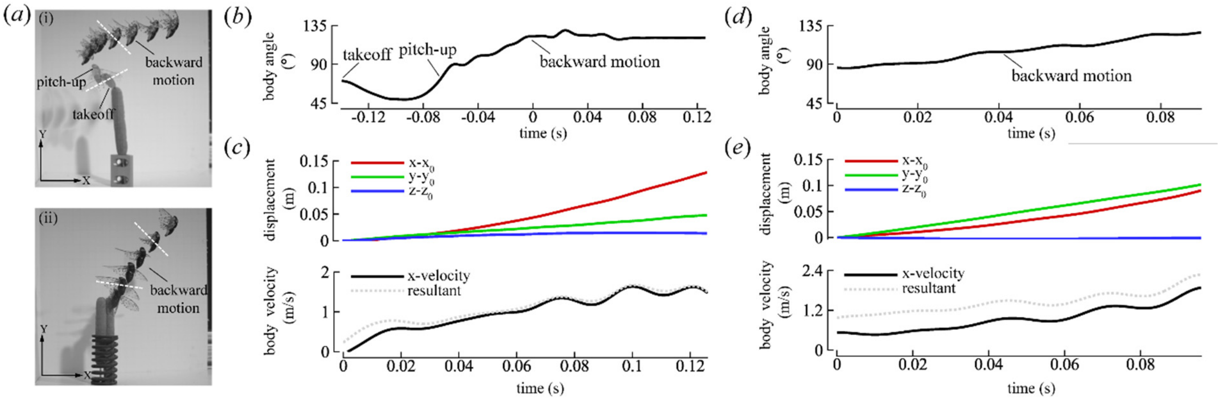

Figure 4.4. Body kinematics. (a) Montage of flight sequences of (i) CCD #1 and (ii) CCD #2. Transparent cicadas in (i) denote the flight phases preceding backward flight (takeoff and pitch-up) of CCD #1. White dashed lines in (i) and (ii) qualitatively denote the stroke plane orientation (b) Body angle and (c) center of mass displacements and the velocity of CCD #1. (d) Body angle and (e) center of mass displacements and the velocity of CCD #2.

4.4.1.2. Wing kinematics

The average stroke plane kinematics of the left and right wings are reported in Figure 4.2(c, d), and summarized in Table 4.3. Although the FW and HW of the cicada were functionally coupled, the FW led the HW with a slight phase difference (<25°), corroborating field observations of cicadas in forward flight [38].

For CCD #1, the wing pairs (FW and HW) traversed a stroke plane inclined at 73±2° relative to the longitudinal axis of the body (β_b). The stroke plane angle relative to the horizontal (β_h) was 46±3° (see Figure 4.2(b) for definition). The stroke amplitude (Φ) was 92±5° and similar for both wings pairs although the average pitch angles (ψ) of the HW were larger. The HW rotation also lagged behind the FW's similar to Lepidopterans with functionally coupled wings [39]. The DS-to-US duration ratio (DS:US) was 0.95, and the DS-to-US ratio of the average effective tip velocity squared ($(\bar{U}_{DS}/\bar{U}_{US})^2_{eff}$) was 0.88. The time histories of the angles of attack (AoA) 0.75R of the FWs are shown in Figure 4.5. α_{geom} was 56±5° and 53±7° in the DS and US, respectively. α_{eff} was 41±7° and 36±5° in the DS and US, respectively.

For CCD #2, β_b and β_h were 69±2° and 37±13°, respectively. Similar to CCD #1, β_b's variation was small, while β_h's variation was more substantial due to changes in body angles over a greater range (86-130°) in flight (Figure 4.2(d)). Φ was 133±5° for both the wing pairs and ψ was higher for the HWs. DS:US was 1.06, and $(\bar{U}_{DS}/\bar{U}_{US})^2_{eff}$ was 0.83. α_{geom} was 52±4° and 43±4° in the DS and US, respectively. α_{eff} was 39±5° and 32±4° in the DS and US, respectively.

In general, the DS AoA was higher than the US's while the wing US velocity was higher than the DS's for both insects (Figure 4.5 and Table 4.3).

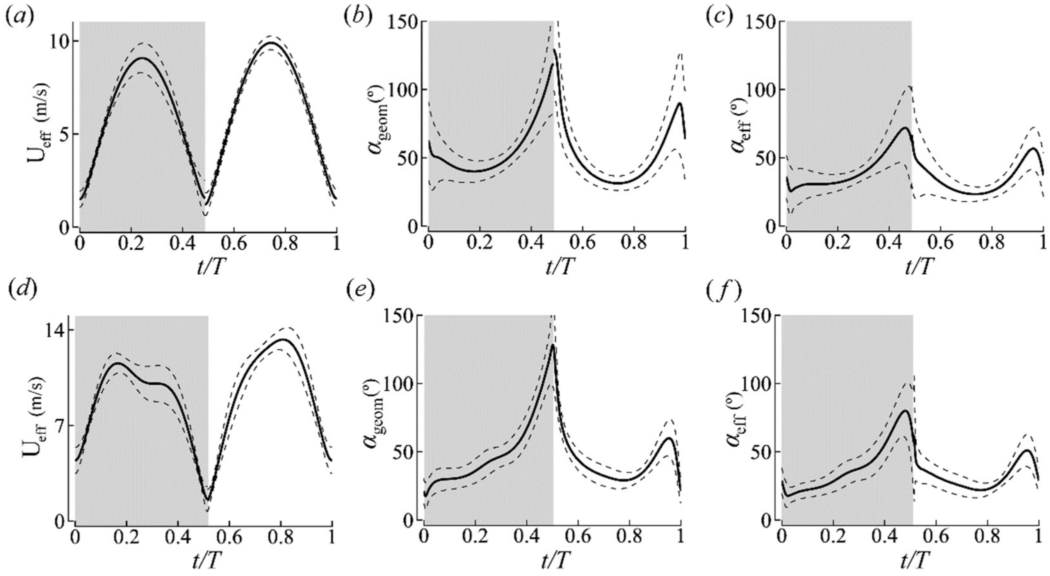

Figure 4.5. Additional forewing kinematics parameters. (a) Effective wing tip speed, (b) Geometric AoA at 0.75R, (c) Effective AoA at 0.75R for CCD #1. (d), (e) and (f) represent CCD #2's data. Solid and dashed lines are the mean and ±standard deviation of the all complete wingbeats, respectively. Grey shading denotes the DS.

Table 4.3. Summary of kinematic parameters of the backward flight of cicadas. The mean and standard deviation for all complete wing beats are documented here.

ID	J	$\bar{U}_b$ (m/s)	$\bar{\chi}$ (°)	β_b (°)	β_h (°)	DS:US	$(\bar{U}_{DS}/\bar{U}_{US})^2_{eff}$	Φ (°)	α_{geom} (°)		α_{eff} (°)	
									DS	US	DS	US
CCD #1	-0.19	-1.0	122±2	73±2	46±3	0.95	0.88	92±5	56±5	53±7	41±7	36±5
CCD #2	-0.17	-0.94	107±14	69±2	37±13	1.06	0.83	133±5	52±4	43±4	39±5	32±4

4.4.2. Aerodynamic force

From the CFD simulation, we obtained the aerodynamic forces by integrating both the shear stress and pressure on the wing. Horizontal forces were produced in the DS for backward propulsion while vertical forces were produced in the US for weight support for CCD #1 (Figure 4.6(a)). In the first half CCD #2's flight (Figure 4.6(b), t=0-46*ms*), both half strokes generated vertical and horizontal forces. The US produced vertical forces for weight support and horizontal forces that opposed the backward motion while the DS generated vertical forces for weight support and horizontal forces that propelled the insect backward. This trend was probably due to the less steep β_{h} (approximately 20°). Nevertheless, in the second half of flight (t=46-96*ms*), CCD #2's force production trend was similar to CCD #1's, whereby horizontal forces were produced predominantly in the DS while vertical forces were produced in the US for weight support. Here, β_{h} had increased to approximately 45°, which is similar to CCD #1's β_{h}. The time-average vertical forces ($\overline{\mathrm{F}}_{\mathrm{V}}$) were 1.3x bodyweight (BW) and 1.5x BW for CCD #1 and #2, respectively, while the time-average horizontal forces ($\overline{\mathrm{F}}_{\mathrm{H}}$) were 1.2x BW and 1.3x BW for CCD #1 and #2, respectively, for all complete strokes.

4.4.3. Force orientation in global and local frame.

In §4.4.2, we quantified the generation of flight forces. However, it is the orientation of the flight forces that is essential for positioning the insect in its intended travel direction. Here, we quantify the force orientation both in the global and local/body frames. A simple technique for orienting flight forces involves tilting the stroke plane [32, 40] which is achieved either (i) through actuation from the wing hinge to rotate the stroke plane relative to the body. Here, the body angle changes slightly. Or (ii) through reorienting the body angle or posture. Here, the stroke plane relative to the body is fixed or changes within a narrow range. The latter (ii) known as force vectoring is employed to reorient flight forces for maneuvers when the aerodynamic force is constrained within the animal's body frame [2, 23, 30, 40].

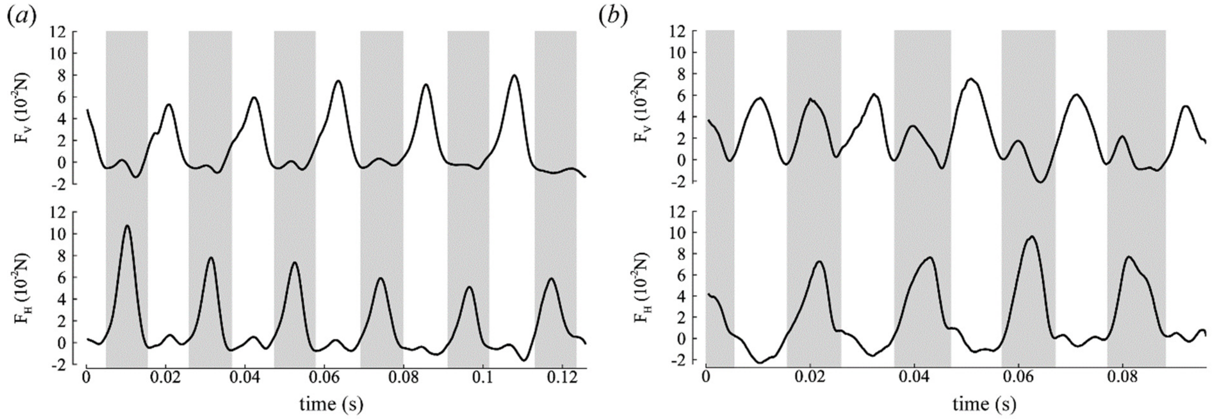

Figure 4.6. Time history of force production in the global frame of (a) CCD #1 and (b) CCD #2. F_{V}-vertical force and F_{H} – horizontal force refers to the force in the Y and X directions, respectively (see Figure 4.4(a)). Gray shading denotes the DS.

β_{b} was relatively fixed during flight (Table 4.3) and Figure 4.4(a) illustrates that the stroke plane in the global frame was reoriented by changes in body angle. The difference in body angle before and after backward flight was initiated was ~80° for CCD #1 (Figure 4.4(b)). CCD #2 also maintained a steep body posture from takeoff. When the body angle was low, the stroke plane was oriented more downward. Conversely, when the body angle increased, the stroke plane was oriented upward (Figure 4.4(a,ii)). The reorientation of the stroke plane due to the body angle is likely the major influence on the orientation of the force vector in the global frame.

In the global frame, the halfstroke-averaged aerodynamic force vectors are presented in the X-Y plane where most of the body motion occurred (Figure 4.7(a,b)). The green arrows and red arrows represent the DS-average ($\overline{F}_{DS}$) and US-average force vectors ($\overline{F}_{US}$), respectively. The US forces point upward (+Y direction), while the DS forces point backward (+X direction). Measured relative to the horizon (+X direction, Figure 4.7) $\overline{F}_{DS}$ and $\overline{F}_{US}$ were oriented at -6±4° and 96±5° for CCD #1, and at 14±18° and 97±10° for CCD #2.

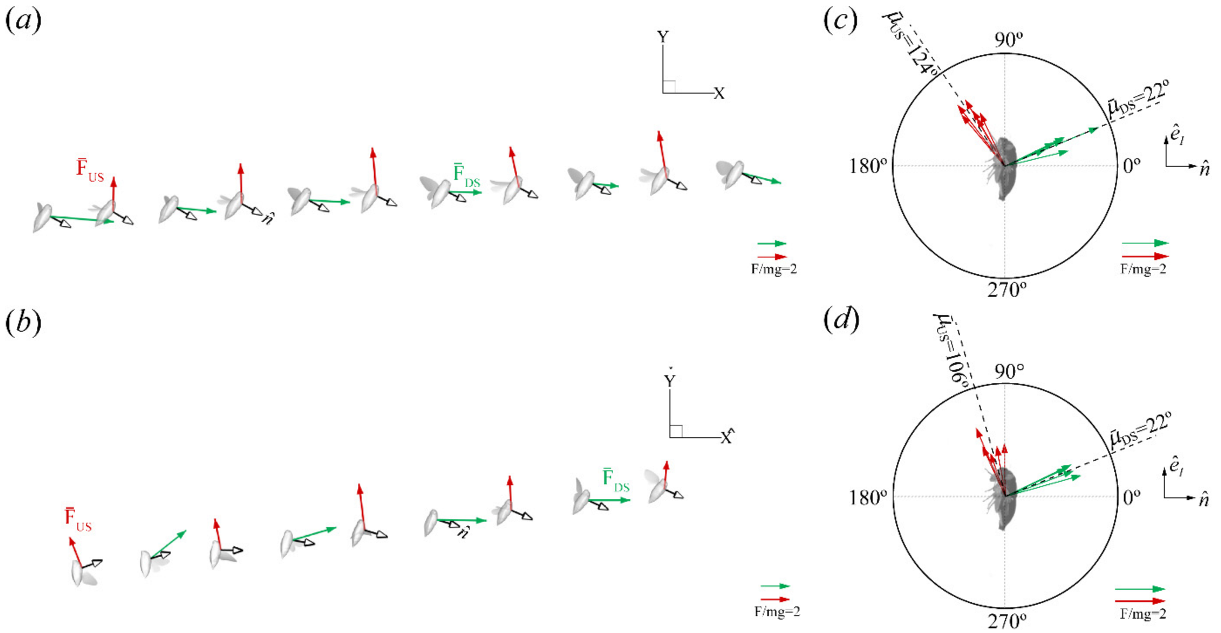

Figure 4.7. Force orientation in the global and local frame. (a, b) Halfstroke-average forces of CCD #1 and #2 respectively in the global frame. Red and green arrows represent $\overline{F}_{US}$ and $\overline{F}_{DS}$, respectively. The force vectors have been supoerimposed on the cicada at midstroke. For illustration purposes, the real spacing between each cicada model in the X-direction has been scaled by ten chord lengths. The vector orientation, as well as the spacing in the Y-direction, were unaffected. (c, d) Orientation of the force vector relative to the body projected on the mid-sagittal plane of CCD #1 and #2 respectively. μ = 0° when $\overline{F}$ is aligned in the same direction as $\hat{n}$.

The orientation of the forces relative to the cicada body (local frame) was obtained by calculating the angle (μ) between $\overline{F}$ and $\hat{n}$ (Figure 4.7(b,d)). $\hat{n}$ which always points outward from the body is perpendicular to the longitudinal axis vector ($\hat{e}_1$) and represents the dorsoventral axis of the body (Figure 4.2(d)). $\bar{\mu}_{DS}$ and $\bar{\mu}_{US}$ were 22±5° and 124±5° for CCD #1, and 22±5° and 106±10° for CCD #2. $\overline{F}$ was produced only in the anterior side of the body which is defined as the half-disk from 0° to 180° counterclockwise (Figure 4.7(b,d)). The forces in dorsoventral stroke (downstroke in the body frame, following Dudley's [7] definition) were produced in the dorsal side (half-disk from 90° to 270°, clockwise), with the major component pointing in the dorsoventral axis. The forces produced in the ventrodorsal stroke (upstroke in the body frame [7]) were produced in the ventral side (half-disk from 90º to 270º, counterclockwise), with the major component pointing in the longitudinal axis. The variation of the orientation of the mean force vector relative to the body (±10º) was within the range reported for other organisms as well as helicopters (±20º), which use force vectoring [30].

4.4.4. Three-dimensional flow features and leading edge vortex circulation

Here, we visualized the flow around the insect using the isosurface of the Q-criterion to understand how flight forces were produced. The evolution of the flow features throughout a representative stroke of CCD #1 (t = 57-80 *ms*) is displayed in Figure 4.8 and colored by the coefficient of pressure.

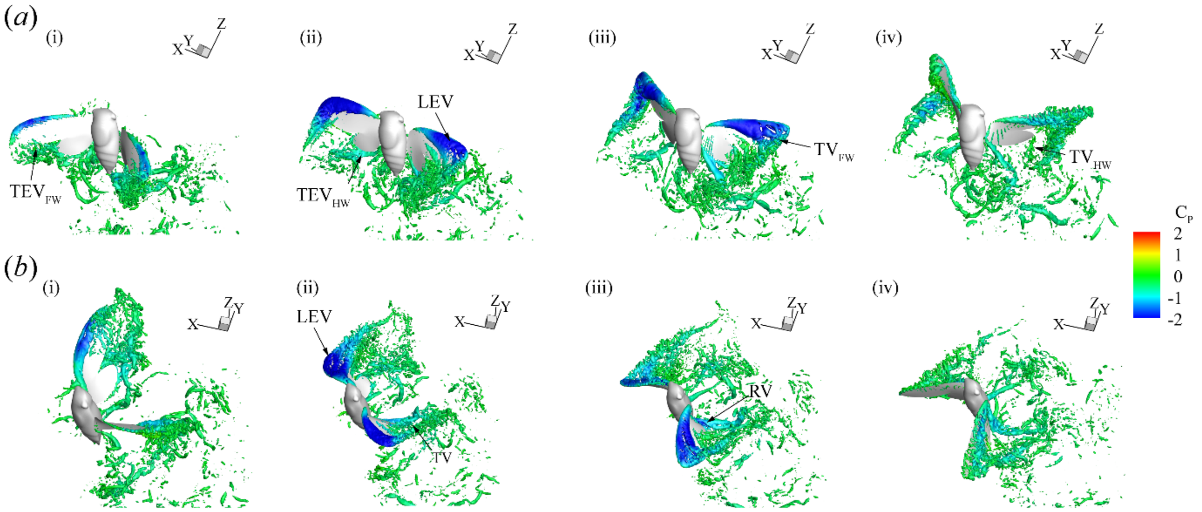

Figure 4.8. Flow structures visualized by the Q-criterion (Q=600) and colored by the pressure of the vortical structures during the third flapping stroke of Cicada #1 (t = 57-80 *ms*). (a) Top row (i-iv) represents snapshots during the DS at t/T=0.13,0.25,0.38,0.48 respectively. (b) Bottom row (i-iv) denote snapshots during the US at t/T=0.63,0.75,0.88,0.98. The flow is colored by the coefficient of pressure ($C_p = p - p_\infty / 0.5\rho \bar{\mathrm{U}}_{\mathrm{eff}}$). TEV-trailing edge vortex; TV-tip vortex. RV- root vortex.

Large coherent structures with strong vorticity around the wings surface were identified. An LEV (a region of low pressure shown in blue) was formed shortly after the inception of both half strokes (Figure 4.8(a, i) and (b, i)) and remained attached for the duration of each half stroke, shedding at the wing reversal. The size of the LEV in both half strokes was similar, qualitatively indicating that comparable amounts of force were generated (Figure 4.6). Other vortex structures such as a trailing edge vortex, tip vortex, and root vortex were also evident. Most of the large vortex structures emanated from the FWs, which may indicate the auxiliary role the HWs play in force production during flight.

To measure the LEV strength, two-dimensional (2D) planes perpendicular to the rotation axis of the LEV were placed along the wing at every time step of the numerical simulation (Figure 4.9(a)). The vorticity (ω) was calculated on this 2D plane by taking the curl of the velocity. The area of integration (*dS*) was identified by a vorticity threshold set at 10% of the maximum spanwise vorticity. Subsequently, the non-dimensional circulation was obtained using (Eqn.(3)).

$$\Gamma^*_{LEV} = \frac{1}{c\bar{U}_{\text{eff}}} \iint_S \omega \cdot dS, \qquad (6)$$

Both the time histories and spanwise distribution of the circulation are reported in Figure 4.9(b) and (c). Consistent with the force measurements, substantial circulation was recorded in both half strokes. Averaged across all strokes, the DS-US LEV circulation ratio was about 1 (Table 4.4), quantitatively indicating similarity in the vortex forces generated during half strokes.

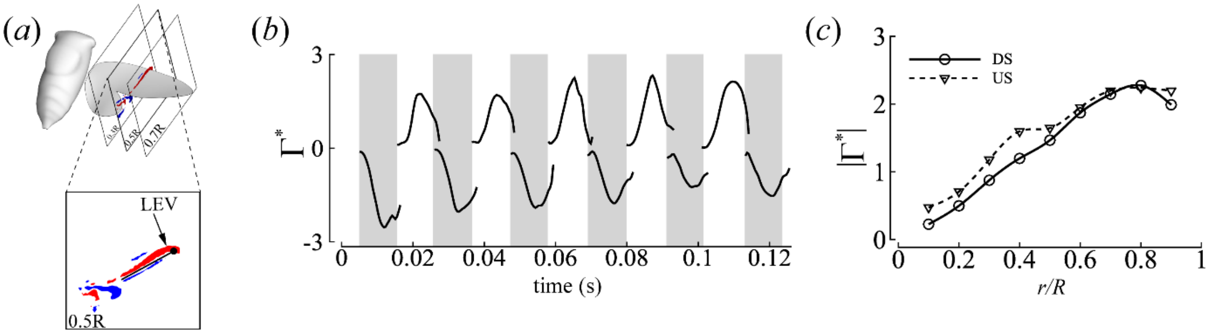

Figure 4.9. LEV circulation. (a) Calculation of LEV circulation. (b) Time history of LEV circulation at mid-span (0.50R) (b). Mean spanwise distribution of circulation at mid-stroke for all complete strokes.

Table 4.4. Half stroke LEV circulation at mid-span. $\bar{\Gamma}^*$ and $\Gamma^*_{\max}$ represent the average and maximum circulation per half stroke, respectively. DS1 corresponds to the first gray shaded region in Figure 4.9(b).

half stroke	$\bar{\Gamma}^*$	$\Gamma^*_{\max}$	$\left\lvert \bar{\Gamma}^*_{DS} / \bar{\Gamma}^*_{US} \right\rvert$	$\left\lvert \Gamma^*_{\max_{DS}} / \Gamma^*_{\max_{US}} \right\rvert$
DS 1	-1.61	-2.58	1.62	1.46
US 1	0.99	1.76		
DS 2	-1.22	-2.07	1.18	1.20
US 2	1.03	1.72		
DS 3	-1.22	-1.94	0.98	0.85
US 3	1.25	2.28		
DS 4	-1.05	-1.80	0.90	0.76
US 4	1.17	2.36		
DS 5	-0.83	-1.27	0.70	0.59
US 5	1.18	2.16		
DS 6	-1.03	-1.55		

4.4.5. Roles of the fore and hind wings

Cicadas have two pairs of wings, of which the HW are the smaller. The HW is attached to the FW in flight to form a functionally two-winged flight apparatus (Figure 4.10(a)). Functionally coupling the FW and HW together is thought to eliminate the conflict between the wing pairs [41]. Here, we quantified the contribution of each wing pair to force generation. We compared two simulation cases, (i) ALL (FW+HW), (ii) FW only (FO). An HW only (HO) case was not simulated because flow cannot separate at the leading edge of the HW where it is connected to the FW's trailing edge.

The time history of the forces of CCD #1 is presented in Figure 4.10(b). The stroke-averaged net force of the ALL case was about 22% greater than the FO case for both Cicadas, with most of the difference between the two cases occurring in the mid-stroke region. The presence of the HW did not significantly affect vortex formation on the FW wing (Figure 4.10(c)). This observation is corroborated by plots of the pressure difference between the top and bottom surfaces of the wings during the mid-stroke (Figure 4.10(d)) for both the ALL and FO cases. Regions of high-pressure difference (shown in red) correspond to where the LEV resided and indicate where most of the force is produced during both half strokes. The size of this region was similar in size for both the ALL and FO cases. The presence of the HW, however, may influence the pressure distribution around the trailing edge of the FW (Figure 4.10(d,iv)). Most of the force contribution from the HW comes from the distal part of the HW where it is no longer connected to the FW and the velocity is highest [22](Figure 4.10(d,i)). The HW forces are not enough for weight support but the HW may be more important for other functions such as evasiveness or turning in flight as seen in functionally two wings flies with well-developed HWs [42].

4.5. Discussion and conclusion

In this study, we investigated a new flight mode of the cicada, that is, backward/reverse flight, which is an avenue for additional maneuverability for this heavy flier. We studied the coordination between the wing and body motion in connection to the production and orientation of the aerodynamic forces. Here, our findings are further discussed and compared to previous literature.

Cicadas typically fly forward with body angles of ~10-50º with the stroke plane inclined downward [21, 43]. During backward flight, however, the stroke plane was tilted upward and χ was large, ranging between 86-130º (Figure 4.4 and Table 4.5). χ was correspondingly larger than the previous measurements of the backward flight of hummingbirds (50-75º) [10], dragonflies (85-95º [15]; 100º [3]), waterlily beetles (50-70º) [5] and cockchafer beetles (87-115º) [14]. Thus far, a steep body posture and an upward titled stroke plane is a common feature of backward flight between pterygota and hummingbirds and is probably a technique shared due to convergent evolution as previously suggested [10]. However, unlike hummingbirds [10] which tilt their stroke plane upward and flatten it relative to the horizontal during backward flight, both cicadas and dragonflies [15] maintain a steeply inclined stroke plane in backward flight just as during forward flight (Table 4.6).

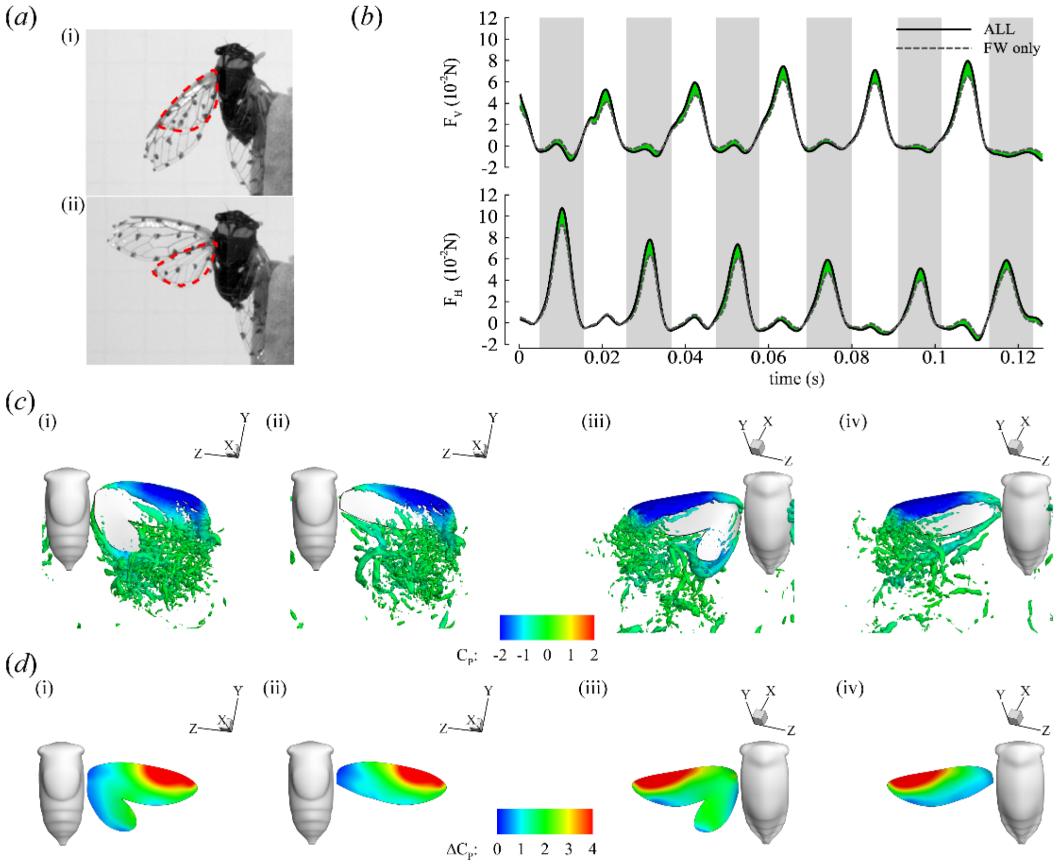

Figure 4.10. Fore and hind wing force generation (a). (i) Wing configuration before flight. The HW (outlined by red dashed lines) is tucked under the FW. (ii) Wing configuration in flight. The HW leading edge is connected to the FW trailing edge (b) Force production of CCD #1. Grey shading denotes the DS. (c) Flow structures at (i) mid-DS when the HW is present versus when absent (ii) and at mid-US when the (iii) HW is present versus when absent (iv). (d) Pressure difference on the wing surface at the exact snapshots shown in (c).

A possible consequence of the upright body posture appropriated during backward flight is an increase in drag. However, if the body angle is very steep, the drag contribution of the body may not be considerably different from forward flight at similar angles relative to the incoming flow. For instance, by maintaining a steep body angle of ~122º (CCD#1), the flow the body experiences is equivalent to orienting the body at 58º in forward flight and is not considerably different from flying at 50º, which is the upper range of body angles used during cicada forward flight. Sapir and Dudley using a hummingbird body model without wings in a wind tunnel [10], showed that although drag during backward flight was higher, it only differed by 3.6% from forward flight although the body angle difference was 33º, that is, an 88% increase in body angle. Bode-Oke et al. [15] also found that the parasite drag coefficient in backward flight was in the range measured for forward flight of dragonflies in wind tunnels at similar *Re*. The parasite (viscous + pressure) drag coefficient, is defined as $\overline{C}_D = \dfrac{\overline{F}_H}{0.5\rho \overline{U}_b^{\,2} S_{\text{frontal}}}$, where $\overline{F}_H$ is the mean body horizontal force and is less than 5% of the horizontal forces produced by the wings, $S_{\text{frontal}} = A_{MF} \sin \overline{\chi}$ is the frontal area where A_{MF} is the cross-sectional area in the mid-frontal plane. $\overline{C}_{\mathrm{D}}$ was 1.18 for CCD #1, which was higher than Liu et al.'s value [22] (0.52). High body drag may be inevitable if force vectoring is the only mechanism by which cicadas elicit backward flight. Typical backward flight speeds are about 1 m/s for dragonflies [15] and Delfly II MAV [44], 1.5m/s for bumblebees [45] and 2 m/s for hummingbirds [10]. At these low flight speeds, drag penalties are not as critical [7, 32].

Table 4.5. Forward versus backward flight of cicada. $\overline{\mathrm{F}}$ is the resultant force normalized by the body weight during each half stroke, while $\overline{\mathrm{F}}_{\mathrm{V}}$ is the component of the resultant force that solely contributes to weight support.

flight mode	J	$\overline{\mathrm{U}}_{\mathrm{b}}$ (m/s)	$\overline{\chi}$ (°)	β_{b} (°)	β_{h} (°)	DS: US	α_{eff} (°)		$\overline{\mathrm{F}}_{\mathrm{DS}}$	$\overline{\mathrm{F}}_{\mathrm{US}}$	$\overline{\mathrm{F}}_{\mathrm{V,DS}}$	$\overline{\mathrm{F}}_{\mathrm{V,US}}$	reference
							DS	US					
forward	--	1.9	25	--	--	--	--	--	--	--	--	--	Zeyghami [46]
	0.32	2.0	28	64	36*	1.0	--	--	3.33	0.53	3.23‡	0.10	Liu et. al [22]
	0.32	2.2	49	62	13*	1.17	62	72	1.91	0.59	1.58‡	0.47	Wan et al. [21]
backward	-0.19	-1.0	122	73	46†	0.95	41	36	2.89	2.96	-0.28	2.87‡	current study
	-0.17	-0.94	107	69	37†	1.06	40	34	3.14	2.35	0.81	2.27‡	

*-stroke plane tilted downward relative to horizontal, † -stroke plane tilted upward relative to horizontal, ‡- predominant weight supporting half stroke.

The slight variation of the mean stroke plane relative to the body (<±5°) observed from the kinematics indicates that cicadas do not considerably control this angle possibly due to a limited range of joint rotation. β_{b} was inclined at approximately 70° for both cicadas and was marginally larger than values measured in forward flight by about 10°, signifying that a small stroke plane tilt away from the body occurred in backward flight (Table 4.5). However, this slight tilt alone did not induce backward flight. Instead, the reorientation of the body in the global frame caused the major reorientation of the force vector in the global frame compared to forward flight (refer to Figure 4.11(a) for illustration). The horizontal motion of the cicadas occurred from left to right (the +X direction, Figure 4.4(a)). Measured relative to the horizon using the components in the midsagittal plane, $\overline{\mathrm{F}}_{\mathrm{DS}}$ and $\overline{\mathrm{F}}_{\mathrm{US}}$ were oriented at -6±4° and 96±5° for CCD #1 and 13±18° and 97±10° for CCD #2, respectively. Likewise, $\overline{\mathrm{F}}_{\mathrm{DS}}$ and $\overline{\mathrm{F}}_{\mathrm{US}}$ were oriented at 91° and 16°, respectively, during forward flight [22]. Our finding indicates that the orientations of force vector in the DS and US in backward flight were reversed relative to forward flight in the global frame. Comparing the final body orientations of the cicada in forward and backward flight moving in the same direction (+X direction), it is as though the DS force vector in forward flight was rotated clockwise by 78-97° while the US force vector was rotated counterclockwise by about 80° simply by changing the body angle. This reorientation of the force vector orientation also reversed the aerodynamic functions of the DS and US in the global frame. In forward flight, the DS and US predominantly provide weight support and forward thrust, respectively. Whereas in backward flight, the DS and US mainly provide backward thrust and weight support, respectively (Figure 4.6).

Table 4.6. Kinematics of backward flight among different fliers. DS:US, α_{eff} and $\overline{\mathrm{F}}$ are split by the contribution of the fore and hind wings, respectively, for functionally four-winged insects. α_{eff} is reported at 0.75R.

animal	$-J$	$\overline{\mathrm{U}}_{\mathrm{b}}$ (m/s)	χ (°)	β_{b} (°)	β_{h} (°)	DS:US	$\alpha_{\mathrm{eff,DS}}$ (°)	$\alpha_{\mathrm{eff,US}}$ (°)	$\overline{\mathrm{F}}_{\mathrm{DS}}$	$\overline{\mathrm{F}}_{\mathrm{US}}$	reference
cockchafer beetle	--	-1.2	87–115	--	--	--	--	--	--	--	Schneider [14]
hummingbird	0.3	-1.5	51–75	57–71	-15 – 6	0.88–1.08	--	--	--	--	Sapir and Dudley [10]
dragonfly	0.3	-1.0	85–95	35	47	0.87 0.83	25 27	21 27	1.44 2.07	2.15 3.17	Bode-Oke et al. [15]
cicada	0.2	-1.0	122	73	46	0.95	41	36	2.89	2.96	current study
	0.2	-0.9	86–130	69	37	1.06	40	34	3.14	2.35	
waterlily beetle	--	--	50–70	40–50	0 –30	--	--	--	--	--	Mukundarajan et al. [5]
delfly II	--	-1.0	70–100	--	--	--	--	--	--	--	Caetano et al. [44]

Because the US now carries the insect's weight in backward flight, the aerodynamic demand on the US increases, and it has to become aerodynamically more active when compared to forward flight (see $\overline{\mathrm{F}}_{\mathrm{V,US}}$ in Table 4.5, for example). Therefore, in the global frame, the half stroke aerodynamic function was not only reversed, but the force magnitude was also influenced. Although the cicadas in this study were accelerating, if they approached cruising where the wing horizontal forces are balanced by body drag, it is expected that the horizontal force magnitude which is generated in the DS in backward flight will decrease [47]. Consequently, the US-DS force asymmetry will become more pronounced. Also, assuming similar net output from the wings during cruising flight in the forward or backward direction, as well as a fixed stroke plane relative to the body, it becomes clearer that the body angle modulates the distribution between vertical and horizontal forces in the global frame.

For insects that employ asymmetric strokes in an inclined stroke plane during hovering or forward flight, the US force, particularly for weight support is minimal [22, 31-33, 48] (Table 4.7). The presence of an active US in backward flight suggests the presence of an LEV on the wing surface, which is essential at low *J* and accelerating flight (Figure 4.8). This is in addition to any enhancements of US velocity due to the backward motion of the cicada. Here, the LEV was stably attached to the FW in both half strokes (Figure 4.8). Since flow separates at the FW's leading edge irrespective of the presence of the HW (Figure 4.10(c)), the FW forces were also substantial due vortex lift which is a consequence of the LEV. Furthermore, when the HW was removed computationally, the LEV characteristics were not greatly influenced corroborating previous results on revolving wings that the FW morphologies match the formation of leading edge vortices [49]. The measured DS-to-US LEV circulation ratio was about 1, indicating the presence of a strong LEV in the US for vertical force production. In past studies on cicada flight [21, 22], the US LEV strength was much smaller than the DS's.

Table 4.7. Half stroke force type and contribution to the resultant aerodynamic force for several insects which use an inclined stroke plane in free flight. *-tethered.

insect	flight mode	DS force (%)	DS force type	US force (%)	US force type	reference
cicada	forward	90	vertical	10	horizontal	Liu et al. [22]
		80	vertical	20	horizontal	Wan et al. [21]
	backward	49	horizontal	51	vertical	current study
		57	horizontal	43	vertical	current study
damselfly	forward	84	vertical	16	horizontal	Bode-Oke et al. [33]
		75	vertical	25	horizontal	Sato et al. [50]
dragonfly	hovering*	77	vertical	23	horizontal	Russell [51]
	backward	33	horizontal	67	vertical	Bode-Oke et al. [15]
	forward	80	vertical	20	horizontal	Azuma and Watanabe [52]
		67	vertical	33	horizontal	Hefler et al. [53]
fruit fly	forward	61	vertical	39	horizontal	Meng and Sun [54]
hawkmoth	forward	80	vertical	20	horizontal	Willmott et al. [55]
	hovering	67	vertical	33	horizontal	Aono and Liu [56]
locust	forward	84	vertical	14	horizontal	Young et al. [57]

Relative to the body, we showed that the flight forces were constrained in the anterior part of the body (Figure 4.7(b) and (d)). During the dorsoventral stroke (downstroke), the forces were directed with the major component pointing in the dorsoventral axis. Whereas, the ventrodorsal stroke (upstroke) was directed majorly in the longitudinal axis. In 3-D space, these force vectors form a cone whose axis is offset by $\bar{\mu}$ from the body normal (ventrodorsal axis), and radii is expressed by the standard deviation of all complete wing beats. $\bar{\mu}_{\mathrm{DS}}$ and $\bar{\mu}_{\mathrm{US}}$ were 22±5° and 124±5° respectively for CCD #1 while $\bar{\mu}_{\mathrm{DS}}$ and $\bar{\mu}_{\mathrm{US}}$ were 22±5° and 106±10° respectively for CCD #2. Prompted by previous work [23], we then asked whether relative to the body, cicadas used a unified force generation strategy irrespective of the flight mode, because of the drastic difference between forward and backward flight body angle, and stroke plane orientation in the global frame. $\bar{\mu}_{\mathrm{DS}}$ and $\bar{\mu}_{\mathrm{US}}$ ranged between 16-27° and 85-135°, respectively in previous work [21-23]. Figure 4.11(b) shows that the backward flight results fell within a similar range as the values recorded for forward flight, and other flight modes.

Although the halfstroke-average aerodynamic forces are fixed in the same direction in the body frame, our finding does not mean that the wing kinematics in all these flight modes are the same. The wing kinematics vary according to the demand for force production or torque generation. For instance, roll and pitch torques can be generated by varying the wing AoA and the wing position relative to the center of mass of the body [23]. Additionally, the contribution of the US to the total force production increases in backward flight compared to a forward flight scenario due to US weight support. Increasing the US magnitude to accommodate weight support in the global frame, indicates an increase in the ventrodorsal stroke's force magnitude (in the body frame). Since the direction of the forces relative to the body is consistent in each half stroke for all flight maneuvers, the dorsoventral (downstroke) and ventrodorsal (upstroke) stroke function are not reversed in the body frame. Nevertheless, the force magnitude is modulated due to the demands of force production that will ensure sustained flight in the global frame.

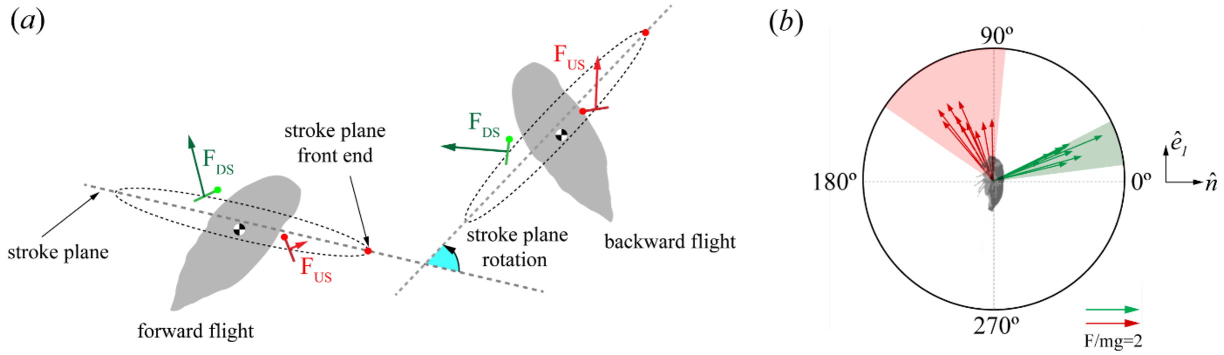

Figure 4.11. Force production and orientation in cicada flight. (a) Schematic illustrating the transition from forward to backward flight (b) Orientation of the aerodynamic force relative to the body normal. Data from previous literature [21-23] are pooled together (shaded sectors on the circles). The arrows are the data from the current study and are also shown in Figure 4.7.

In the context of the work presented here, our understanding of cicadas can now be extended to backward flight. We showed that cicadas elicit backward flight by changes in body posture to reorient both the stroke plane and the force vector in the global frame. We found that the steep body posture also influenced the wing aerodynamics by reversing the aerodynamic roles of the half strokes compared to forward flight in the global frame. However, the orientation of aerodynamic force relative to the body, compared to other flight modes remains relatively fixed despite significantly different body orientations and motions. An aerodynamically active upstroke signified by the presence of an LEV and high wing velocity was identified and the upstroke was principally responsible for weight support during backward flight. The LEV was present on the FWs which generated most of the flight forces in comparison to the smaller HWs. Our results also clarify what the aerodynamics and kinematic adjustments may look like for other simple fliers (with limited range of stroke plane motion relative to the body) such as beetles [5, 14] which appropriate backward flight for both obstacle avoidance and interfacial flight, as well as MAVs which may use backward flight during free flight or takeoff from vertical surfaces [44].

4.6. References

[1] Sane, S.P. 2003 The aerodynamics of insect flight. *The journal of experimental Biology* **206**, 4191-4208.
[2] Dickinson, M.H. & Muijres, F.T. 2016 The aerodynamics and control of free flight manoeuvres in Drosophila. *Phil. Trans. R. Soc. B* **371**, 20150388.
[3] Rüppell, G. 1989 Kinematic analysis of symmetrical flight manoeuvres of Odonata. *Journal of Experimental Biology* **144**, 13-42.
[4] Rüppell, G. & Hilfert, D. 1993 The flight of the relict dragonfly Epiophlebia superstes (Selys) in comparison with that of the modern Odonata (Anisozygoptera: Epiophlebiidae). *Odonatologica* **22**, 295-309.
[5] Mukundarajan, H., Bardon, T.C., Kim, D.H. & Prakash, M. 2016 Surface tension dominates insect flight on fluid interfaces. *Journal of Experimental Biology* **219**, 752-766. (doi:10.1242/jeb.127829).
[6] Yokoi, T. & Fujisaki, K. 2009 Hesitation behaviour of hoverflies Sphaerophoria spp. to avoid ambush by crab spiders. *Naturwissenschaften* **96**, 195-200.
[7] Dudley, R. 2002 *The biomechanics of insect flight: form, function, evolution*, Princeton University Press.

[8] Lannoo, M.J. & Lannoo, S.J. 1993 Why do electric fishes swim backwards? An hypothesis based on gymnotiform foraging behavior interpreted through sensory constraints. *Environmental biology of fishes* **36**, 157-165.

[9] Flammang, B.E. & Lauder, G.V. 2016 Functional morphology and hydrodynamics of backward swimming in bluegill sunfish, Lepomis macrochirus. *Zoology* **119**, 414-420. (doi:http://dx.doi.org/10.1016/j.zool.2016.05.002).

[10] Sapir, N. & Dudley, R. 2012 Backward flight in hummingbirds employs unique kinematic adjustments and entails low metabolic cost. *The Journal of experimental biology* **215**, 3603-3611.

[11] Duysens, J., Tax, A.A., Murrer, L. & Dietz, V. 1996 Backward and forward walking use different patterns of phase-dependent modulation of cutaneous reflexes in humans. *Journal of Neurophysiology* **76**, 301-310. (doi:10.1152/jn.1996.76.1.301).

[12] Collett, M., Graham, P. & Collett, T.S. 2017 Insect Navigation: What Backward Walking Reveals about the Control of Movement. *Current Biology* **27**, R141-R144. (doi:https://doi.org/10.1016/j.cub.2016.12.037).

[13] Zeil, J. & Wittmann, D. 1989 Visually controlled station-keeping by hovering guard bees ofTrigona (Tetragonisca) angustula (Apidae, Meliponinae). *Journal of Comparative Physiology A* **165**, 711-718.

[14] Schneider, P. 1981 Flugmanöver der käfer. *Mitteilungen der Deutschen Gesellschaft für Allgemeine und Angewandte Entomologie* **3**, 259-263.

[15] Bode-Oke, A.T., Zeyghami, S. & Dong, H. 2018 Flying in reverse: kinematics and aerodynamics of a dragonfly in backward free flight. *Journal of The Royal Society Interface* **15**. (doi:10.1098/rsif.2018.0102).

[16] Tiegs, O.W. 1955 The flight muscles of insects-their anatomy and histology; with some observations on the structure of striated muscle in general. *Philosophical Transactions of the Royal Society of London. Series B, Biological Sciences* **238**, 221-348. (doi:doi:10.1098/rstb.1955.0001).

[17] Bennet-Clark, H.C. & Daws, A.G. 1999 Transduction of mechanical energy into sound energy in the cicada cyclochila australasiae. *Journal of Experimental Biology* **202**, 1803-1817.

[18] Williams, K.S. & Simon, C. 1995 The Ecology, Behavior, and Evolution of Periodical Cicadas. *Annual Review of Entomology* **40**, 269-295. (doi:10.1146/annurev.en.40.010195.001413).

[19] BARTHOLOMEW, G.A. & BARNHART, M.C. 1984 Tracheal Gases, Respiratory Gas Exchange, Body Temperature and Flight in Some Tropical Cicadas. *Journal of Experimental Biology* **111**, 131-144.

[20] Kelleher, S.M., Habimana, O., Lawler, J., O' Reilly, B., Daniels, S., Casey, E. & Cowley, A. 2016 Cicada Wing Surface Topography: An Investigation into the Bactericidal Properties of Nanostructural Features. *ACS Applied Materials & Interfaces* **8**, 14966-14974. (doi:10.1021/acsami.5b08309).

[21] Wan, H., Dong, H. & Gai, K. 2015 Computational investigation of cicada aerodynamics in forward flight. *Journal of The Royal Society Interface* **12**, 20141116.

[22] Liu, G., Dong, H. & Li, C. 2016 Vortex dynamics and new lift enhancement mechanism of wing–body interaction in insect forward flight. *Journal of Fluid Mechanics* **795**, 634-651.

[23] Zeyghami, S., Babu, N. & Dong, H. 2016 Cicada (Tibicen linnei) steers by force vectoring. *Theoretical and Applied Mechanics Letters*. (doi:http://dx.doi.org/10.1016/j.taml.2015.12.006).

[24] OberdÖRster, U.T.A. & Grant, P.R. 2007 Predator foolhardiness and morphological evolution in 17-year cicadas (Magicicada spp.). *Biological Journal of the Linnean Society* **90**, 1-13. (doi:10.1111/j.1095-8312.2007.00702.x).

[25] Bode-Oke, A. & Dong, H. 2018 On the Backward Flight of a Cicada: Kinematics and Aerodynamics. *Bulletin of the American Physical Society*.

[26] Zhiwei, L., Xiaojun, Y., Mingjing, Q., Yangsheng, Z., Dawei, H., Xiaoyong, Z. & Liwei, L. 2017 Artificial insect wings with biomimetic wing morphology and mechanical properties. *Bioinspiration & Biomimetics* **12**, 056007.

[27] Ma, K.Y., Chirarattananon, P., Fuller, S.B. & Wood, R.J. 2013 Controlled Flight of a Biologically Inspired, Insect-Scale Robot. *Science* **340**, 603-607. (doi:10.1126/science.1231806).

[28] Pfau, H. 1991 Contributions of functional morphology to the phylogenetic systematics of Odonata. *Advances in Odonatology* **5**, 109-141.

[29] Wakeling, J. & Ellington, C. 1997 Dragonfly flight. II. Velocities, accelerations and kinematics of flapping flight. *Journal of experimental biology* **200**, 557-582.

[30] Ros, I.G., Bassman, L.C., Badger, M.A., Pierson, A.N. & Biewener, A.A. 2011 Pigeons steer like helicopters and generate down- and upstroke lift during low speed turns. *Proceedings of the National Academy of Sciences* **108**, 19990-19995. (doi:10.1073/pnas.1107519108).

[31] Wang, Z.J. & Russell, D. 2007 Effect of forewing and hindwing interactions on aerodynamic forces and power in hovering dragonfly flight. *Physical review letters* **99**, 148101.

[32] Ellington, C.P. 1999 The novel aerodynamics of insect flight: applications to micro-air vehicles. *Journal of Experimental Biology* **202**, 3439-3448.

[33] Bode-Oke, A., Zeyghami, S. & Dong, H. 2017 Aerodynamics and flow features of a damselfly in takeoff flight. *Bioinspiration & biomimetics* **12**, 056006.

[34] Koehler, C., Liang, Z., Gaston, Z., Wan, H. & Dong, H. 2012 3D reconstruction and analysis of wing deformation in free-flying dragonflies. *The Journal of experimental biology* **215**, 3018-3027.

[35] Mittal, R., Dong, H., Bozkurttas, M., Najjar, F., Vargas, A. & von Loebbecke, A. 2008 A versatile sharp interface immersed boundary method for incompressible flows with complex boundaries. *Journal of computational physics* **227**, 4825-4852.

[36] Li, C., Dong, H. & Zhao, K. 2018 A balance between aerodynamic and olfactory performance during flight in Drosophila. *Nature Communications* **9**, 3215. (doi:10.1038/s41467-018-05708-1).

[37] Hunt, J.C., Wray, A. & Moin, P. 1988 Eddies, streams, and convergence zones in turbulent flows. *Center for Turbulence Research Report CTR-S88*, 193–208.

[38] Brackenbury, J. 1995 *Insects in flight*, Blandford.

[39] Willmott, A.P. & Ellington, C.P. 1997 The mechanics of flight in the hawkmoth Manduca sexta. I. Kinematics of hovering and forward flight. *The Journal of Experimental Biology* **200**, 2705-2722.

[40] Hsu, S.-J., Thakur, N. & Cheng, B. 2019 Speed control and force-vectoring of bluebottle flies in a magnetically levitated flight mill. *The Journal of Experimental Biology* **222**, jeb187211. (doi:10.1242/jeb.187211).

[41] Grodnitsky, D.L. 1995 Evolution and Classification of Insect Flight Kinematics. *Evolution* **49**, 1158-1162. (doi:10.2307/2410440).

[42] Jantzen, B. & Eisner, T. 2008 Hindwings are unnecessary for flight but essential for execution of normal evasive flight in Lepidoptera. *Proceedings of the National Academy of Sciences* **105**, 16636-16640. (doi:10.1073/pnas.0807223105).

[43] Moore, T.E., Huber, F., Weber, T., Klein, U. & Back, C. 1993 Interaction between visual and phonotactic orientation during flight in Magicicada cassini (Homoptera: Cicadidae). *The Great Lakes Entomologist* **26**, 3.

[44] Caetano, J.V., de Visser, C.C., Remes, B.D., De Wagter, C., Van Kampen, E.-J. & Mulder, M. 2013 Controlled flight maneuvers of a Flapping Wing Micro Air Vehicle: a step towards the DelFly II Identification. In *AIAA Atmospheric Flight Mechanics (AFM) Conference* (p. 4843.

[45] Bomphrey, R.J., Taylor, G.K. & Thomas, A.L.R. 2009 Smoke visualization of free-flying bumblebees indicates independent leading-edge vortices on each wing pair. *Experiments in Fluids* **46**, 811-821. (doi:10.1007/s00348-009-0631-8).

[46] Zeyghami, S. 2015 Wing in the Loop: Integrating the Wing Into Dynamics of Insect Flight. Charlottesville, VA, University of Virginia, Department of Mechanical and Aerospace Engineering, PHD, 2015.

[47] Ellington, C. 1984 The aerodynamics of hovering insect flight. III. Kinematics. *Philosophical Transactions of the Royal Society of London B: Biological Sciences* **305**, 41-78.

[48] Ellington, C.P. 1984 The Aerodynamics of Flapping Animal Flight1. *American Zoologist* **24**, 95-105. (doi:10.1093/icb/24.1.95).

[49] Chen, D., Kolomenskiy, D., Nakata, T. & Liu, H. 2017 Forewings match the formation of leading-edge vortices and dominate aerodynamic force production in revolving insect wings. *Bioinspiration & Biomimetics* **13**, 016009. (doi:10.1088/1748-3190/aa94d7).

[50] Sato, M. & Azuma, A. 1997 The flight performance of a damselfly Ceriagrion melanurum Selys. *Journal of Experimental Biology* **200**, 1765-1779.

[51] Russell, D.B. 2004 Numerical and experimental investigations into the aerodynamics of dragonfly flight [PhD Dissertation], Cornell University.

[52] Azuma, A. & Watanabe, T. 1988 Flight performance of a dragonfly. *Journal of Experimental Biology* **137**, 221-252.

[53] Hefler, C., Noda, R., Shyy, W. & Qiu, H. 2017 Unsteady Vortex Interactions for Performance Enhancement of a Free Flying Dragonfly. In *ASME 2017 Fluids Engineering Division Summer Meeting* (pp. V01CT21A010-V001CT021A010, American Society of Mechanical Engineers.

[54] Meng, X. & Sun, M. 2016 Wing Kinematics, Aerodynamic Forces and Vortex-wake Structures in Fruit-flies in Forward Flight. *Journal of Bionic Engineering* **13**, 478-490. (doi:https://doi.org/10.1016/S1672-6529(16)60321-9).

[55] Willmott, A.P., Ellington, C.P. & Thomas, A.L. 1997 Flow visualization and unsteady aerodynamics in the flight of the hawkmoth, Manduca sexta. *Philosophical Transactions of the Royal Society B: Biological Sciences* **352**, 303-316.

[56] Aono, H. & Liu, H. 2006 Vortical Structure and Aerodynamics of Hawkmoth Hovering. *Journal of Biomechanical Science and Engineering* **1**, 234-245. (doi:10.1299/jbse.1.234).

[57] Young, J., Walker, S.M., Bomphrey, R.J., Taylor, G.K. & Thomas, A.L.R. 2009 Details of Insect Wing Design and Deformation Enhance Aerodynamic Function and Flight Efficiency. *Science* **325**, 1549-1552. (doi:10.1126/science.1175928).

Chapter 5

The reverse flight of the monarch butterfly *(Danaus plexippus)* is characterized by a positively loaded upstroke and postural changes.

5.1. Abstract

Here, we studied the backward flight of a butterfly using high-speed photogrammetry, three-dimensional reconstruction, and computational fluid dynamics simulations. Backward flight was characterized by body angles (>90º), with pitch-down and pitch-up motions in the downstroke and upstroke, respectively, and accompanied by the reversal of the aerodynamic functions of the half strokes in comparison to forward flight due to stroke plane reorientation via body postural adjustments. The upstroke dominated force generation providing weight support, while the downstroke generated horizontal force. An LEV was formed in both half strokes. The upstroke's LEV topology was consistent with a Class II LEV previously reported, albeit, during the downstroke in forward flight, and the LEV rested on the forewing's ventral surface. The LEV and large upstroke velocity increased the upstroke's contribution to the net force from 32% in forward to 60% in backward flight. Likewise, upstroke weight support increased from 8% to 85%. Despite different trajectories, body postures and force orientations in the global frame, the stroke plane was fixed to the body and the halfstroke-average forces in both forward and backward flight pointed in a uniform direction relative to the body, indicating that the helicopter model is used by butterflies for low-speed (-1 to 2m/s) flight.

Keywords: butterfly, backward flight, active upstroke, helicopter model.

5.2. Introduction

Under the influence of their ecosystem, volant insects use different techniques for aerial prowess via wing and body kinematics adjustments and deformations, varied wing shapes and configurations, and the use of aerodynamic mechanisms which are distinct in the translational and rotational phases [1-5]. Butterflies are among the most agile insects, having developed this ability to evade predators [6]. Butterflies have a low wing loading (bodyweight to wing area ratio), and with each wingbeat, they can cover substantial distances while changing their flight trajectory considerably. Their varied body motion is characterized by changes in abdominal deformation which has a rigid phase relationship with wing motion [7], and body orientation [8-10], the latter which affects the wing aerodynamics substantially on a half stroke basis.

The flapping frequency is low, and the time scales of flapping and body motion are similar (signified by high advance ratios in forward flight) [11]. Moreover, body rotations (particularly pitch) are exaggerated. Thus, both the body and wing motion of butterflies play pivotal roles in their flight performance in comparison to other insects, such as dragonflies, and so on. To inspire insect-like robots [12, 13] and to clarify the underlying physics of flight, several studies have evaluated the behaviors that delineate the flight envelope of butterflies such as hovering, takeoff, flap-gliding, forward, climbing, and turning flights [6, 9, 10, 14].

Ellington [15] described the novel use of a vertical stroke plane during the takeoff and hovering flight of a cabbage butterfly (*Pieris braisscae*) in a seminal work. The wings were strongly supinated in the upstroke (US), while large angles of attack (AoA) characterized the downstroke (DS). Accordingly, the vertical force was produced by pressure drag in the DS, signified by the shedding of a large vortex ring from the wingtips, while the US produced little force. Associated with the wing kinematics adjustments were alterations in the body kinematics whereby the thorax was horizontal and vertical in the DS and US, respectively. Sunada et al. [9] also arrived at similar conclusions as Ellington [15], by analyzing the aerodynamics, in addition to the kinematics, of a related species (*Pieris melete*). They showed that the variation of the body posture influences the stroke plane orientation and is the key mechanism in flight. The aerodynamic torques from the wings, which raise the thorax, and the moments generated by abdominal deflection to suppress thoracic motion, modulated stroke plane inclination.

Using smoke visualization under free-flight conditions, Srygley and Thomas [16], showed that butterflies (*Vanessa atalanta*) use unsteady aerodynamic mechanisms. However, butterflies could switch the wing aerodynamics either on a stroke by stroke basis or flight mode basis. The generation of large forces was signified qualitatively by the presence of a leading edge vortex (LEV), connected from tip to tip over the thorax (Class II LEV) during the DS. In some strokes, additional circulation was generated during the dorsal contact between the wings (‘clap and peel’), as well as during wake capture.

Using computational fluid dynamics (CFD) simulations, Zheng et al. [17] investigated the forward flight with constant inflow. For *Vanessa cardui*, they reported that wing deformation, especially wing twist, improves the lift to power ratio in flight. For a different species (*Kallima inachus*), Fei and Yang [18], studied the effect of transient body motion and noted that failing to consider the variation of flight speed within the stroke cycle may lead to an overestimate of lift or underestimate of the flight speed and thrust. They [8] also investigated the influence of body rotations and reported that in addition to stroke plane modulation, body rotations controlled the shed vortex ring orientation in each half stroke. Moreover, the initial body angle determined the obliqueness of flight from the horizontal.

A common denominator in the studies above was the dominance of the DS in force production. Since butterflies move their wing in a steeply inclined stroke plane in hovering and forward flight [11, 17, 19] the half stroke kinematics and forces are asymmetric [3, 15]. Butterflies generate 59-74% of the net aerodynamic forces during the DS, and the US is less dominant [17, 18, 20]. The DS is always aerodynamically active, whereas the US can switch between an active and inactive/near-inactive US [16]. The inactive US is zero (neutrally) loaded when the airstreams around the insect are undisturbed by the wing, and no substantial momentum is imparted to the flow. Feathering the US also reduces the force generated in that half stroke, and attached flows dominate [21, 22].

Conversely, if active, the US is either negatively (downward) loaded or positively (upward). The DS generates the force for weight support (due to its positively loaded nature) while the US provides the thrust force for flight (due to its negatively loaded nature). However, body postural changes can effect changes in wing function and aerodynamics as the authors have noted in previous work [23]. Nowhere in the literature has evidence been presented that the US (ventrodorsal stroke [3]) generates substantial forces for weight support of butterflies.

Here, we show that when the advance ratio (*J*) is negative ($J<0$; backward flight) that an active (lift generating or positively loaded) US is present, thus, providing new insight into the wing function and versatility of butterflies. Although the occurrence of backward flight has been observed among hawkmoths [24, 25], it has not been documented among butterflies hitherto. Moreover, the mechanics and aerodynamics of backward flight are unknown for any Lepidoptera species. Backward flight was appropriated for takeoff from walls/vertical surfaces, 'normal' and accelerating flight, obstacle avoidance, turning, and escape response by the monarch butterfly (*Danaus plexippus*) in the laboratory. Nectar-feeding volant organisms may use backward flight to render immediate turning after feeding unnecessary [3, 26]. We are interested in understanding the techniques of force generation in the backward flight of butterflies, viz., the aerodynamic functions of the half strokes, the role of the wing pairs, and the importance of body motion in the overall flight performance. Also, we are interested in the kinematic changes or trends that may differentiate backward flight from other flight modes. To this end, we extracted quantitative data (both transient body motion [18] and wing deformation [17]) from the three-dimensional surface reconstruction of high-speed videos. Afterward, a high-fidelity CFD solver was used to compute flight forces and flow features.

5.3. Material and methods

5.3.1. Insects, experimental setup and three-dimensional (3-D) surface reconstruction

The monarch butterfly (*Danaus plexippus*) was selected because of its availability. We captured monarchs outside during the summer and transported them to the lab for video capture. The insects were placed in a filming area comprising of a takeoff platform, and two sidewalls and flight was initiated voluntarily (Figure 5.1(a)). We did not train the butterflies to fly backward. We used three high-speed cameras (Photron Fastcam SA3 60K; Photron USA, Inc., San Diego, CA) arranged orthogonally and recording 1000 frames per second with 1024x1024 pixels. Backward flight naturally ended when the insect by transitioned to another flight mode or by coming to rest in the shooting area. We captured multiple sequences for an individual whose morphological parameters are documented in Table 5.1. After motion capture, 3-D reconstruction was performed in Autodesk Maya using a template-based technique [27]. The template comprised of a body and wings which were matched to the high-speed images by following the patterns on the butterfly's wings as well as body deformations (Figure 5.1(c)).

Table 5.1. Morphological parameters. Wing parameters are reported for one wing. Length and mass measurements uncertainties are ±1mm and ±1mg, respectively.

body mass (mg)	body length (mm)	forewing length (mm)	forewing area (mm^2)	hindwing length (mm)	hindwing area (mm^2)
500	35	51	800	35	753

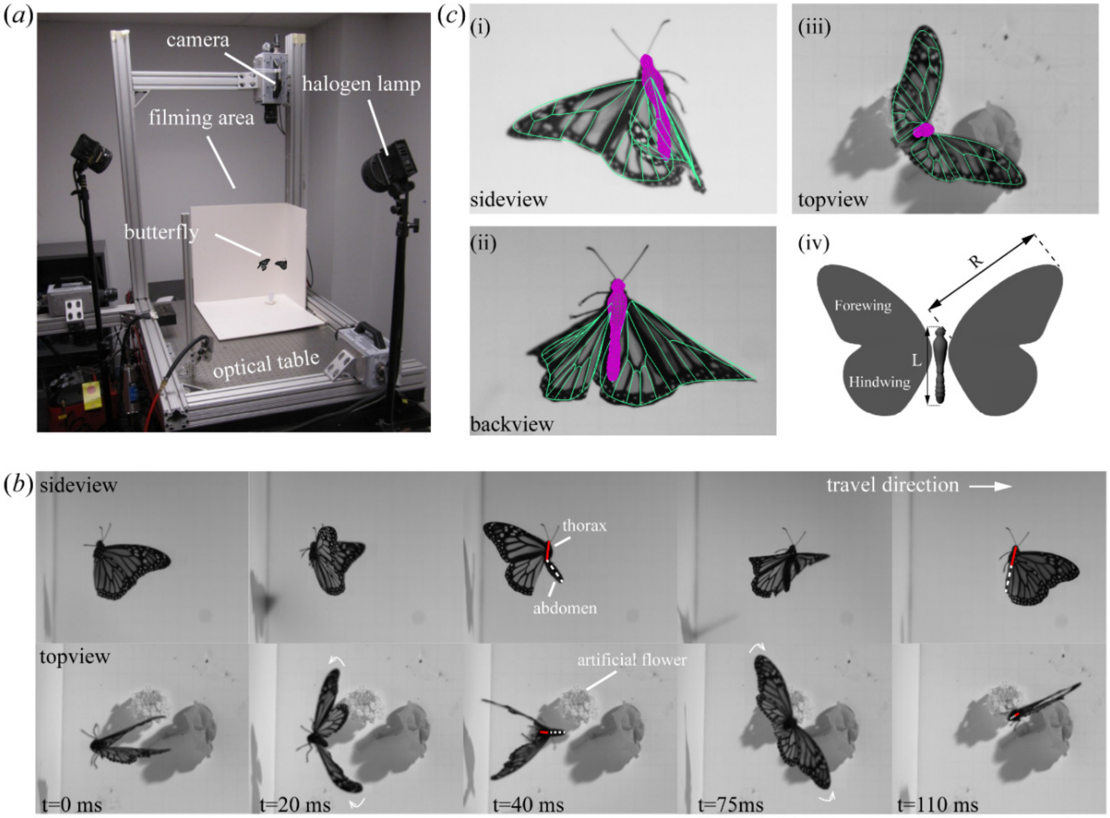

Figure 5.1. Butterfly in backward flight (a). Experimental set-up. (b) Montage of a typical stroke. (c) (i-iii) Template based reconstruction. (iv) Morphological parameters labeled on an anecdotal butterfly.

5.3.2. Kinematics definitions

A coordinate system was placed at the wing root, and the wing kinematics were measured relative to the mean stroke plane. The stroke plane relative to body (β_b) was calculated relative to the longitudinal axis ($\hat{e}_1$) which is the line connecting the head and hinge point of the abdomen. The Euler angles, flap (ϕ), deviation (θ), and pitch (ψ), denote the rigid wing orientation in the mean stoke plane (Figure 5.2 (a)). ϕ is the back and forth motion of the wing. θ is the angle between the wing and its projection on the stroke plane. ψ is the angle between the wing chord and the mean stroke plane, ψ_{DS} is less than 90º. The effective AoA (α_{eff}) is the angle between the wing chord and the vector sum of the body and wing velocities (Figure 5.2(b)). J is the ratio of the body to wing velocity and negated to indicate backward flight. *Vis-à-vis* body kinematics, the abdominal angle (θ_{t}) is the angle between $\hat{e}_1$ and the abdomen's tip. The dominant frequency of both the body and wing angles were computed using the fast Fourier transform (FFT) in Tecplot 360 (Tecplot, Bellevue, WA).

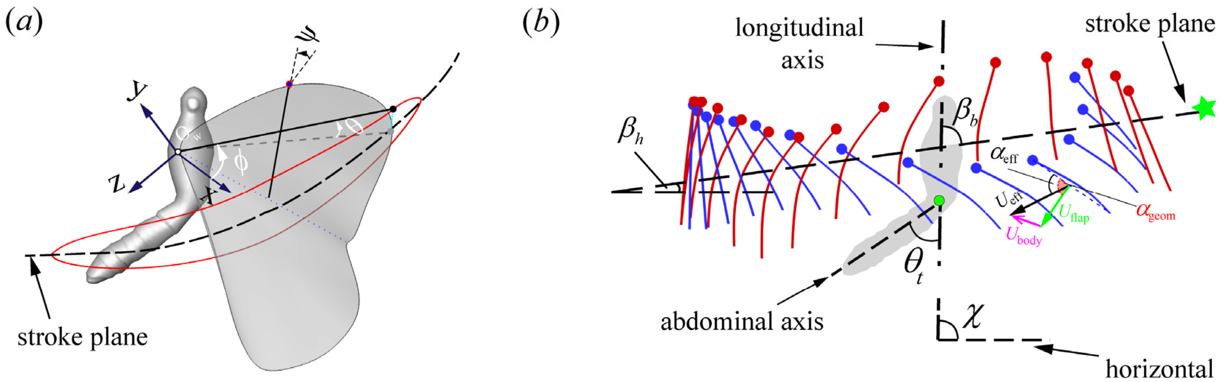

Figure 5.2. Kinematics quantification. (a) Wing Euler angle definitions. (b) Additional kinematics definitions. Green star denotes the front end of the stroke plane. Symbols definitions are found in the text.

5.3.3. Computational fluid dynamics simulation set-up

We used an in-house immersed boundary method CFD code. A detailed exposition on the algorithm has been published [28] with validations [29]. The incompressible Navier-Stokes equation (Eqn. (1))

$$\nabla \cdot \mathbf{u} = 0; \quad \frac{\partial \mathbf{u}}{\partial t} + \mathbf{u} \cdot \nabla \mathbf{u} = -\frac{1}{\rho}\nabla p + \upsilon \nabla^2 \mathbf{u}, \qquad (7)$$

where $\mathbf{u}$ is the velocity vector, ρ is the density, υ is the kinematic viscosity and p is the pressure, was solved using a finite difference method with 2nd order accuracy in space and a fractional step method for time-stepping. The momentum equation was solved using a second-order Adams-Bashforth scheme for the convective terms and an implicit Crank–Nicolson scheme for the diffusive terms. The simulation domain size was 30R x 30R x 30R, and the size of the dense regions was selected based on the range of the motion of each butterfly trajectory and designed to resolve the vortex structures (Figure 5.3). The domain boundary conditions (BC) of both the pressure and velocity were homogeneous Neumann BC, i.e., zero gradient. The Reynolds number was defined as $Re = \frac{\overline{U}R}{\upsilon}$, where $\overline{U}$ is the body speed, and R is the forewing (FW) length, following Kang et al. 's [10] work. Re ranged between 1700 and 3300. A grids refinement study is shown for a stroke in one of the flight sequences in this study. The fine grids were deemed sufficient for our following analyses.

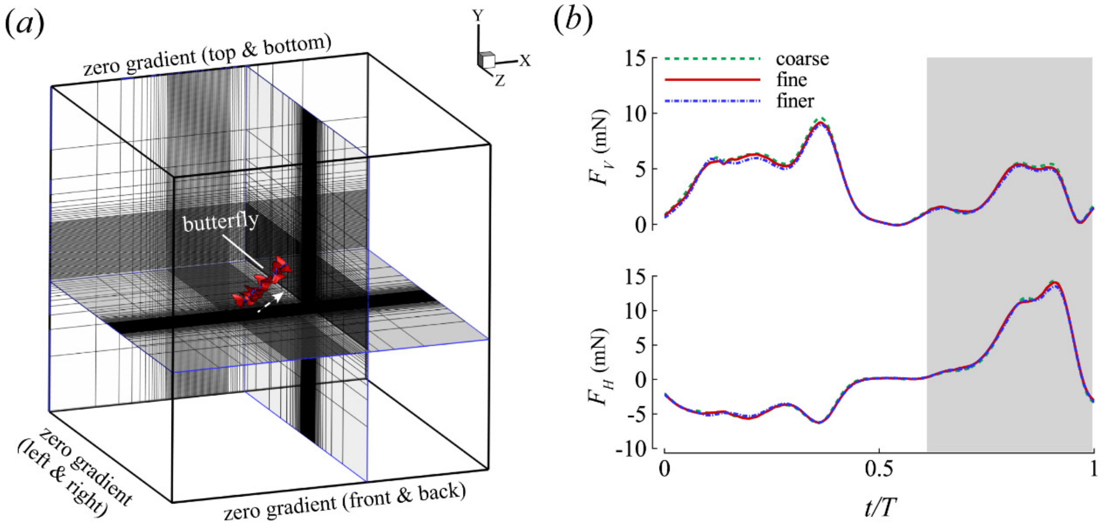

Figure 5.3. Computational setup. (a) Sample of background mesh-grids used for the CFD simulation coarsened five times in each direction. (b) CFD grid refinement.

Table 5.2. Force coefficients for three different mesh set-ups.

	meshes	$\overline{F}_V$	$F_{V_{max}}$	$\overline{F}_H$	$F_{H_{max}}$
coarse	217x265x169	4.18	9.59	-0.81	14.2
fine	281x345x217	4.08	9.17	-0.86	14.1
finer	385x353x241	3.95	8.95	-0.86	13.5

5.4. Results

5.4.1. Kinematics

5.4.1.1. Body kinematics

The body kinematics are reported in Figure 5.4 and Table 5.4. As expected, the flight trajectories greatly varied from horizontal to oblique backward flight (Figure 5.4(a)). By way of example, the body angles and velocities during some of the flight sequences are displayed in Figure 5.4(b) and (c), respectively.

A steep body posture was maintained throughout the flight, and body motion was characterized by substantial abdominal and body rotations within each wing beat. The mean body angles ($\overline{\chi}$) measured during the DS were less the US's by about 10º indicating that the body pitched-down and pitched-up during the DS and US, respectively. In contrast to the body rotation, the abdomen pitched-up, and pitched-down in the DS and US, respectively, with $\overline{\theta}_t$ of 50º. Both the body (n_b) and tail (n_t) frequencies were less than 15Hz and sometimes had the same value. However, the tail and wing (n_w) frequencies were more closely linked. The gray shadings denoting the DS in Figure 5.4(b) usually coincided with the tail but not necessarily with the body. The body pitching motion led the wing motion by about 40º-60º (see Figure 5.4(b-i,iii), and Table 5.3) whereas the wings and tail moved out of phase by approximately 180º (Table 5.3). The butterflies flew with speeds typically less than 1 m/s, which varied on a half stroke basis (Figure 5.4(c)). During the DS, the backward velocity increased while the vertical velocity decreased. The reverse occurred during the US.

Table 5.3. Body kinematics. $\varphi_{b,w}$ and $\varphi_{t,w}$ are the phase shifts between the body and wing flapping angle, and tail and wing flapping angle, respectively, and calculated only when the frequencies of the two parameters were similar. ID is the trajectory number in Figure 4(a). *-escape maneuver. Other symbol definitions are found in the text.

ID	duration (ms)	$\bar{\chi}$ (°)	$\bar{\chi}_{\mathrm{DS}}$ (°)	$\bar{\chi}_{\mathrm{US}}$ (°)	$\bar{\theta}_{\mathrm{t}}$ (°)	n_{b} (Hz)	n_{t} (Hz)	$\varphi_{\mathrm{b,w}}$	$\varphi_{\mathrm{t,w}}$
1	440	85	82	87	51	10.2	9.09	44.6	181.4
2	301	106	100	111	51	7.01	9.97	--	199.0
3*	147	119	116	133	28	6.81	13.6	--	--
4	270	99	91	103	42	7.41	7.41	39.6	142.5
5	190	107	103	112	43	5.24	15.7	--	--
6	220	108	100	114	60	9.09	9.09	59.0	157.4
7	290	108	103	114	56	3.44	10.3	--	191.6

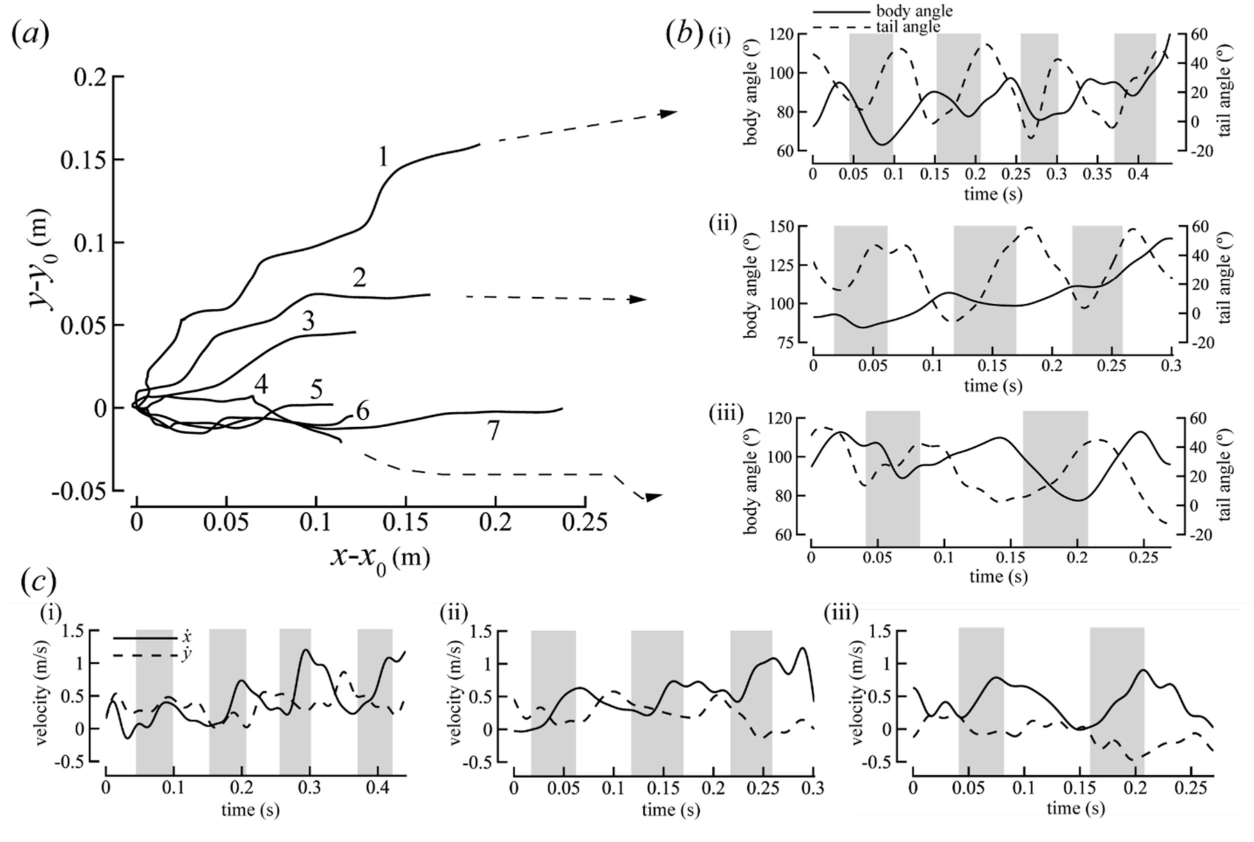

Figure 5.4. Body kinematics. (a) Flight trajectories of the flight sequences. (b) Body and tail angles. (c) Flight velocities. Gray shadings denote the DS.

5.4.1.2. Wing kinematics

The wing kinematics of the left and right wings were averaged. The time histories were presented in Figure 5.5 and summarized in Table 5.4. β_{b} was approximately perpendicular to $\hat{\mathrm{e}}_{\mathrm{l}}$. The stroke plane angle relative to the horizontal (β_{h}) was inclined (<40º), with the front end being above the horizontal (see star symbol in Figure 5.2(b)). β_{h} was more inclined during the US than in the DS (>10º) as a result of $\bar{\chi}$ being higher by about 10º in the US (Table 5.3). The US-to-DS duration ratio (US:DS [11]) varied among flights, but the US duration was usually longer than the DS's. Likewise, the US velocities were larger.

The wings flapped with large amplitudes (approximately 130º) and with high pitch angles ψ in both half strokes (Figure 5.5). ψ_{US} differed between the proximal location (0.25R) and distal location (0.75R) indicating that the wings were twisted. α_{eff} was measured at the same locations as ψ. In general, the proximal effective AoA ($\alpha_{\mathrm{eff,p}}$) was larger than the distal effective AoA ($\alpha_{\mathrm{eff,d}}$) in the US similar to ψ, while the reverse trend occurred in the DS. Both ψ and α_{eff} were larger in the DS.

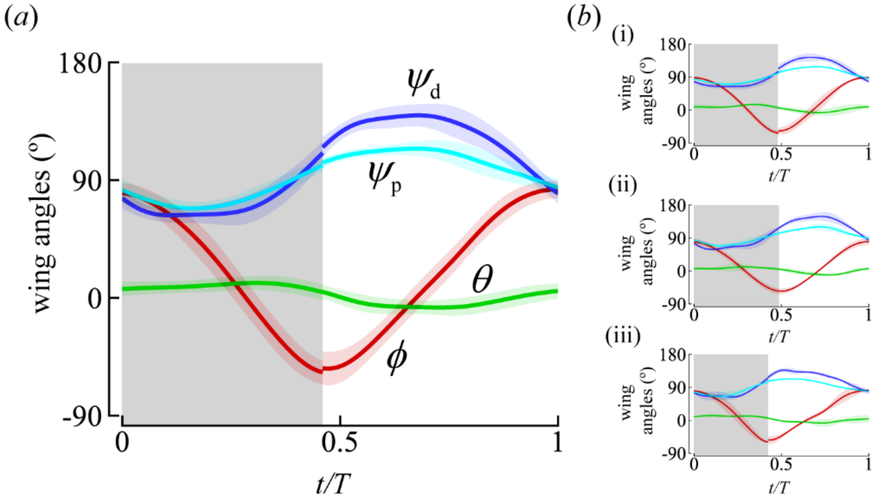

Figure 5.5. Wing kinematics. (a). Pooled mean ± standard deviation (SD; shaded) of the wing angles from all flights (b) Mean ± SD for selected sequences (see Figure 5.4(b,c)). A discontinuity exists due to the half stroke averaging process (see Ros et al. [30] for a similar artifact).

Table 5.4. Wing kinematics parameters. *-escape maneuver

ID	J	$\bar{\mathrm{U}}_{\mathrm{b}}$ (m/s)	US:DS	$\left(\bar{\mathrm{U}}_{\mathrm{US}}/\bar{\mathrm{U}}_{\mathrm{DS}}\right)^2_{\mathrm{eff}}$	$\bar{\beta}_{\mathrm{b,DS}}$ (°)	$\bar{\beta}_{\mathrm{b,US}}$ (°)	$\bar{\beta}_{\mathrm{h,DS}}$ (°)	$\bar{\beta}_{\mathrm{h,US}}$ (°)	n_{w} (Hz)	Φ (°)	$\alpha_{\mathrm{eff,p}}$ (°)		$\alpha_{\mathrm{eff,d}}$ (°)	
											DS	US	DS	US
1	0.29	0.44	1.07	1.33	82	82	0	5	9.08	148	44	41	53	37
2	0.28	0.54	1.06	1.62	85	85	16	26	9.97	135	44	41	58	33
3*	0.28	0.83	0.82	--	--	--	--	--	13.6	142	--	--	--	--
4	0.27	0.42	1.36	0.96	87	83	4	20	7.41	142	85	65	72	51
5	0.30	0.57	0.85	1.71	78	78	25	35	10.6	115	44	54	56	42
6	0.29	0.54	1.45	1.04	86	83	14	32	9.06	144	69	53	67	44
7	0.40	0.82	1.25	1.39	85	82	18	32	10.3	132	55	49	58	39

5.4.2. Aerodynamic force and power

The aerodynamic force was obtained from integrating the pressure and shear stress on the wing. The aerodynamic power is defined as $p_{\mathrm{aero}} = -\iint (\vec{\sigma} \cdot \vec{n})\vec{u}\, ds$ where $\vec{\sigma}$ is the stress tensor, $\vec{u}$ is the velocity of the fluid adjacent to the wing, and $\vec{n}$ and ds are the unit normal and area of each element, respectively. The muscle-mass specific aerodynamic power is $p^*_{aero} = p_{aero}/M_{\mathrm{m}}$, and the muscle mass (M_{m}) is 30% of the body mass [31]. Before reporting the wing forces, we performed a force balance based on the motion of sequence 1 (Figure 5.4(a)). The mean vertical force ($\bar{\mathrm{F}}_{\mathrm{V}}$) was estimated from body motion:

$$\bar{\mathrm{F}}_{\mathrm{V}} = \mathrm{m}(\bar{\mathrm{a}}_{\mathrm{v}} + \mathrm{g}), \tag{8}$$

where m is the body mass, g is the acceleration due to gravity (9.81 m/s^2) and $\bar{\mathrm{a}}_{\mathrm{V}}$ is the average upward acceleration (0.8 m/s^2) obtained from the time derivative of the body velocity (Figure 5.4(c, i)). $\bar{\mathrm{F}}_{\mathrm{V}}$ was 5.3mN (1.08 x bodyweight), which was similar to the result obtained from the CFD simulation (5.3mN, 1.08 x bodyweight, Table 5.5)

Across the flight sequences, the DS generated horizontal forces primarily but also vertical force in some of the strokes and negative lift at times. The US produced vertical forces for weight support primarily but also generated forward horizontal forces (drag). The forward force reduced the backward impulse of the DS but not enough to prevent backward flight (Figure 5.6(b)). p^*_{aero} ranged between 63 and 121 W/kg, which was within the scope of values measured for forward flight [17].

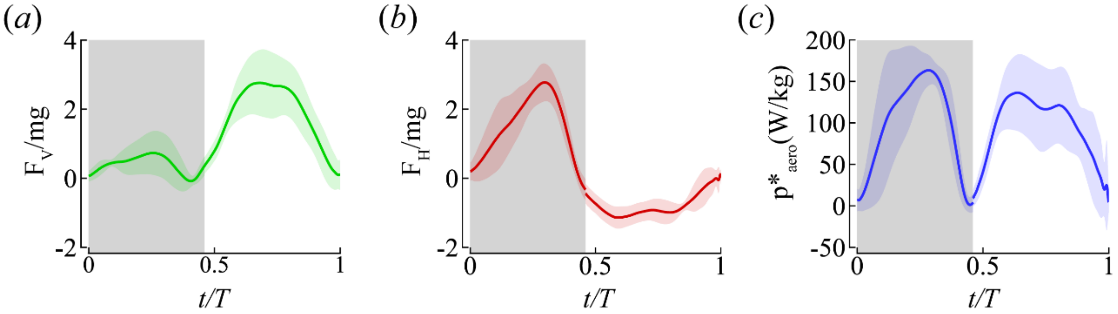

Figure 5.6. Force production and aerodynamic power. Pooled mean ± SD (shaded). Gray shading denotes the DS.

5.4.3. Force orientation

In the global frame, the halfstroke-average aerodynamic force vectors are presented in the X-Y plane (Figure 5.7(a)). The DS-average ($\overline{F}_{DS}$) pointed backward (+X direction) and upward (+Y direction), while the US-average forces ($\overline{F}_{US}$) pointed upward and forward (-X direction). The angle between the force and -X direction is denoted as γ. $\bar{\gamma}_{DS}$ and $\bar{\gamma}_{US}$ were 166° and 64°, respectively.

Figure 5.7(b) shows the force orientation relative to $\hat{e}_1$. Despite the different trajectories in the global frame (Figure 5.4(a)) and large variation of the force orientation in the global frame (Figure 5.7(a)), the force vectors were clumped up in a consistent direction during each half stroke. The angle between the force and $\hat{e}_1$ is denoted as ξ. The half stroke forces were only produced in the anterior side of the body (half-disk from 90° to -90°, clockwise; Figure 5.7(b)). Furthermore, the forces in dorsoventral stroke (downstroke) were produced in the dorsal side (half-disk from 0° to 180°, counterclockwise), with the major component pointing toward $\hat{n}$ ($\bar{\xi}_{DS}$=68°). The forces produced in the ventrodorsal stroke (upstroke) were produced in the ventral side (half-disk from 0° to 180°, clockwise), pointing in between the longitudinal axis and dorsoventral axis ($\bar{\xi}_{US}$=-43°). The range of variation of the mean force vector relative to the body among flight sequences was 15° (DS), and 13° (US) was within the scope of values (±20°) recorded for biological fliers as well as helicopters, that appropriate force vectoring [30].

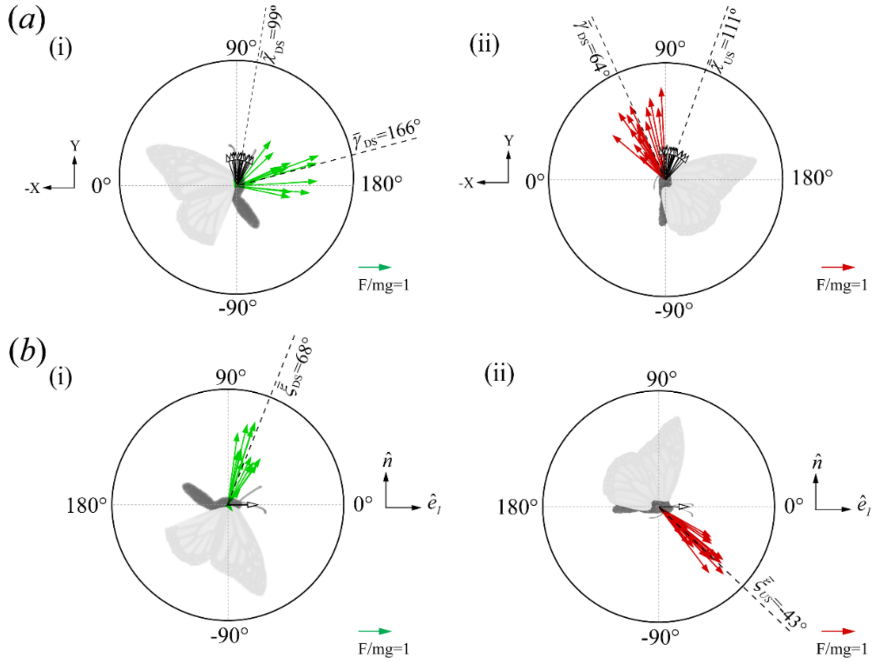

Figure 5.7. Force orientation. (a) Halfstroke-average force in the global frame (measured relative to -X) (i) downstroke (ii) upstroke. (b) Halfstroke-average force relative to $\hat{e}_1$, (i) downstroke, (ii) upstroke. Dashed lines denote average values. Black vectors with white arrowhead – body longitudinal axis, red vectors- upstroke forces, green vectors- downstroke forces.

Table 5.5. Force magnitude, orientation, and muscle-mass specific power consumption. 3* was excluded.

ID	$\bar{F}_{DS}$	$\bar{F}_{US}$	$\bar{F}_{V,DS}$	$\bar{F}_{V,US}$	$\bar{\gamma}_{DS}$	$\bar{\gamma}_{US}$	$\bar{\xi}_{DS}$	$\bar{\xi}_{US}$	p^*_{aero}
							(°)	(°)	(W/kg)
1	1.70	1.69	0.88	1.28	146	50	64	-37	85.3
2	1.90	2.24	0.35	2.06	171	74	70	-38	100.4
4	1.46	1.35	0.58	1.05	156	53	65	-50	62.9
5	1.34	2.59	-0.03	2.32	177	72	64	-41	107.0
6	2.11	2.33	0.35	2.04	168	65	68	-49	120.8
7	1.75	2.22	0.22	2.03	175	72	79	-42	98.7

5.4.4. Three-dimensional flow features

We elucidated the flow features around the butterfly using the isosurface of the Q-criterion. The evolution of the flow features over a representative stroke is shown for sequence 1 (Figure 5.8).

An LEV was formed following the separation of the wing pairs at the start of the DS (Figure 5.8(a,i)). The LEV, which is characterized by low-pressure regions around the leading edge of the wing, grew and remained attached on the wing surface for most of the stroke, shedding only at wing reversal. The LEV fed into a strong tip vortex. The LEV was present on the FW but absent on the HW. Attached vortex structures could be seen on the periphery of the HW, but their contribution toward force production may not substantial.

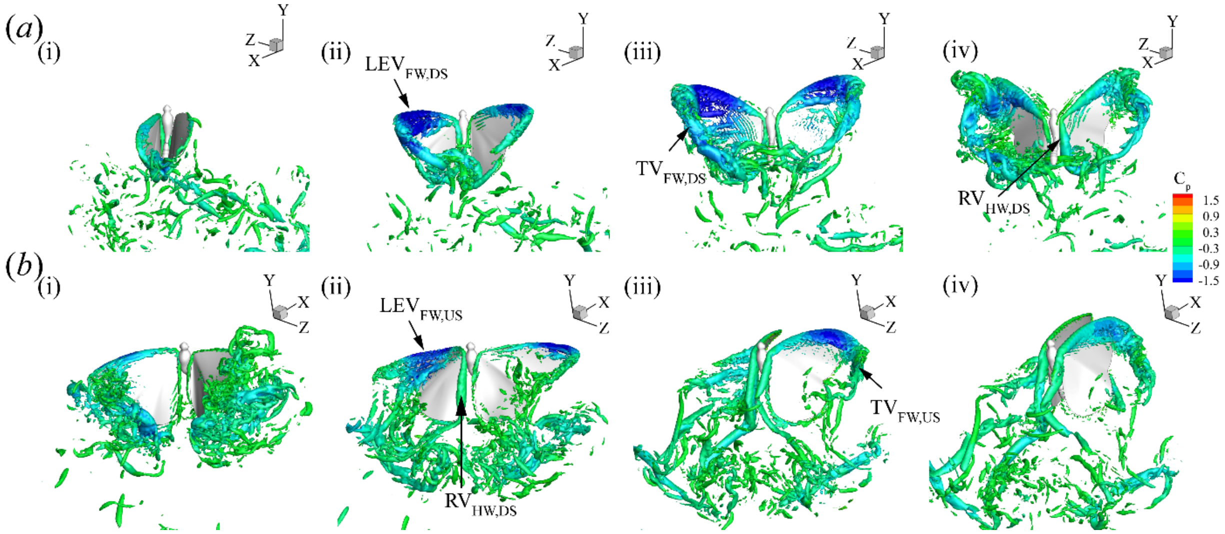

Figure 5.8. Flow structures in a selected stroke. The Isosurface of Q (Q=1600) is colored by non-dimensional pressure. (a) Top row (i-iv) is the DS flow at t/T=0.13,0.25,0.38,0.48, respectively. (b) Bottom row (i-iv) is the US flow at t/T=0.63,0.75,0.88,0.98. The flow is colored by the coefficient of pressure ($C_p = (p - p_\infty)/0.5\rho\bar{U}_{\text{eff}}^2$). TEV-trailing edge vortex; TV-tip vortex. RV- root vortex. FW-forewing, HW-hindwing.

The simulation (Figure 5.8) was performed similarly to Zheng et al. [17] in that only the wings were simulated. However, when the body was placed in the simulation of one of the flight sequences (sequence 4, Figure 5.9(a,ii)), the LEV extended from tip to tip across the thorax in the US and resembled a Class II LEV [32], albeit in the US. The root vortices disappeared, and the flow that otherwise would have been lost was harnessed by the body, forming the LEV on the thorax (Figure 5.9(b)). Both Figure 5.8(a) and Figure 5.9(a), show a strong interaction between the wing pairs, which could potentially enhance force production. Nonetheless, true 'clap and peel' was only observed in one stroke in sequence 4.

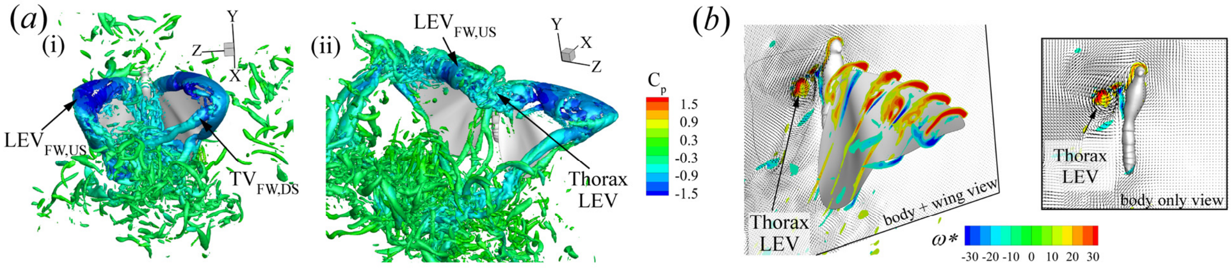

Figure 5.9. Mid-stroke flow structures of sequence 4 (a) 3D flow at (i) mid-DS and (ii) mid-US (b) 2D slices at mid-US to elucidate the LEV that runs across the body (Class II LEV). Contours of non-dimensional spanwise vorticity and velocity vectors are shown.

5.4.5. Fore and hindwings contribution to force generation

Butterfly wing motion is driven by the action of the FWs, although both wing pairs are well developed. The HW of the monarch contributes 52% of the total wing area [6, 12]. During flight, the wings pairs are uncoupled but overlap effectively acting as a single airfoilHere we investigate the contribution of each wing pair to the force production in backward flight by simulating an FW only (FO) and the FW+HW (ALL) case. The HW only (HO) case is not simulated to prevent flow separation at the HW's leading edge, which is improbable under most free flight conditions (Figures 5.8 and 5.9). The time histories are shown in Figure 5.10. The FW contributed about 65% of the net forces for flight and generated 70-80% of weight support in the flight sequences reported in Figure 5.10. The HW helped with both vertical and backward force production but also increased the drag force produced in the US.

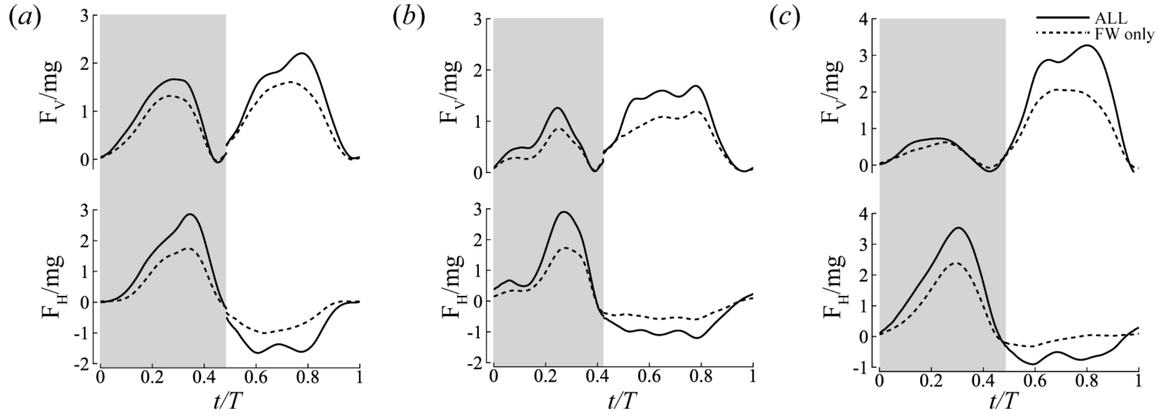

Figure 5.10. Contribution of the fore and hindwings to force production. The mean forces of all complete half stroke are plotted.

5.5. Discussion and conclusion

As a means of examining the wing half stroke function and aerodynamics of butterflies, we investigated a previously uncharacterized flight mode. Backward flight was used for retreating from walls, for 'normal' and accelerating flight, obstacle avoidance, turning, and as an escape response. Among nectar-feeding Lepidopterans, short backward flight had been previously observed in hawk moths; *Manduca sexta* [25, 33] and *Macroglossum stellatarum* [24]. Uncontrollable backward flight was elicited when the flagella of the antenna were severed, while controlled backward flight occurred in response to visual cues [24, 33]. Here, the backward flight of the Monarch was self-motivated without visual cues or alteration to the sensory organs. We discuss our findings in light of the current literature.

In the flight sequences captured, backward flight was accomplished by maintaining a steep body posture which oscillated around a mean value that was greater than 90º. However, not all the flights involved large-amplitude pitching of the body (see Figure 5.4(b)). $\bar{\chi}_{\mathrm{DS}}$ was about 10º less than $\bar{\chi}_{\mathrm{US}}$. Likewise, for hovering[15], takeoff [9], climbing[10], and forward flight [18], $\bar{\chi}$ was less during the DS. The steep body angle technique for backward flight is shared among vastly different organisms; hummingbirds (50-75º) [34], dragonflies (85-95º[23]; 100º[35]) waterlily beetles (50-70º) [36], cockchafer beetles [37] and cicadas (86-130º; Bode-Oke and Dong, under review), although without the high-amplitude body rotations, and indicates that body postural adjustments are necessary for reverse flight for different flying species.

A steep body angle, however, does not indicate that every time a butterfly assumes that posture, it flies backward. Monarchs appropriate a steep posture (mean: 65º; min: 31º, max: 85º) in steep vertical climbs (A. T. Bode-Oke, unpublished data). Leaf butterflies (*K. inachus)*, also possess large χ (60°-90º) in forward flight. *K. inachus* relies on drastic body rotation in each half stroke so that the forward (thrust) force of the US counteracts the backward (drag) force of the DS, to preclude backward flight.

Body rotations have been reported to perform the function of wing rotation due to reduced wing degrees of freedom of a butterfly [8, 38]. Although substantial body oscillation occurred in backward flight with $\Delta\bar{\chi} < 25^{\circ}$ (Figure 5.4(b, i)), large body rotation in each half stroke was not necessary (Figure 5.4(b, i)). Thus, effecting wing rotation using the body motion only, as previously described [8, 38] may not completely characterize the backward flight of the monarch since the monarch can supinate the FWs to an extent (Figure 5.5 and Figure 5.2(b)). Instead, the US is characterized by wing supination and a pitch up motion of the body to aid the wings. It is also interesting to note that body rotation leads the wing motion (Figure 5.4(b)), which may also signify the importance of body motion on the wing motion.

Table 5.6. Relevant parameters of the forward flight of the monarch.

ID	J	$\bar{U}_b$ (m/s)	US:DS	$\bar{\chi}_{DS}$ (º)	$\bar{\chi}_{US}$ (º)	$\bar{\beta}_{b,DS}$ (º)	$\bar{\beta}_{b,US}$ (º)	$\bar{\beta}_{h,DS}$ (º)	$\bar{\beta}_{h,US}$ (º)	$\bar{\theta}_t$ (º)	n_w (Hz)	n_b (Hz)	n_t (Hz)	Φ (º)	$\alpha_{eff,d}$ (º)		ξ (º)	
															DS	US	DS	US
1	0.90	1.75	0.61	24	32	93	93	69	61	15	9.92	9.91	9.91	110	28	30	**77**	-66
2	0.42	0.91	0.65	40	61	78	91	38	30	14	9.92	9.91	9.91	129	52	37	69	-32

Comparing backward to forward flight kinematics listed in Tables 5.6 and 5.7, both Φ and n were similar to both forward and climbing flight values. Likewise, $\bar{\beta}_b$ was comparable, indicating that there was no substantial change in its inclination though the flight modes are distinct in terms of wing aerodynamic function and body posture. The effect of fixed $\bar{\beta}_b$ influenced the force orientation and is discussed later. Backward flight was slower than forward flight (approximately 1-2m/s, Table 5.6) and also occurs at low speeds for other fliers; 1 m/s for dragonflies [23], cicadas and Delfly II MAV [39], 1.5m/s for bumblebees [40], and 2 m/s for hummingbirds [26]. The upper limit of backward flight speeds in the wild is still unknown for any animal.

Table 5.7. Forward versus backward flight of the butterfly. $\bar{F}$ is normalized by body weight. †See Table 1 in [11] for the species information. Dudley's [11] data is the only result based on quasi-steady aerodynamic analysis.

flight mode	species	J	$\bar{U}_b$ (m/s)	$\bar{\chi}$ (º)	β_b (º)	β_h (º)	US: DS	Φ (º)	$\bar{F}_{DS}$	$\bar{F}_{US}$	$\bar{F}_{V,DS}$	$\bar{F}_{V,US}$	ξ_{DS} (º)	ξ_{US} (º)	p^*_{aero} (W/kg)	reference
forward	*Vanessa cardui*	0.4	1.14	6	85	79	0.77	120	2.46	1.16	2.37	-0.87	85	-56	120.7	Zheng et al. [17]
	Kallima inachus	0.5	0.7	77	--	--	1.0	115	3.02	2.10	1.93	-0.03	69	-85	--	Fei and Yang [18]
	†	0.4 – 2.0	0.55–3.16	3–32	83	67	0.5-1.35	61–144	--	--	0.97–1.41	--	--	--	--	Dudley [11, 41]
	Parantica sita	1.2	1.6	28	--	--	1.0	92	2.27	0.74	2.19	0.23	55	-33	--	Yokoyama et al. [20]
	Danaus plexipus	0.4	0.91–1.75	27–51	90	63	0.6	103	2.35–2.42	1.05–1.17	2.14–2.27	-0.03–0.45	69-77	-32–-66	65.0–86.9	current study
backward	*Danaus plexipus*	-0.3 – -0.4	-0.44–-0.83	85–119	83	19	0.82-1.45	115-148	1.34–2.11	1.34–2.59	-0.03–0.88	1.05-2.32	64-79	-37–-50	62.9–120.8	current study

Comparing backward flight of butterflies to those of other insects indicates similarities in kinematics. The US duration is longer than the DS, likewise the effective velocities (Table 5.8 and [23]). Whereas α_{eff} is slightly lower in the US. The higher US velocity compensates for the lower US AoA. $\bar{\beta}_{\mathrm{h}}$ is smaller than angles recorded for dragonflies and cicadas. Because butterfly $\bar{\beta}_{\mathrm{b}}$ is higher than those other fliers, a higher body angle has to be appropriated to achieve similar force partition in both half strokes as those insects, for example, dragonflies. Even with the larger χ substantial forward force was produced in the US due to the inability to supinate the whole (fore + hind) wing (Figures 6(b) and 5). Supination may aid the FWs to have more directional control of the forces than the hindwings (HWs). If χ is too large, the flight may become uncontrollable.

Butterflies can generate as much as six times the body weight during the DS in forward and climbing flight [14, 17, 18]. During the US, however, the butterfly generates little to no vertical force in forward flight [8]. If any lift, the US generates negative lift (see Table 4.5). Negative lift result from the inability to supinate the whole wing completely in a steeply inclined stroke plane. The US net forces are also smaller compared to the DS; a consequence of the steep stoke plane which induces a force asymmetry, and also wing feathering. When large forces are produced in the US in forward flight, the forces are generated to counteract the drag generated during the DS. This is particularly common in species such as *K. inchus* that maintain large body angles in the DS (approximately 70°) [18].

Our results indicate that peak vertical force in backward flight was about three times the body weight (Figures 5.8 and 5.9). The US produced vertical forces primarily while the DS generated horizontal (backward) force primarily. Negative lift was rare, and when it occurred, it occurred during the DS (Figure 5.7(a,i) and Table 5.5). On average, the US force was higher than the DS's. The wing AoA was substantial in both half strokes (Table 5.4) and sufficient to form an LEV. Although the US AoA was lower than the DS's, the US wing velocity was higher.

Table 5.8. Backward flight of different organisms in free flight. α_{eff} is measured at 0.75R.

animal	$-J$ (°)	$\bar{\mathrm{U}}_{\mathrm{b}}$ (m/s)	$\bar{\chi}$ (°)	β_{b} (°)	β_{h} (°)	US:DS	$\alpha_{\mathrm{eff,DS}}$ (°)	$\alpha_{\mathrm{eff,US}}$ (°)	$\bar{\mathrm{F}}_{\mathrm{DS}}$	$\bar{\mathrm{F}}_{\mathrm{US}}$	reference
cockchafer beetle	--	-1.2	101	--	--	--	--	--	--	--	Schneider [37]
hummingbird	0.3	-1.5	51–75	57–71	-15–6	0.93–1.14	--	--	--	--	Sapir and Dudley [26]
dragonfly	0.3	-1.0	90	35	47	1.15 1.20	25 27	21 27	1.4 2.1	2.2 3.2	Bode-Oke et al. [23]
cicada	0.2	-1.0	107-122	69–73	37–46	0.94-1.05	40-41	34-36	2.9-3.1	2.4-3.0	Bode-Oke et al. (under review)
waterlily beetle	--	--	50–70	40–50	0–30	--	--	--	--	--	Mukundarajan et al. [36]
delfly II	--	-1.0	70–100	--	--	--	--	--	--	--	Caetano et al. [39]
butterfly	0.3–0.4	-0.4 – -0.8	85-119	78–86	0–35	0.82-1.45	53-72	33-51	1.3–2.1	1.3–2.6	current study

In insect flight, the production of large lift is attributed to an LEV. Wing-wing interactions are also important in butterfly flight, although 'clap and peel' does not occur in every stroke. Ancel et al. [12], showed that during gliding flight at different AoA for different butterfly wing shapes, the LEV was restricted to the FW surface. Srygley and Taylor [16] reported the absence of an LEV in

V. atalanta in steady forward flight in a wind tunnel. During forward flight with acceleration, however, an LEV was formed on the wing surface, typically extending from tip to tip. Zheng et al. [17] and Yokoyama [20] also observed LEVs from their CFD simulations. *J* indicates the ratio of steady to unsteady effects in flapping flight. For butterflies, the body motion is unsteady (*J* changes continually) [18]. Since $|\bar{J}|$ ranged between 0.3-0.4 here, unsteady effects were important. We observed LEVs in both half strokes. The LEV extended from tip to tip, when the body was considered in the simulations, matching previous observations of a Class II LEV in forward flight [16].

Unlike previous works, a strong LEV was formed during the US. The LEV in both half strokes was absent on the HW and FW dominated force production, generating about 65% of the net force and 70-80% of the bodyweight. In functionally two-winged insects with smaller HWs, it had been shown that the LEV resides on the FW, and the HW does not affect its formation [42]. We expect that the same applies to butterflies. Although the HW has been reported to be unnecessary for flight, our results indicate that without wing kinematics adjustments of the FW such as an increase in frequency as observed when the HWs were ablated [6], weight support during backward flight may not be possible (Figure 5.10).

Since the US carried the bodyweight primarily, we compared the mechanism of upstroke lift in forward and backward flight. The assumption of an active US is dependent on what part of the wing, either the ventral or dorsal, the oncoming flow strikes [43, 44]. Srygley and Thomas [16] verified these assumptions [43] using smoke visualization. They identified both a positively and negatively loaded US. Although only a wingtip vortex was visualized in the negative loaded US in Srygley and Thomas's study [16], CFD simulations indicate that an LEV, with a reversed sign of circulation, may reside on the wing on the ventral surface [17]. This US LEV was smaller than the DS's, and contributed to negative lift and thrust forces [17]. In the case of the positively loaded US, an LEV of the same sign of circulation as DS rested on the dorsal surface of the wings. The body of the butterfly was horizontal, and the wings were also negatively cambered but not strongly supinated. The raised leading edge, however, possessed a high enough AoA so that the incoming flow separated over the wing forming the vortex. The stagnation point was located on the wing's ventral surface and indicated that the US was lifting (see both Figure 4(d) and the supplementary video in [16]). The occurrence of a positively loaded US, however, is rare. It occurred only in one US at the inception of flight in Srygley and Thomas's study [16] and has not been reported in any other forward free flight studies [17, 18, 20]. The positively loaded US may be an artifact of the incoming flow or unique kinematics of *V. atalanta* in the experiment.

The mechanics of the US in our study is different because the LEV was stably attached on the ventral surface, indicating that sense of circulation of the DS and US was reversed. The US loading was changed due to the reorientation of the body posture. We also did not observe any inactive US in any of the flight sequences. Since the forces generated during the US support the insect's weight, feathering the US is not a viable option in backward flight.

As aforementioned, butterflies elicit backward flight by noticeable postural changes reminiscent of the backward flight observed in other species [23, 26]. A butterfly is likely not to elicit backward flight with a horizontal posture because the range of motion of the wing stroke plane is constrained within a narrow range relative to the body, in the anterior side, due to reduced wing degree of freedom (Tables 5.3 and 5.7). Although the wing forces varied considerably in the global frame (Figure 5.7(a)), the angle between the body and aerodynamic force vector was relatively constant (Figure 5.7(b)). To generalize our findings, we compared our results to the forward flight data of the monarch presented in Table 5.6 and literature values for other butterfly species (Figure 5.11). Similar to backward flight, the forward flight forces were constrained in the anterior side. The DS forces were constrained in the dorsal side with the forces tilted toward the dorsoventral axis. Likewise, the US forces were produced in the ventral side, in between the longitudinal axis and dorsoventral axis. The uniformity of the results in forward and backward flight indicates that the helicopter model is being used by butterflies at least within the range of speeds -1 to 2m/s or $-0.4 \leq J \leq 0.9$. This finding does not indicate that forward, and backward kinematics are the same. The kinematics and half stroke force magnitudes are different, and the wing aerodynamic functions in the global frame have reversed between forward and backward flight. Nevertheless, the force orientation is in a uniform direction relative to the body (local frame) in both flight scenarios.

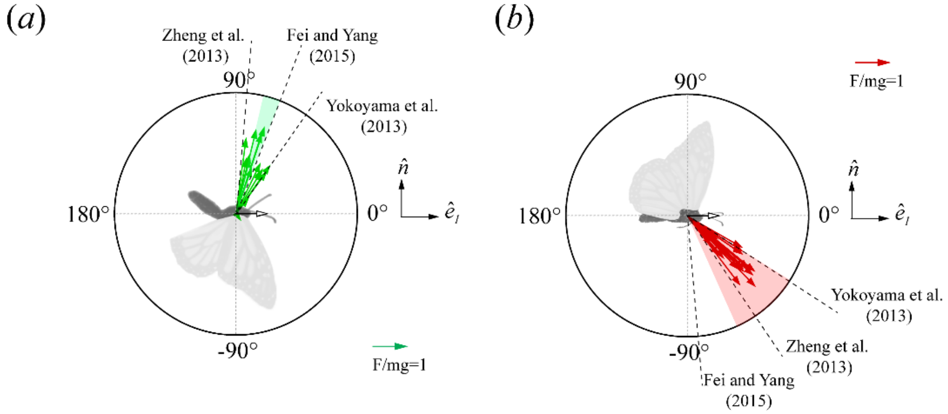

Figure 5.11. Butterflies rely on the helicopter model for rectilinear flight. (a) Dorsoventral stroke (downstroke). (b) Ventrodorsal stroke (upstroke). The arrows are the backward flight results from Table 5.5. Shaded sectors of the circle are the forward flight results of the monarch (Table 5.6). The dashed lines are the forward flight results of other butterfly species from Zheng et al. 's [17], Fei and Yang's [18], and Yokoyama et al. 's [20] work (Table 4.5).

Table 5.9. Half stroke contribution to the net force and force type produced predominantly in each half stroke, for insects which use an inclined stroke plane *-tethered

insect	flight mode	DS force (%)	DS force type	US force (%)	US force type	reference	
butterfly	forward	74	vertical	26	horizontal	Zheng et al	[17]
		75	vertical	25	horizontal	Yokoyama et al.	[20]
		59	vertical	41	horizontal	Fei and Yang	[18]
	backward	40	horizontal	60	vertical	current study	
cicada	forward	90	vertical	10	horizontal	Liu et al.	[45]
		80	vertical	20	horizontal	Wan et al.	[46]
	backward	50	horizontal	50	vertical	Bode-Oke and Dong. (under review)	
damselfly	forward	84	vertical	16	horizontal	Bode-Oke et al.	[21]
		75	vertical	25	horizontal	Sato et al.	[47]
	backward	33	horizontal	67	vertical	Bode-Oke et al.	[23]
	forward	80	vertical	20	horizontal	Azuma and Watanabe	[48]
		67	vertical	33	horizontal	Hefler et al.	[49]
fruit fly	forward	61	vertical	39	horizontal	Meng and Sun	[50]
hawkmoth	forward	80	vertical	20	horizontal	Willmott et al.	[51]
locust	forward	84	vertical	14	horizontal	Young et al.	[52]

5.6. References

[1] Bomphrey, R.J., Nakata, T., Phillips, N. & Walker, S.M. 2017 Smart wing rotation and trailing-edge vortices enable high frequency mosquito flight. *Nature* **544**, 92-95.

[2] Sane, S.P. 2003 The aerodynamics of insect flight. *The journal of experimental Biology* **206**, 4191-4208.

[3] Dudley, R. 2002 *The biomechanics of insect flight: form, function, evolution*, Princeton University Press.

[4] Dickinson, M.H., Lehmann, F.-O. & Sane, S.P. 1999 Wing rotation and the aerodynamic basis of insect flight. *Science* **284**, 1954-1960.

[5] Le Roy, C., Debat, V. & Llaurens, V. Adaptive evolution of butterfly wing shape: from morphology to behaviour. *Biological Reviews* **0**. (doi:10.1111/brv.12500).

[6] Jantzen, B. & Eisner, T. 2008 Hindwings are unnecessary for flight but essential for execution of normal evasive flight in Lepidoptera. *Proceedings of the National Academy of Sciences* **105**, 16636-16640. (doi:10.1073/pnas.0807223105).

[7] Obara, Y. 1975 Mating behavior of the cabbage white butterfly,Pieris rapae crucivora. *Journal of comparative physiology* **102**, 189-200. (doi:10.1007/bf01464355).

[8] Fei, Y.-H.J. & Yang, J.-T. 2016 Importance of body rotation during the flight of a butterfly. *Physical Review E* **93**, 033124. (doi:10.1103/PhysRevE.93.033124).

[9] Sunada, S., Kawachi, K., Watanabe, I. & Azuma, A. 1993 Performance of a butterfly in take-off flight. *Journal of Experimental Biology* **183**, 249-277.

[10] Kang, C.-k., Cranford, J., Sridhar, M.K., Kodali, D., Landrum, D.B. & Slegers, N. 2018 Experimental Characterization of a Butterfly in Climbing Flight. *AIAA Journal* **56**, 15-24. (doi:10.2514/1.j055360).

[11] DUDLEY, R. 1990 Biomechanics of Flight in Neotropical Butterflies: Morphometrics and Kinematics. *Journal of Experimental Biology* **150**, 37-53.

[12] Ancel, A.O., Eastwood, R., Vogt, D., Ithier, C., Smith, M., Wood, R. & Kovač, M. 2017 Aerodynamic evaluation of wing shape and wing orientation in four butterfly species using numerical simulations and a low-speed wind tunnel, and its implications for the design of flying micro-robots. *Interface Focus* **7**, 20160087. (doi:doi:10.1098/rsfs.2016.0087).

[13] Tanaka, H., Matsumoto, K. & Shimoyama, I. 2008 Design and performance of micromolded plastic butterfly wings on butterfly ornithopter. In *2008 IEEE/RSJ International Conference on Intelligent Robots and Systems* (pp. 3095-3100.

[14] Sridhar, M., Kang, C.-K. & Landrum, D.B. 2016 Instantaneous lift and motion characteristics of butterflies in free flight. In *46th AIAA Fluid Dynamics Conference* (p. 3252.

[15] Ellington, C. 1980 Vortices and hovering flight. *Instationare Effekte An Schwingended Fluegeln*, 64-101.

[16] Srygley, R.B. & Thomas, A.L.R. 2002 Unconventional lift-generating mechanisms in free-flying butterflies. *Nature* **420**, 660. (doi:10.1038/nature01223 https://www.nature.com/articles/nature01223#supplementary-information).

[17] Zheng, L., Hedrick, T.L. & Mittal, R. 2013 Time-Varying Wing-Twist Improves Aerodynamic Efficiency of Forward Flight in Butterflies. *PLOS ONE* **8**, e53060. (doi:10.1371/journal.pone.0053060).

[18] Fei, Y.-H.J. & Yang, J.-T. 2015 Enhanced thrust and speed revealed in the forward flight of a butterfly with transient body translation. *Physical Review E* **92**, 033004. (doi:10.1103/PhysRevE.92.033004).

[19] BETTS, C.R. & WOOTTON, R.J. 1988 Wing Shape and Flight Behaviour in Butterflies (Lepidoptera: Papilionoidea and Hesperioidea): A Preliminary Analysis. *Journal of Experimental Biology* **138**, 271-288.

[20] Yokoyama, N., Senda, K., Iima, M. & Hirai, N. 2013 Aerodynamic forces and vortical structures in flapping butterfly's forward flight. *Physics of Fluids* **25**, 021902. (doi:10.1063/1.4790882).

[21] Bode-Oke, A., Zeyghami, S. & Dong, H. 2017 Aerodynamics and flow features of a damselfly in takeoff flight. *Bioinspiration & biomimetics* **12**, 056006.

[22] Wang, J.K. & Sun, M. 2005 A computational study of the aerodynamics and forewing-hindwing interaction of a model dragonfly in forward flight. *Journal of Experimental Biology* **208**, 3785-3804. (doi:10.1242/jeb.01852).

[23] Bode-Oke, A.T., Zeyghami, S. & Dong, H. 2018 Flying in reverse: kinematics and aerodynamics of a dragonfly in backward free flight. *Journal of The Royal Society Interface* **15**. (doi:10.1098/rsif.2018.0102).

[24] Farina, W.M., Kramer, D. & Varjú, D. 1995 The response of the hovering hawk moth Macroglossum stellatarum to translatory pattern motion. *Journal of Comparative Physiology A* **176**, 551-562. (doi:10.1007/BF00196420).

[25] Sane, S.P., Dieudonné, A., Willis, M.A. & Daniel, T.L. 2007 Antennal mechanosensors mediate flight control in moths. *science* **315**, 863-866.

[26] Sapir, N. & Dudley, R. 2012 Backward flight in hummingbirds employs unique kinematic adjustments and entails low metabolic cost. *The Journal of experimental biology* **215**, 3603-3611.

[27] Koehler, C., Liang, Z., Gaston, Z., Wan, H. & Dong, H. 2012 3D reconstruction and analysis of wing deformation in free-flying dragonflies. *The Journal of experimental biology* **215**, 3018-3027.

[28] Mittal, R., Dong, H., Bozkurttas, M., Najjar, F., Vargas, A. & von Loebbecke, A. 2008 A versatile sharp interface immersed boundary method for incompressible flows with complex boundaries. *Journal of computational physics* **227**, 4825-4852.

[29] Li, C., Dong, H. & Zhao, K. 2018 A balance between aerodynamic and olfactory performance during flight in Drosophila. *Nature Communications* **9**, 3215. (doi:10.1038/s41467-018-05708-1).

[30] Ros, I.G., Bassman, L.C., Badger, M.A., Pierson, A.N. & Biewener, A.A. 2011 Pigeons steer like helicopters and generate down- and upstroke lift during low speed turns. *Proceedings of the National Academy of Sciences* **108**, 19990-19995. (doi:10.1073/pnas.1107519108).

[31] Marden, J.H. & Chai, P. 1991 Aerial Predation and Butterfly Design: How Palatability, Mimicry, and the Need for Evasive Flight Constrain Mass Allocation. *The American Naturalist* **138**, 15-36.

[32] Bomphrey, R.J., Lawson, N.J., Harding, N.J., Taylor, G.K. & Thomas, A.L.R. 2005 The aerodynamics of Manduca sexta: digital particle image velocimetry analysis of the leading-edge vortex. *Journal of Experimental Biology* **208**, 1079-1094. (doi:10.1242/jeb.01471).

[33] Cheng, B., Deng, X. & Hedrick, T.L. 2011 The mechanics and control of pitching manoeuvres in a freely flying hawkmoth (Manduca sexta). *The Journal of Experimental Biology* **214**, 4092-4106. (doi:10.1242/jeb.062760).

[34] Thomas, A.L., Taylor, G.K., Srygley, R.B., Nudds, R.L. & Bomphrey, R.J. 2004 Dragonfly flight: free-flight and tethered flow visualizations reveal a diverse array of unsteady lift-generating mechanisms, controlled primarily via angle of attack. *Journal of Experimental Biology* **207**, 4299-4323.

[35] Rüppell, G. 1989 Kinematic analysis of symmetrical flight manoeuvres of Odonata. *Journal of Experimental Biology* **144**, 13-42.

[36] Mukundarajan, H., Bardon, T.C., Kim, D.H. & Prakash, M. 2016 Surface tension dominates insect flight on fluid interfaces. *Journal of Experimental Biology* **219**, 752-766. (doi:10.1242/jeb.127829).

[37] Schneider, P. 1981 Flugmanöver der käfer. *Mitteilungen der Deutschen Gesellschaft für Allgemeine und Angewandte Entomologie* **3**, 259-263.

[38] Huang, H. & Sun, M. 2012 Forward flight of a model butterfly: Simulation by equations of motion coupled with the Navier-Stokes equations. *Acta Mechanica Sinica* **28**, 1590-1601. (doi:10.1007/s10409-012-0209-1).

[39] Caetano, J.V., de Visser, C.C., Remes, B.D., De Wagter, C., Van Kampen, E.-J. & Mulder, M. 2013 Controlled flight maneuvers of a Flapping Wing Micro Air Vehicle: a step towards the DelFly II Identification. In *AIAA Atmospheric Flight Mechanics (AFM) Conference* (p. 4843.

[40] Bomphrey, R.J., Taylor, G.K. & Thomas, A.L.R. 2009 Smoke visualization of free-flying bumblebees indicates independent leading-edge vortices on each wing pair. *Experiments in Fluids* **46**, 811-821. (doi:10.1007/s00348-009-0631-8).

[41] DUDLEY, R. 1991 Biomechanics of Flight in Neotropical Butterflies: Aerodynamics and Mechanical Power Requirements. *Journal of Experimental Biology* **159**, 335-357.

[42] Chen, D., Kolomenskiy, D., Nakata, T. & Liu, H. 2017 Forewings match the formation of leading-edge vortices and dominate aerodynamic force production in revolving insect wings. *Bioinspiration & Biomimetics* **13**, 016009. (doi:10.1088/1748-3190/aa94d7).

[43] Srygley, R.B. & Ellington, C.P. 1999 Estimating the relative fitness of local adaptive peaks: the aerodynamic costs of flight in mimetic passion–vine butterflies <i>Heliconius</i>. *Proceedings of the Royal Society of London. Series B: Biological Sciences* **266**, 2239-2245. (doi:doi:10.1098/rspb.1999.0914).

[44] Willmott, A.P. & Ellington, C.P. 1997 The mechanics of flight in the hawkmoth Manduca sexta. II. Aerodynamic consequences of kinematic and morphological variation. *The Journal of Experimental Biology* **200**, 2723-2745.

[45] Liu, G., Dong, H. & Li, C. 2016 Vortex dynamics and new lift enhancement mechanism of wing–body interaction in insect forward flight. *Journal of Fluid Mechanics* **795**, 634-651.

[46] Wan, H., Dong, H. & Gai, K. 2015 Computational investigation of cicada aerodynamics in forward flight. *Journal of The Royal Society Interface* **12**, 20141116.

[47] Sato, M. & Azuma, A. 1997 The flight performance of a damselfly Ceriagrion melanurum Selys. *Journal of Experimental Biology* **200**, 1765-1779.

[48] Azuma, A. & Watanabe, T. 1988 Flight performance of a dragonfly. *Journal of Experimental Biology* **137**, 221-252.

[49] Hefler, C., Noda, R., Shyy, W. & Qiu, H. 2017 Unsteady Vortex Interactions for Performance Enhancement of a Free Flying Dragonfly. In *ASME 2017 Fluids Engineering Division Summer Meeting* (pp. V01CT21A010-V001CT021A010, American Society of Mechanical Engineers.

[50] Meng, X. & Sun, M. 2016 Wing Kinematics, Aerodynamic Forces and Vortex-wake Structures in Fruit-flies in Forward Flight. *Journal of Bionic Engineering* **13**, 478-490. (doi:https://doi.org/10.1016/S1672-6529(16)60321-9).

[51] Willmott, A.P., Ellington, C.P. & Thomas, A.L. 1997 Flow visualization and unsteady aerodynamics in the flight of the hawkmoth, Manduca sexta. *Philosophical Transactions of the Royal Society B: Biological Sciences* **352**, 303-316.

[52] Young, J., Walker, S.M., Bomphrey, R.J., Taylor, G.K. & Thomas, A.L.R. 2009 Details of Insect Wing Design and Deformation Enhance Aerodynamic Function and Flight Efficiency. *Science* **325**, 1549-1552. (doi:10.1126/science.1175928).

Chapter 6

The backward flight aerodynamics of a damselfly (*Hetaerina americana*) is linked to changes in flight speed.

6.1. Abstract

It has been reported that insects appropriate rearward flight to transition to other flight modes. Here, we show that before the transition to forward flight, the backward flight of damselflies involves a speed-up (accelerating) and slow-down (deceleration) phase. During speed-up, an upright posture and high angles of attack (AoA) in both half strokes were appropriated. The upright posture rotated the stroke plane in the inertial frame in comparison to forward flight, causing the reversal of the aerodynamic functions of the half strokes. An active upstroke signified by the presence of a leading edge vortex was the principal means of force production and weight support, while the downstroke produced backward forces. During slow-down, however, the body and stroke plane angles reduced and a pronounced asymmetry in the half stroke AoA was observed. The upstroke AoA increased while the downstroke's reduced in comparison to the speed-up phase. Consequently, the upstroke remained aerodynamically active, though it assumed a dual function, generating both (i) weight support and (ii) negative horizontal forces (drag) to counteract the backward forces still being produced in the downstroke. If the downstroke angle of attack was low enough, the downstroke's force production diminished substantially, and the half stroke became aerodynamically inactive. Associated with the inactive downstroke was the switch from separated to attached flow. After the transition to accelerating forward flight, the body angle reduced and the aerodynamic roles of the half strokes reverted to their normal functions: downstroke lift, upstroke thrust. Our findings indicate that the half stroke kinematics and aerodynamics are different, and distinct in each flight phase, being characterized by adjustments mainly in body angle, stroke plane angle, and wing AoA.

Keywords: damselfly, backward flight, active upstroke, downstroke-upstroke reversal, leading edge vortex, attached flow.

6.2. Introduction

Adroit flying insects exhibit different flying modes which are elicited by the adjustments of both the wing and body kinematics, along with the use of different lift-enhancing mechanisms [1, 2], that can vary substantially on a stroke by stroke basis [3]. Of the flight modes which delineate the repertoire of flying insects, here, we focus on backward flight, which is less studied and understood but commonly exhibited in the natural world especially among agile fliers such as Odonates (damselflies and dragonflies) [4-6]. Volant taxa employ backward flight for takeoff, slow flight, predator evasion, prey capture, territorial fights, when retreating from or assessing flowers ("hesitation behaviors"[7]), obstacle avoidance, during mating, after haematophagy, etc. [4, 5, 7-11]. The possibility of backward flight thus offers an alternative to forward motions by extending the flight envelope of the insect. Moreover, backward flight studies have provided new insights essential both for biology and micro aerial vehicles (MAVs) *vis-à-vis* half stroke function, aerodynamics, coordination between wing and body motion, energetics and convergent evolution [4, 8].

Recent works [4, 8] have revealed that the trends that characterize backward flight are not merely direct extrapolations or opposites of forward or hovering flight. For example, weight support is manifest in the upstroke (US) during backward flight. Other qualitative [12] and quantitative studies [4, 8, 13] have also documented that an upright posture is preferred in backward flight, although flight with a horizontal posture characterizes the forward flight many insects. Transforming the body posture from horizontal to upright reorients the stroke plane and flight forces to initiate and maintain backward flight [4]; a behavior that is not more expensive than hovering [4, 8].

It has, nevertheless, been suggested that biomechanical constraints prescribe that maximum flight speed is achieved when flying forward and that insects inevitably reorient themselves in the posture for flying forward [5, 13, 14]. Rightly so, during video capture in the laboratory, if we waited long enough, a transition to another flight mode from backward flight occurred. If backward flight then is for transitioning to other flight modes, we suggest that the flight velocity profile of the insect will comprise of a phase of increasing speed (speed-up/acceleration) and decreasing speed (slow-down/deceleration) which will enable the insect to prepare for the transition to another rectilinear flight mode such as forward flight. Anecdotal studies support this claim and have indicated that hoverflies often accelerate and decelerate to switch between forward and backward flight as an antipredator strategy [7]. European Hawkmoths also exhibit similar behavior, albeit in response to visual cues while hovering at flowers [15]. Our lab observation of damselflies-the insects of choice in this paper, and field observations of Rüppell [5, 10] show that they speed up or slow down to avoid obstacles or transition from backward to forward flight or vice versa. The aerodynamics of this type of flight with this 'unsteady' body motion have not been elucidated. Previous quantitative studies on backward flight have focused solely on flights where the acceleration/speed-up phase is dominant [4] or flights with constant inflow [8]. However, the trends which characterize the slow down (deceleration) phase have not been studied. For damselflies, which are generally slower fliers than dragonflies, the slow-down duration is substantial, accounting for as much as half the flight duration of the backward flight.

To speed up and slow down, we suggest that damselflies modulate the patterns of force production of the wings by adjustment of wing kinematics and aerodynamics mechanisms based on flight phase and the wing kinematics in the up and down stroke are quite different and correlated changes in flight velocity. How the kinematics and aerodynamics during the speed-up and slow-down phases are modulated, how forces are produced, which flow mechanisms are dominant, the functions of the wing pairs, and the aerodynamics roles of the half strokes during each flight phase, in this kind of backward flight has not been reported before now for any species. Therefore, we used a high-speed camera system to capture the flight as well as a surface reconstruction technique to extract wing and body kinematics. A high fidelity CFD simulation was used to quantify flight forces and also identify the relevant flow features.

6.3. Material and methods

6.3.1. Damselflies, high-speed photogrammetry, and three-dimensional surface reconstruction

We caught damselflies at a pond, and after transportation to the laboratory, we dotted their wings for tracking purposes and then placed the insects on a platform for filming. Individuals initiated flight voluntarily, and their motion was captured using a high-speed camera set-up comprising of three synchronized cameras positioned orthogonally. These cameras recorded at 1000 frames per second with a resolution of 1024x1024 pixels. Transient and lengthy backward flight sequences consisting of rectilinear flight, turning maneuvers and short takeoff were common in the recorded flight footages. From the footage, we selected sequences of rectilinear motion (~4). The body kinematics were reconstructed from the videos using a template-based surface reconstruction technique [16], and we quantified the velocity profiles by taking the time derivative of the body displacement. The backward motion of the insects consisted of a phase of increasing speed (speed-up) and decreasing speed (slow-down), respectively (See section §6.4.1.1 for the quantification of the body velocities). Their wing motions were also reconstructed to capture both the kinematics and deformations. By way of example, we selected two damselflies (DaF#1 and DaF#2 in Table 6.1) for the analyses in the text.

Table 6.1. Morphological characteristics of the insects**.** Chord values are measured at mid-span. n_w -flapping frequency $\bar{U}_b$ -body velocity. The uncertainties in the length and mass measurements are ±1mm and ±1mg, respectively.

species	ID	flight time (*ms*)	body weight (mg)	body length (mm)	FW length (mm)	FW chord (mm)	HW length (mm)	HW chord (mm)	n_w (Hz)	$\bar{U}_b$ (m/s)	$U_{b,max}$ (m/s)
Hetaerina americana	DaF #1	140	95	44	29	6	28	6	25	0.63	0.86
	DaF #2	235	75	42	29	6	29	6	26	0.34	0.50
	DaF #3	140	75	42	29	6	29	6	28	0.37	0.53
	DaF #3	160	78	44	28	5	28	5	27	0.30	0.45

6.3.2. Wing kinematics definitions

A coordinate system was placed at the wing root, and the kinematics were measured relative to the mean stroke plane. The mean stroke plane was determined by calculating a least-squares plane based on the points that comprised the wing root and tip coordinates and averaged for all complete strokes. The rigid wing orientation in the mean stroke plane is defined by the Euler angles, flap (ϕ), deviation (θ), and pitch (ψ) (Figure 6.1). ϕ is the back and forth motion of the wing in the stroke plane. θ is the angle between the wing and its projection on to the stroke plane while ψ is the angle between the wing chord and stroke plane (Figure 6.1(a)). The effective AoA (α_{eff}) is the angle between the wing section and vector sum of the body (U_{body}) and wing velocity

($\mathrm{U}_{\mathrm{flap}}$). α_{eff} is based on the flapping kinematics and does not consider any influence of induced flows or wing-wing and wing-wake interactions.

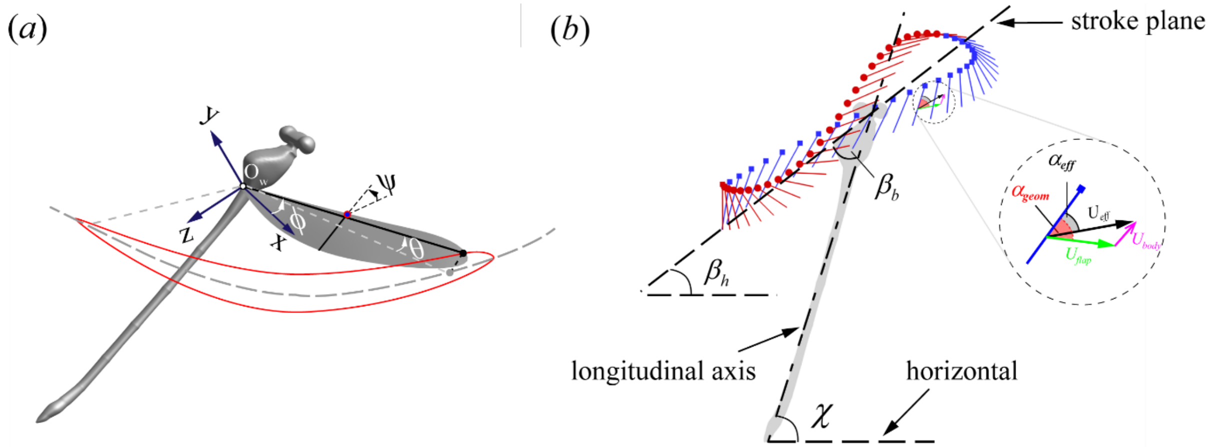

Figure 6.1. Kinematics definitions. (a). Wing Euler angle definition. (b) β_{h} and β_{b} are the stroke plane angles with respect to the horizontal plane and body longitudinal axis, respectively. χ is the body angle relative to the horizon. α_{geom} and α_{eff} are geometric and effective AoA, respectively.

6.3.3. Computational fluid dynamics simulations

We used an in-house immersed boundary method based CFD solver for the simulations in this study and briefly outlined the methods here (see [17] for details). We solved the time-dependent incompressible viscous Navier-Stokes (N-S) Equation (Eqn. (1))

$$\nabla \cdot \mathbf{u} = 0; \quad \frac{\partial \mathbf{u}}{\partial t} + \mathbf{u} \cdot \nabla \mathbf{u} = -\frac{1}{\rho} \nabla p + \upsilon \nabla^2 \mathbf{u}, \tag{9}$$

where $\mathbf{u}$ is the velocity vector, ρ is the density, υ is the kinematic viscosity and p is the pressure, using a finite difference method with 2nd order accuracy in space and a fractional step method for time stepping. The computational domain is shown in Figure 6.2(a). A zero-gradient boundary condition of velocity and pressure, that is, homogeneous Neumann boundary conditions set to zero was imposed at all boundaries. The domain size was $60c \times 60c \times 60c$, where c is the chord length at mid-span, with a large dense region to capture the full motion of the insect, and the wake left behind. A grids refinement study is reported in Figure 6.2(b) and Table 6.2. The Reynolds number is defined as $Re_c = \frac{\bar{\mathrm{U}}_{\mathrm{eff}} c}{\upsilon}$, where $\bar{\mathrm{U}}_{\mathrm{eff}}$ is the average effective wing tip speed (tip speed + body motion), and υ is the kinematic viscosity of air at room temperature ($1.5\mathrm{x}10^{-5}$ m^2/s). The *Re* was about 1000 for the selected damselflies.

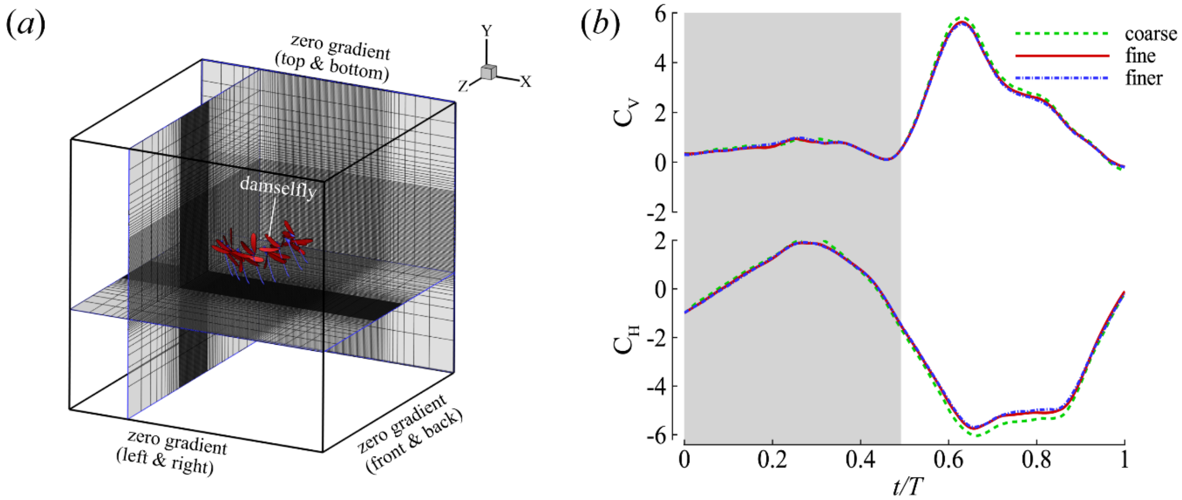

Figure 6.2. Numerical simulation set-up (a) Computational domain used in the current simulation. For display, the meshes are coarsened thrice in each direction. (b) Grid Refinement. The vertical (C_V) and horizontal (C_H) force coefficients during the second stroke of DaF#1 are shown. Gray shading denotes the forewing downstroke. Coarse= 10.8 million; fine=21.5 million; finer=24.4 million. The fine grids are shown in (a).

Table 6.2. Force coefficients for three different mesh set-up for DaF#1.

	mesh set-up	$\overline{C}_V$	$\overline{C}_{V,max}$	$\overline{C}_H$	$\overline{C}_{H,max}$
coarse	279x221x175	1.66	5.82	-1.82	-6.04
fine	353x281x217	1.58	5.62	-1.73	-5.74
finer	369x289x229	1.56	5.55	-1.69	-5.69

6.4. Results

6.4.1. Kinematics

6.4.1.1. Body kinematics

The body kinematics of the damselflies is shown in Figure 6.3(c). The insects traveled backward along a relatively straight flight path with minimal body rotations. Accompanying the backward motion were changes in body velocity. The general trend was that the damselflies increased their backward velocity during the first half of flight (measured in non-dimensional time, normalized by the duration of flight of each insect) and slowed down during the second half (Figure 6.3(c,ii)). The maximum flight speeds recorded were less than 1 m/s, indicating slow flight. In addition to changes in velocity, the body posture was also varied, whereby during the speed-up phase, the damselflies usually maintained higher body angles (χ) than during the slow-down phase (Table 6.3 and Table 6.4).

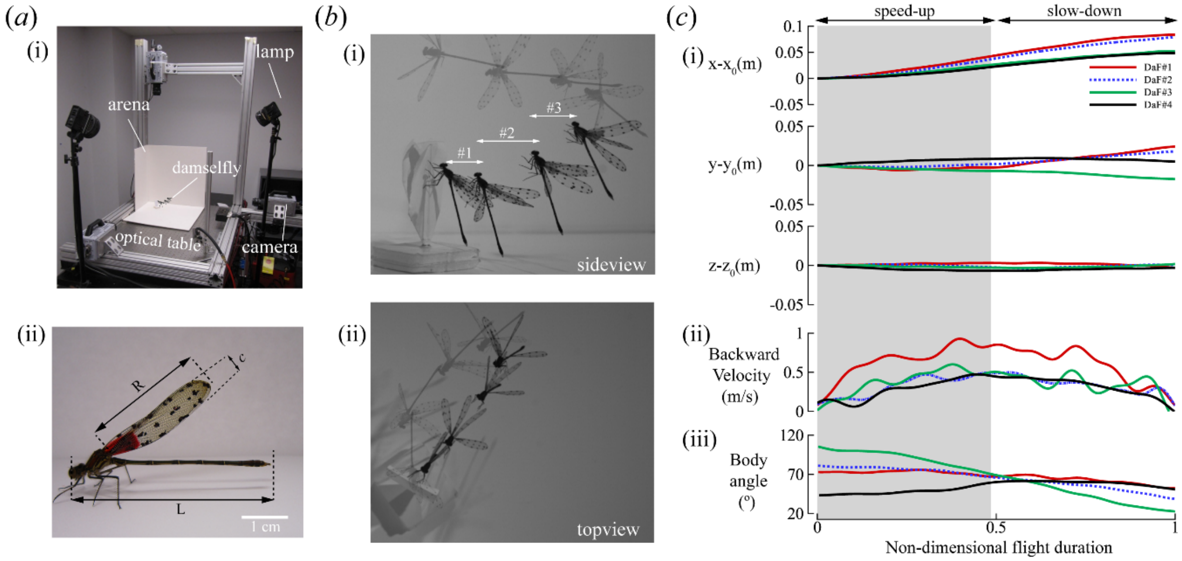

Figure 6.3. Experimental set-up and body kinematics (a)(i) flight arena (ii) damselfly species and morphological parameters where c is the chord length, L is the body length, R is the wing length. (b) Montage of high-speed images (i) side view (the wing strokes are numbered), (ii) top view. Transparent damselflies indicate flight phase post backward flight. (C) Body (i) displacement, (ii) velocity, (iii) angle. Gray shading qualitatively denotes the speed-up phase.

6.4.1.2. Wing kinematics

The time series of the fore and hind wing kinematics are reported in Figure 6.4 and summarized in Table 6.3 and Table 6.4 on a flight phase basis. The forewings (FW) led the hindwings (HW) typical of damselfly flight, as the wings traversed an inclined stroke plane [14, 18, 19].

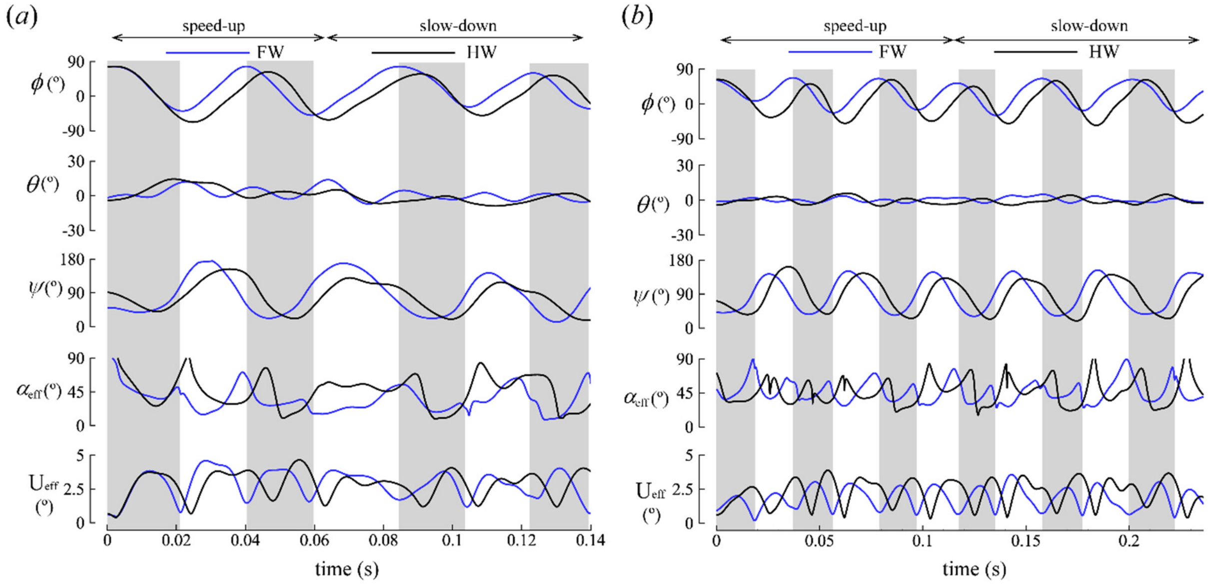

Figure 6.4. Wing kinematics. The time series of the kinematics of (a) DaF#1 and (b) DaF#2 are reported. Gray shading denotes the forewing's downstroke. Symbol meanings are found in the text.

For DaF #1, averaged across both flight phases, the stroke plane angle relative to the longitudinal axis of the body (β_{b}) was 35±4°(FW) and 42±6°(HW). The stroke plane angle relative to the horizontal (β_{h}) was inclined at 34±8°(FW) and 33±9°(HW). The flapping amplitudes (Φ) were 113±15°(FW) and 122±15°(HW). *Vis-à-vis* flight phase, β_{h} reduced in each stroke, that is, becoming more horizontal (flattened) because of the adjustments of both β_{b} and body angle (χ) (Figure 6.3(c,iii), Tables 6.3 and 6.4). During slow-down, β_{b} was tilted away from the longitudinal axis by 5° compared with the speed-up phase, and at the same time, χ reduced by 9°. Larger Φ occurred during the speed-up phase (Figure 6.4). The difference in Φ between the speed-up and slow-down phase was about 20° for both wing pairs. From speed-up to slow-down, there was a reduction in downstroke (DS) AoA while there was an increase in US AoA, and the changes in AoA were more drastic for the HW. The drop in $\alpha_{\mathrm{eff,DS}}$ was 12° (FW) and 19° (HW). In contrast, the increase in $\alpha_{\mathrm{eff,US}}$ was 3° (FW) and 13° (HW). The drop in $\alpha_{\mathrm{eff,mid\text{-}DS}}$ was 20° (FW) and 9° (HW). In contrast, the increase in $\alpha_{\mathrm{eff,mid\text{-}US}}$ was 17° (FW) and 36° (HW).

Table 6.3. Speed-up kinematic parameters. $\alpha_{\mathrm{eff,mid}}$ is the instantaneous effective angle of attack at mid-stroke.

		χ	β_{b}	β_{h}	Φ	$\alpha_{\mathrm{eff,mid}}$		α_{eff}	
		(°)	(°)	(°)	(°)	(°)		(°)	
						DS	US	DS	US
DaF #1	FW	77	32	45	121	34	19	39	35
	HW	77	38	39	134	23	30	42	45
DaF #2	FW	76	33	43	73	39	40	47	49
	HW	75	40	35	99	31	39	42	50

For DaF#2, averaged across all complete strokes, β_{b} was 35±3°(FW) and 41±4°(HW) while β_{h} was 30±15° (FW) and 23±14°(HW), respectively. Φ was 78±12°(FW) and 104±11° (HW). Relative to the flight phase, there was also a flattening of the stroke plane relative to the horizontal similar to DaF #1. During slow-down, β_{b} was tilted away from the longitudinal axis by about 4° while χ reduced by 20° in comparison to the speed up phase (Figure 6.3(c,iii)). Unlike DaF#1, the flapping amplitude increased during the slow down phase by 11° for both wing pairs. From speed-up to slow-down, there was a reduction in DS AoA while there was an increase in US AoA. Similar to DaF#1, the changes in AoA were more evident for the HW. The drop in $\alpha_{\mathrm{eff,DS}}$ was 2° for the FW and HW. In contrast, the increase in $\alpha_{\mathrm{eff,US}}$ was 8° (HW) while there was 4° reduction for the FW. The decrease in $\alpha_{\mathrm{eff,mid\text{-}DS}}$ was 3° (FW) and 5° (HW). In contrast, the increase in $\alpha_{\mathrm{eff,mid\text{-}US}}$ was 20° (HW).

Table 6.4. Slow-down kinematic parameters.

		χ (°)	β_b (°)	β_h (°)	Φ (°)	$\alpha_{eff,mid}$ (°)		α_{eff} (°)	
						DS	US	DS	US
DaF #1	FW	68	37	31	104	14	36	27	38
	HW	70	44	26	111	14	56	23	58
DaF #2	FW	57	36	20	84	36	40	45	45
	HW	55	44	11	110	26	51	40	58

6.4.2. Force generation and orientation

6.4.2.1. Global frame

The instantaneous aerodynamic forces obtained from the CFD simulation were computed from the integration of the pressure and shear stress on the wing and documented in Figure 6.5. For visualization, the magnitude and direction of the halfstroke-average forces are displayed in Figure 6.6. The colors of the force vectors in Figure 6.6 correspond to the line colors in Figure 6.5.

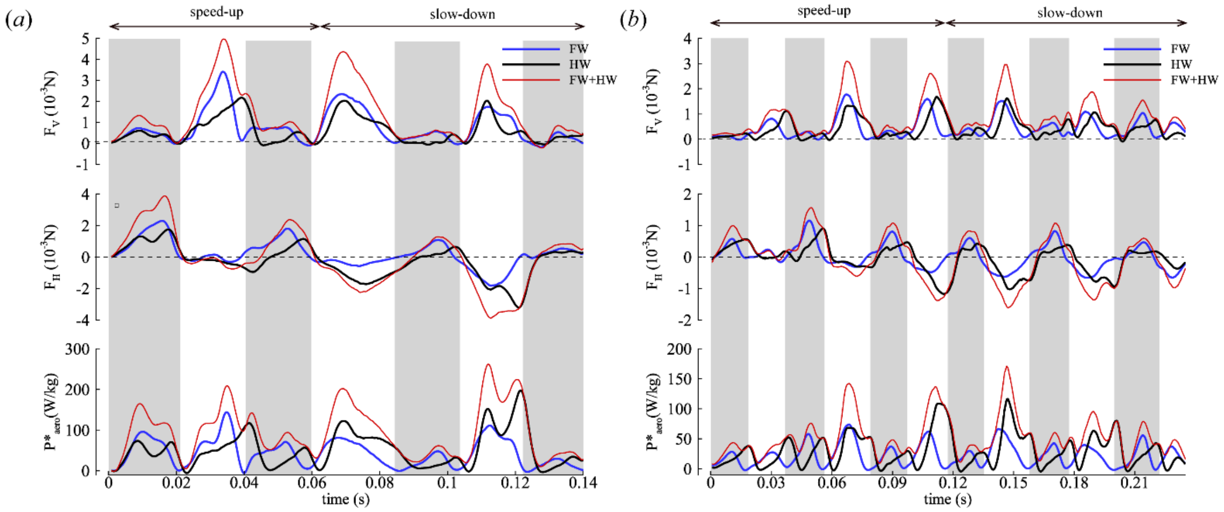

Figure 6.5. Force generation. The time history of the aerodynamic forces produced by (a) DaF#1 and (b) DaF#2 are reported. The gray shading denotes the DS of the forewings. Short dashed lines represent the zero line.

DaF#1 produced an average vertical force of 1.5 times its body weight (BW). Most of the vertical force was produced in the US while the horizontal force was produced both in the DS or US depending on the phase of flight. Positive horizontal forces (backward) forces were produced in the DS while negative horizontal (forward) forces were produced in the US.

Vis-à-vis flight phase, the force vectors pointed backwards and upward in the DS (DS 1 and 2 for FW and HW; Figure 6.6(a,i)), while the force vectors during pointed upward the US (US 1 for FW and HW; Figure 6.6(a,i)) during speed-up. During slow-down, first, although the DS force vectors still pointed backward and upward, the magnitude of the backward forces (positive horizontal forces) diminished substantially (DS 3 for FW and DS 2 & 3 for HW (Figure 6.6(a,i)).

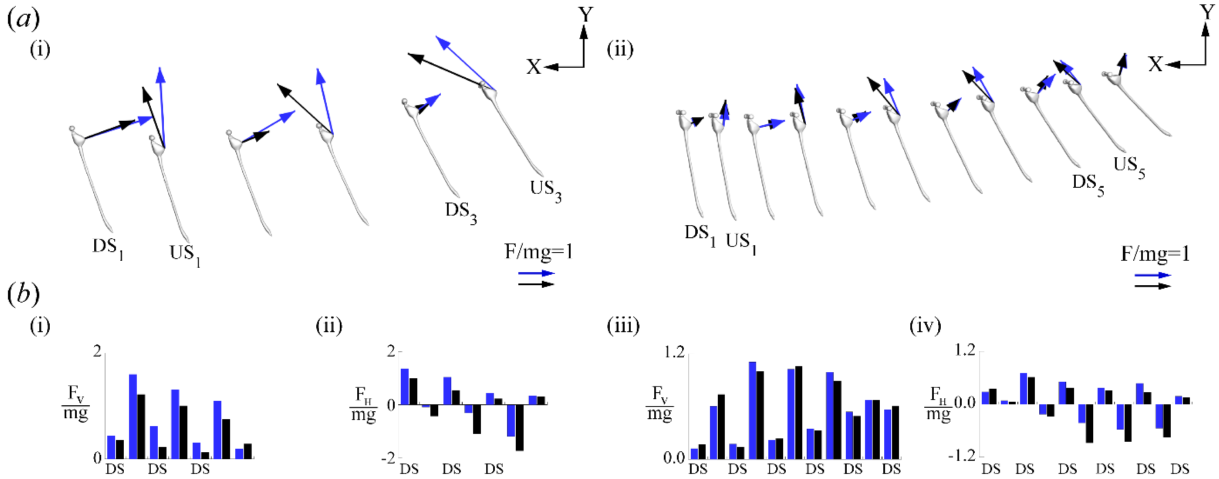

Figure 6.6. Force orientation in the global frame. (a) Halfstroke-average force vectors of (i) DaF#1 and (ii) DaF#1 for all the complete half strokes in Figure 6.5. Blue and black arrows represent the fore and hindwing forces, respectively. The force vectors are superimposed on the instantaneous body posture at the average midstroke of the fore and hindwings (b) Contribution of each half stroke to vertical and horizontal force production.

Second, the aerodynamic function of the US became dual, producing both vertical forces and negative horizontal (or forward) forces to keep the insect aloft and reduce the flight speed, respectively. The US force vectors which were initially pointing upward during speed-up were significantly tilted forward (-X direction) (US 3 for FW, US 2 & 3 for HW (Figure 6.6(a,i))) with the HW force vectors being more tilted forward than the FW's. The US's role in horizontal force generation followed a reverse trend in comparison to the DS as the magnitude of the horizontal (forward) force increased from speed-up to slow-down (Figure 6.6(b,ii)). The average muscle-mass specific power consumed by the damselfly (DaF#1) was ~94W/kg (FW: 43W/kg; HW: 51W/kg).

DaF#2 produced an average vertical force of 1.2x BW to stay aloft. Similar to DaF#1, the majority of the vertical force was generated during the US, while the horizontal force was produced in the DS or US depending on the phase of flight. During speed up, backward force was produced in the DS. Unlike DaF#1, the DS force magnitude did not diminish in each subsequent stroke (Figure 6.6(b,iv)).

The US generated little amounts of horizontal force during speed-up. During slow-down, the US generated mainly negative horizontal forces to counteract the positive horizontal forces produced by the DS. During slow-down, however, the DS also generated lift some lift as shown by the orientation of the force vector. The average muscle-mass specific power consumed by the damselfly (DaF#1) was ~52W/kg (FW: 22W/kg; HW: 30W/kg).

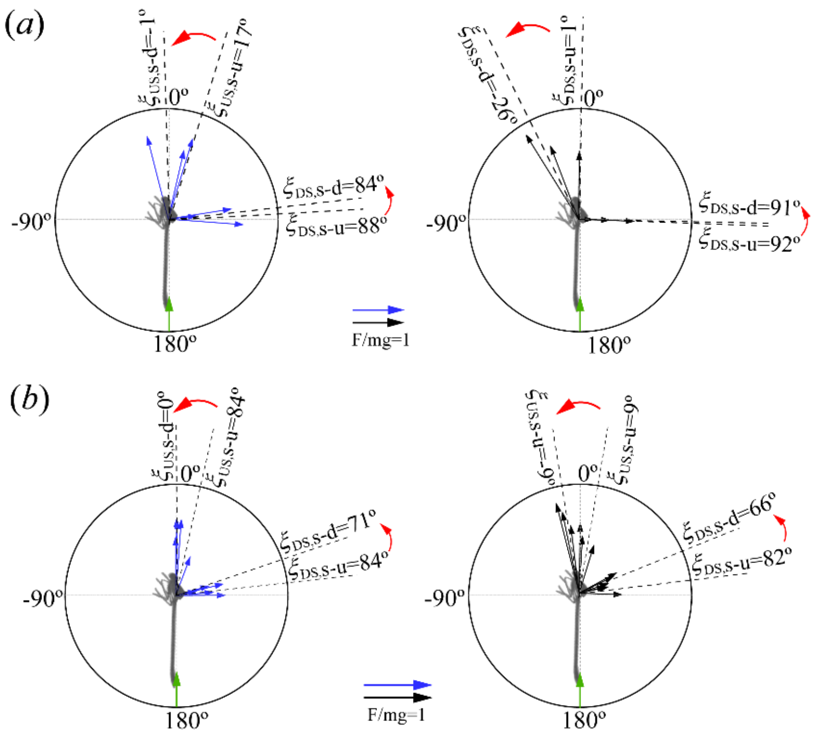

Figure 6.7. Force orientation relative to the body. (a) DaF#1 (b) DaF#2. Negative values of ξ, indicate that the force vector is in front of (or below) the longitudinal axis. The curved red arrow shows the tilt of the force vector from the speed-up to the slow-down phase. Subscripts s-u and s-d are speed-up and slow-down. Blue vector- FW. Balck vector-HW. Green arrow- longitudinal axis.

6.4.2.2. Local frame

The tilt (ξ) of the force vector relative to the longitudinal axis is shown in Figure 6.7. The results indicate that the tilt of the force vector in the global frame was also due to the rotation (shown by red curly arrows) of the force vector relative to the long axis of the body in addition to body angle adjustments. For Daf#1 (Figure 6.7(a)), during speed up, ξ_{DS} was 88° (FW) and 92(HW) while ξ_{US} was 17 (FW) and 1(HW). During slow-down, ξ_{DS} was 84° (FW) and 91° (HW) while ξ_{US} was -1° (FW) and -26° (HW). For Daf#2 (Figure 6.7(b)), during speed up, ξ_{DS} was 84(FW) and 82° (HW) while ξ_{US} was 12° (FW) and 9° (HW). During slow-down, ξ_{DS} is 71° (FW) and 66° (HW) while ξ_{US} is 0° (FW) and -9° (HW). Negative values of ξ indicate that the force vector is in front of (or below) the longitudinal axis. There was a more significant reliance force tilt relative to the body in the US in DaF#1 than #2 to slow down.

The roles of the wing pairs can be elucidated both from their orientation. The hindwing forces are more tilted away than the forewing forces from the longitudinal axis as well as in the global frame, in addition to having a larger magnitude during the slow down phase. Therefore, the HW was more instrumental in slowing the insect down.

6.4.3. Three-dimensional vortex structures

Here, we visualized the 3D flow features during a representative stroke of the speed-up and slow-down phase of DaF #1 and 2, by taking snapshots when the maximum force was produced (Figures 6.8 and 6.9). The flow structures are presented for the fore and hindwings separately because the FW leads during flight. We identified the relevant flow features and juxtaposed both flight phases.

During speed-up, the flow is separated on both wing pairs (Figure 6.8(a)) in the DS. An LEV which feeds into a TV which extends as a contrail during wing excursion is present. In the US, an LEV is also evident (Figure 6.8(b)) and indicates that both half strokes generate substantial forces during speed-up (Figure 6.5).

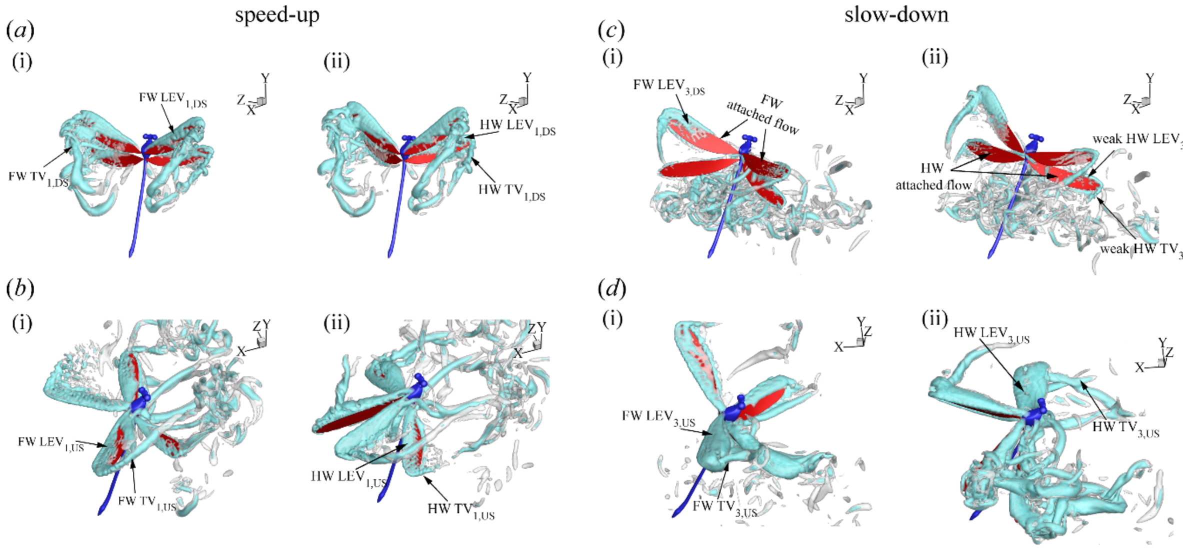

Figure 6.8. Three-dimensional flow features of DaF #1 visualized by the Q-criterion during maximum force production. TEV-trailing edge vortex. TV-Tip vortex. Subscripts 1, 3 signify vortices formed in those respective flapping strokes 1 (speed-up) and 3 (slow-down). Q=200,400 (1.25 and 2.5% of maximum Q, respectively). Top row (a, c) represents the DS, and the bottom row (c, d) represents the US.

During the slow-down phase, however, the flow did not separate on both wing pairs during the DS. Attached flows characterized most of the flow on the wings (Figure 6.8(c)). Although a much smaller LEV compared to the speed-up phase can be observed on the FW (Figure 6.8(c,i)), it was confined to the tip region. On the HW, there is no LEV formation. This is different from the speed-up phase, where the HW DS has an LEV stably attached to the wing surface (Figure 6.8(a)). During the US, an LEV covered the entire wing surface (Figure 6.8(d)). The absence of the LEV in the DS and its presence in the US indicates that the US dominates force production during the slow-down phase.

For DaF#2, the flow in the speed-up phase is similar to DaF#1's. In the slow-down phase, however, the flow is separated during the DS. Although the DS AoA is smaller than the US's, the DS AoA is above the attached flow threshold (Figure 6.9(c)).

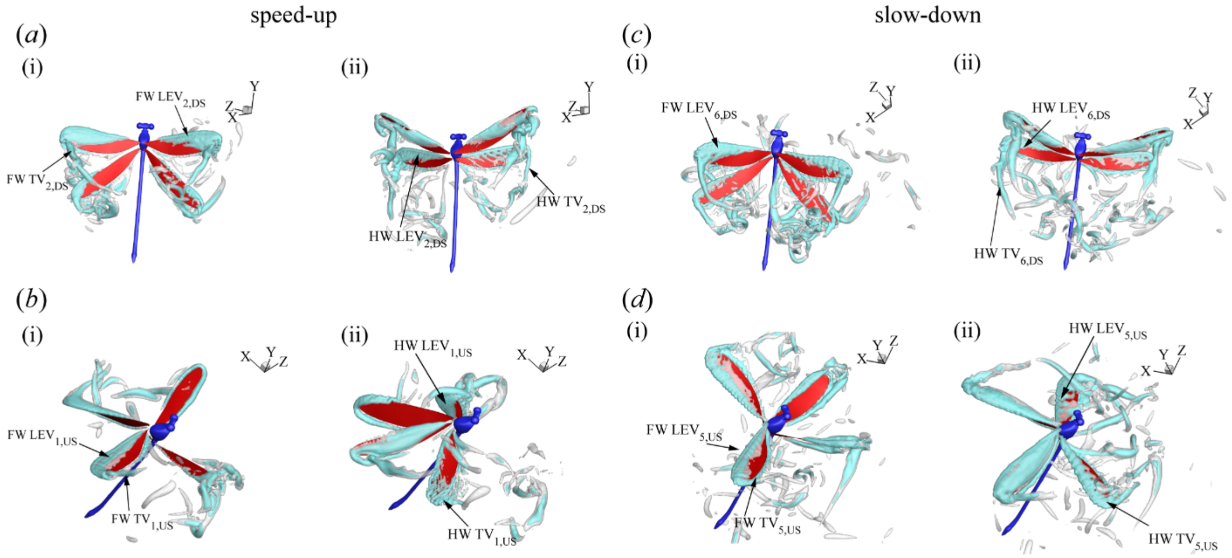

Figure 6.9. Three-dimensional flow features of DaF #2 visualized by the Q-criterion during maximum force production (DaF#2). Subscripts 1,2,5,6 signify vortices formed in those respective strokes. Top row (a,c) represents the DS, and the bottom row (b, d) represents the US.

6.4.4. Leading edge vortex circulation

The flow features indicate that the flow in the speed-up and slow-down phase are particularly distinct for DaF#1. Thus we quantified the LEV strength and pressure distribution (§6.4.5) for this damselfly. The strength of the LEV on the wing surface was measured by quantifying its circulation. 2D planes normal to the axis of the LEV were constructed at every time step of the CFD simulation (Figure 6.10(a)). On each 2D plane, the vorticity (ω) along the LEV axis was calculated. The circulation is defined as the flux of vorticity (Eqn. 3).

$$\Gamma^*_{LEV} = \frac{1}{c\bar{\mathrm{U}}_{\mathrm{eff}}} \iint_S \omega \cdot dS. \tag{10}$$

The closed surface of integration (dS) is bound by a vorticity threshold ~10% of maximum spanwise vorticity to capture the LEV. However, using a vorticity threshold means one cannot distinguish between a vortex and the shear layer [20]. Thus, over-estimates are possible, especially at low *Re* where the viscous shear layer is thicker. We showed the time history of LEV circulation at mid-wing (0.5R) in Figure 6.10(c). At wing reversal, an LEV was shed, and another developed on the opposite surface of the wing. Hence a discontinuity exists in the circulation curves.

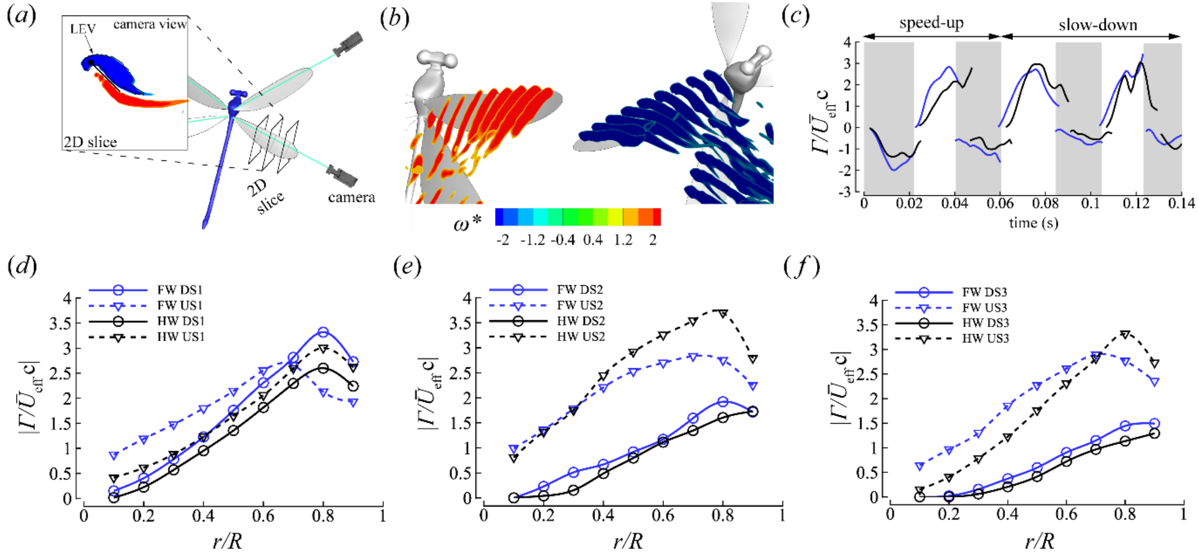

Figure 6.10. LEV circulation. (a). Depiction of the calculation of LEV circulation. The cyan lines depict the axis passing through the vortex core (b). Non-dimensional spanwise vorticity on each 2D slice at mid-stroke (i) DS (ii) US (c). Time history of LEV circulation at 0.5R (d-f). Spanwise distribution of circulation at mid-stroke for the 1st, 2nd and 3rd strokes respectively.

During the 1st stroke, corresponding to a significant part of the speed-up phase, the LEV circulation was large in both half strokes. In subsequent strokes, the LEV circulations during the DS diminished significantly (Figure 6.10(c)) commensurate with the force measurements (Figure 6.5(a)). The attenuation of circulation observed in the 2nd, and 3rd DS corresponds to the presence of to the attached flows or a very weak LEV for both wing pairs but especially for the hindwings identified in Figure 6.8(c).

The spanwise distribution of LEV circulation the mid-strokes are reported in Figure 6.10(d-f). The circulation increases along the span and tapers near the wingtip with maximum circulation occurring around 0.7-0.8R. The US's LEV circulation, shown in dashed lines, is greater than the DS's circulation, which decreases in each successful stroke (compare solid lines in Figure 6.10(d-f)). Quantitative values of LEV circulation are included in Table 6.5. All the US-to-DS ratios of LEV circulation are greater than 1. The ratio gets larger as the insect transitions from the speed-up to slow-down phase, increasing from 1.42 to 3.74 and 1.47 to 5.04 for the FW and HW, respectively.

To further describe the flow topology, it is common to use a combination of two or more criteria to identify the vortex structures [21]. Here, streamlines are superimposed on vorticity contours and shown in Figure 6.11. Flow separation is evident at the leading edge of the wing during speed-up in both half strokes and is signified strong vorticity and spiraling streamlines (Figure 6.11(a,b –i,ii)). The focus of the streamlines coincides with a vorticity maximum. Looking from the same point of view through the axis of the LEV, during slow-down, there is no flow separation during the DS (Figure 6.11(a,b –iii)). The shear layer is visible, but there is not an LEV or spiraling streamlines that coincide with vorticity maximum. Rather the streamlines run parallel to the wing surface. In contrast, during the US, an LEV rests on the wing surface (Figure 6.11(a,b -iv)). These findings corroborate our visualizations using the Q-criterion.

Table 6.5. Leading edge vortex circulation quantification. $\overline{\Gamma}^*$ represents the time half stroke averaged values. $\Gamma^*_{\max}$ represents the maximum circulation per half stroke. All values are measured at midspan (0.5R).

flapping stroke			$\overline{\Gamma}^*$	$\Gamma^*_{\max}$	$\left\lvert \frac{\overline{\Gamma}^*_{US}}{\overline{\Gamma}^*_{DS}} \right\rvert$	$\left\lvert \frac{\Gamma^*_{\max_{US}}}{\Gamma^*_{\max_{DS}}} \right\rvert$	$\left\lvert \frac{\overline{\Gamma}^*_{US} - \overline{\Gamma}^*_{DS}}{\overline{\Gamma}^*_{DS}} \right\rvert \%$
1st	FW	DS	-1.32	-2.00	1.42	1.42	42%
		US	1.87	2.84			
	HW	DS	-0.99	-1.37	1.47	1.58	47%
		US	1.46	2.16			
2nd	FW	DS	-0.98	-1.63	1.87	1.66	87%
		US	1.83	2.71			
	HW	DS	-0.75	-1.01	2.67	2.94	167%
		US	2.00	2.97			
3rd	FW	DS	-0.50	-0.80	3.74	4.05	274%
		US	1.87	3.26			
	HW	DS	-0.37	-0.57	5.06	5.34	405%
		US	1.87	3.04			

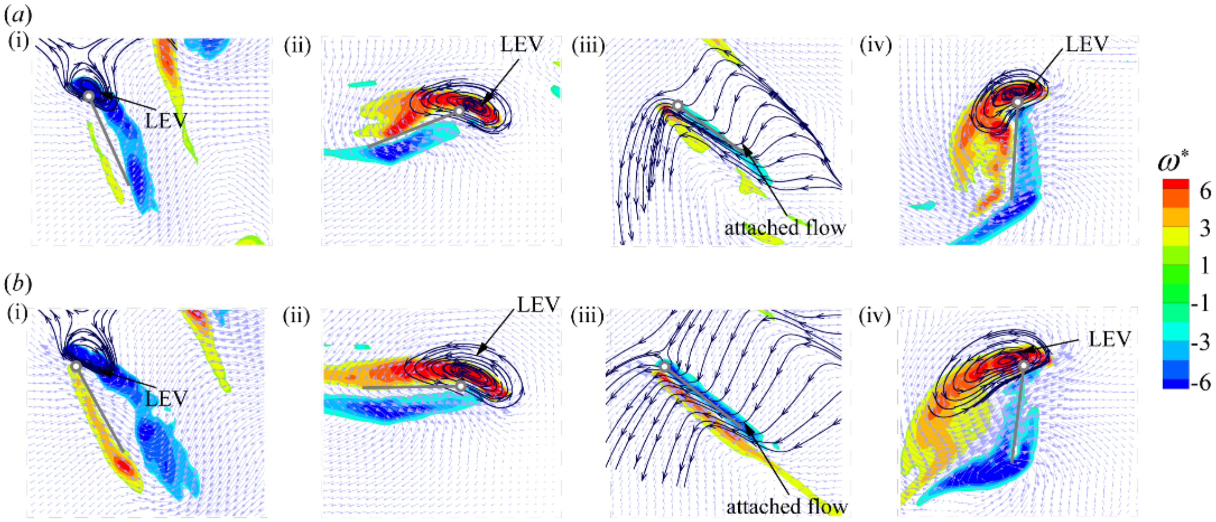

Figure 6.11. Flow topology during the speed-up and slow-down phases visualized using vorticity contours and streamlines, on the left hindwings of DF#1 at the same instant as Figure 6.8 (a, ii) and (c, ii). Top row (a) and Bottom row (b) are the cross-sections at 0.5R and 0.7R, respectively. DS (i) speed-up phase, (iii) slow-down phase. US (ii) speed-up phase, (iv) slow-down phase.

6.4.5. Pressure distribution

The pressure difference between the dorsal and ventral surface of the wing at the same time instant as Figure 6.8 is projected onto a representative wing model (Figure 6.11) and indicates what part of the wing produces the greatest velocity-difference or circulation. Figure 6.12 shows the pressure difference contours with the darker shade (blue) contours indicating regions of high-pressure difference at a location that coincides with the location of the LEV on the wing as well as the wingtip in both half strokes (Figure 6.8). In contrast, Figure 6.12(b,i) which corresponds to a DS during the slow down phase shows that the pressure difference is minimal (light shade contours) indicating low force generation and the lack of flow separation (absence of LEV) in the DS (Figure 6.11(b)). Figure 6.12(a-ii, b-ii) shows that large pressure differences occur during the US in all flight phases due to the presence of the LEV on the wing.

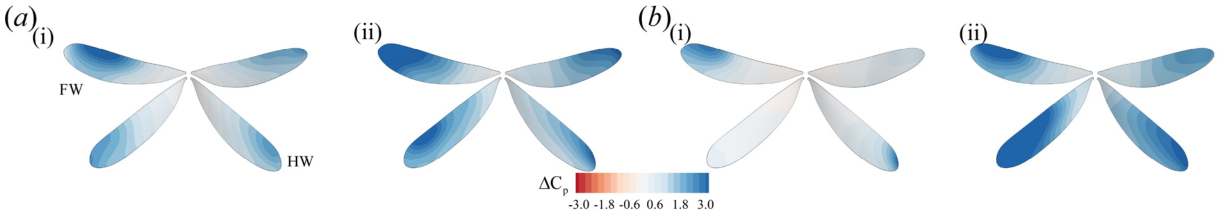

Figure 6.12. Pressure difference (ΔC_p) of the wing at mid-stroke during (a) the speed-up phase's (i) DS and (ii) US and during (b) the slow-down phase's (i) DS and (ii) US. The pressure on the side that contains the LEV is subtracted from the other side of the wing that does not. The pressure is non-dimensionalized as follows: $C_p = (p - p_\infty) / 0.5\rho\bar{\mathrm{U}}_{\mathrm{eff}}^{\;2}$ where p_∞ is the freestream pressure.

6.5. Discussion and conclusion

Different from previous studies on backward flight which typically focused on one phase of flight, mainly acceleration [4] or cruise [8], here, we investigated flight which consisted of both a speed-up (accelerating) and slow-down (decelerating) phase. This unsteady body motion, that is, speed-up and slow-down, usually preceded a transition to a forward flight mode. This flight pattern is readily observed in the wild [5, 7, 10] and is not particularly unique to damselflies, the insects we studied in this work. To understand what happened in both flight phases, we quantified the body and wing kinematics, the flight forces and flow features. Our findings are discussed in light of previous works below.

All the flight sequences were initiated with a steep body posture (Figure 6.3(d, iii)) which supports previous observations during the backward flight of hummingbirds (50-75º) [22], dragonflies (85-95º[4]; 100º[5]) waterlily beetles (50-70º) [23], cockchafer beetles [13] and cicadas (86-130º). Thus, steep body postures are a consistent feature of backward flight regardless of whether the stroke plane is horizontal or steeply inclined. Field recordings [5, 10], have indicated that damselflies can also fly backward with a horizontal posture (~0º), however. While we did not observe backward flight with a horizontal posture in the lab, further work will need to be done to address the differences between the steep and low body angles technique of backward flight in Zygoptera both in terms of wing and body kinematics and aerodynamics. Of the extant Odonata, dragonflies have only been observed to fly backward using a high body posture [4, 5]. Damselflies (Zygoptera) are similar to dragonflies (Anisoptera), although not exactly alike [5, 14, 19, 24-27]. The anisozygoptera (*Epiophlebia superstes*) which exhibits morphological characteristics of both the Anisoptera (dragonflies) and Zygoptera (damselflies) can perform backward flight with the low body angle technique [28]. However, the wing joint structure and wing planform shape of the Anisozygoptera is most similar to the Zygoptera [29].

Previous works on forward flight [25, 28] have reported that damselfly body alignment is independent of resultant (vertical + horizontal) force direction. Hence, large variation of the force vector in the body frame is possible due to more degrees of freedom of the wing actuation mechanism [24, 25, 28] and larger angle between the line connecting the wing joints and the longitudinal axis of damselflies than dragonflies [18]. More degrees of freedom indicates larger variation in stroke plane orientation relative to the body. Because of larger stoke plane variation in Zygoptera (approximately 60° [25]), it is possible that backward flight can be achieved without whole-body rotations. After all, the main function of the high body angles in backward flight is to rotate the stroke plane, which reorients the forces in the global frame, analogous to force vectoring by a helicopter [4]. Reduction in degrees of freedom of the wing also indicates that the metathoracic wing stroke motor system is simplified [24] and the stroke plane is more constrained relative to the body. Thus, rotating the body, which in turn rotates the stroke plane in the global frame for force reorientation is a simpler alternative to rotating the stroke plane relative to the body through actuation at the wing hinge without any changes in body posture. When implementing designs in MAVs, an upright body posture is the easier for inducing backward flight because it can be performed with reduced complexity of wing actuation. Insects like cicadas and beetles [13, 23] with constrained stroke planes rely on force vectoring alone. The Delfly-II MAV has been shown to initiate backward flight by modulating the body angle to about 100º from its stable flight configuration [30] with even fewer wing degrees of freedom than a real insect.

Upright body postures may incur a drag penalty, however. The typical measurement of parasite drag is performed on an isolated body with inflow to mimic flight speed [8, 31]. Sapir and Dudley [8], showed that drag forces generated only differed by 3.6% between the backward and forward flight of Hummingbirds despite the drastically different body postures. Since the flight speeds are low, typically less than 3 m/s during backward free flight [4, 11], the drag penalty may not be significant [6]. The measured parasite drag coefficient for dragonfly backward flight was in the measured range (0.31-0.84) for forward flight [4]. The parasite drag coefficient is defined as $\bar{C}_D = \frac{\bar{\mathrm{F}}_{\mathrm{H,b}}}{0.5\rho\bar{U}_b^2 S_{\mathrm{frontal}}}$, where $\bar{\mathrm{F}}_{\mathrm{H,b}}$ is the mean horizontal force of the body with the same motion as in flight, $\bar{\mathrm{U}}_{\mathrm{b}}$ is the average backward velocity. $S_{\mathrm{frontal}} = A_{\mathrm{MF}}\sin(\bar{\chi})$ is the frontal area presented to the flow, where A_{MF} is the mid-frontal area of the insect. $\bar{C}_{\mathrm{D}}$ was 1.92 and 2.38 for DaF#1 and #2, respectively. $\bar{C}_{\mathrm{D}}$ was greater than values (0.91-1.66) measured by Wakeling [31] for normal forward flight angles (10-30º) for a damselfly (*Calopteryx splendens*) under steady conditions (*Re*=2770). Yet, $\bar{C}_{\mathrm{D}}$ was much smaller than those measured traveling forward with an angle of 70º where $\bar{C}_{\mathrm{D}}$=4.58 [31].

Slender bodied insects are likely not to rely on the body to actively produce drag since the body force are marginal in comparison to the wing forces. During the slow-down phase, where the body angles should increase to a more upright posture (~90º) to maximize frontal area, the body angle decreased (Figure 6.3(d)) probably due to the desire to switch the flight mode after slowing down. Thus, indicating the priority of using the body for force reorientation over body drag to slow down. If the body is already horizontal, acceleration to the new flight mode can occur without waiting for body angle to tilt [32]. Appropriating a steep body angle thus necessitates that the slow-down phase is prolonged (as in the case of damselflies) as the insect tries to reorient its body to a more horizontal posture during slow-down before the transition to another flight mode can occur. The coordination of the body and wings which was achieved through a combination of stroke plane rotation relative to the body and large AoA variation was responsible for reorienting flight forces by rotating the force vector relative to the body (Figure 6.7). Furthermore, in the global frame additional adjustment of the body angle (Figure 6.3(c)) flattened the stroke plane relative to the horizon (Figure 6.13) and rotated the force vector (Figure 6.6).

Table 6.6. Net force generation in forward and backward flight of Odonata. The averages are reported based on all complete half strokes. The speed-up and slow-down phase for the damselflies are combined.

insect		flight mode	$\overline{F}_{DS}/mg$ (FW)	$\overline{F}_{US}/mg$ (FW)	$\overline{F}_{DS}/mg$ (HW)	$\overline{F}_{US}/mg$ (HW)	reference
damselfly		forward	1.22	0.32	1.60	0.30	Bode-Oke et al. [19]
			0.69	0.24	1.22	0.39	Sato et. al [18]
	1	backward	0.90	1.55	0.61	1.64	current study
	2		0.60	0.98	0.63	0.96	
dragonfly		forward	1.21	0.27	1.06	0.32	Azuma and Watanabe [33]
			0.94	0.38	1.06	0.53	Hefler et al. [34]
		backward	1.44	2.15	2.07	3.17	Bode-Oke et. al. [4]

In backward flight, backward force is produced predominantly in the DS. Increasing or maintaining a large AOA in the DS (Figure 6.13(b)) during slow-down will increase the pressure drag and produce backward and even vertical forces (Figure 6.5 (b)). To slow down, the damselfly may compensate by actively generating more negative (forward) thrust forces than positive (backward) thrust forces produced by the aerodynamically active DS (Figure 6.5 (b)). This trend was exhibited more by DF#2.

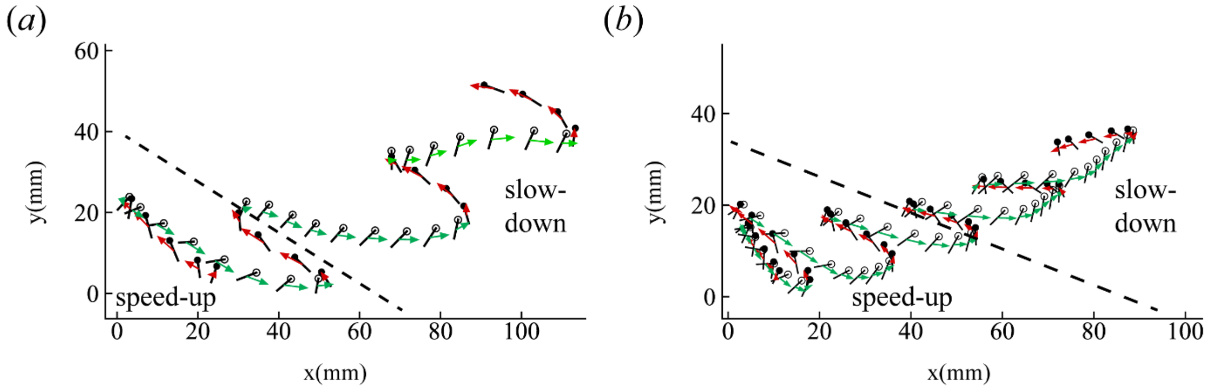

Figure 6.13. Wing motion of the hindwing in the global frame. (a) DaF#1 (b) DaF#2. Lollipop figures with open and closed circles signify the US and DS, respectively. Green arrow- US velocity, red arrow- DS velocity. Dashed lines demarcate the speed-up and slow-down phases.

Due to morphological constraints on wingspan and area reduction, most insects cannot fold or flex their wings like birds do to render the half stroke inactive to reduce both the inertial and aerodynamic costs in flight [35, 36]. Thus, to slow down, a viable alternative is to modulate wing AoA such that the half stroke responsible for producing the backward force (that is, the DS in backward flight) operated at very low AoA (Figure 6.13(a)). This will reduce the pressure drag on the wings, prevent further backward motion and reduce the aerodynamic power consumption because it renders to renders the half stroke aerodynamically inactive. We observed this in the flight of DaF#1 (Figures 6.8, 6.10, 6.11, and 6.12).

During backward flight of DaF#1, the wings sliced forward (DS) at a much lower angle attack and pushed backward (US) at a much higher angle to generate negative horizontal force to slow down (Figure 6.4(a) and Figure 6.13(a)). The large drag (negative horizontal forces) generated during slow down occurred predominantly in the US. In forward flight, when negative thrust was generated, it is usually produced during the DS [18, 19]. Rüppel's [5] observation of an increase in US AoA and reduction in DS AOA during the transition from backward to forward flight of the damselfly (*Megaloprepus coerulatus*) in the field corroborate our findings.

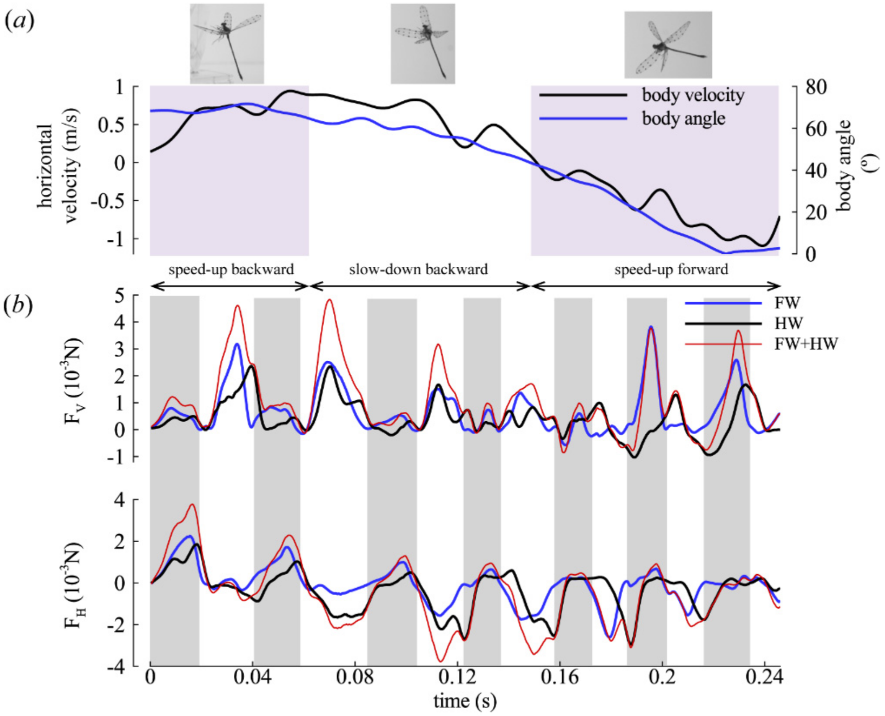

Figure 6.14. Transitioning from backward to forward flight (a) body velocity and body angle; purple shadings denote the flight phases qualitatively. The damselfly posture in the middle of each phase is shown (b) Forces. Gray shading denotes the forewing DS.

Only a few studies have analyzed the flow over damselfly wings [14, 19]. The CFD simulations here indicated that the main vortex structure on the wings was an LEV. The LEV is a well-known lift enhancing mechanism used in insect flight [14, 22, 37]. However, the presence of the LEV or and its strength varied depending on flight phase commensurate with the wing kinematics (Figure 6.6 and Figure 6.11). Studies of insects that use asymmetric strokes in an inclined stroke plane have also reported that the LEV circulation is substantially higher in the DS compared to US where there may be no sign of an LEV [14, 22, 38, 39]. Attached flow usually dominate due to low AoA leading to an aerodynamically inactive US [19, 22].

Consequently, in forward flight, the DS dominates vertical force production, and the US produces thrust (horizontal force) [5, 40, 41] (Table 4.7). The forces produced during the US are considerably smaller compared to the DS forces [19, 32, 38]. We observed that the LEV was present on both wing pairs and in both half strokes during speed-up commensurate with the wing AoA (Figure 6.8). The US LEV was stronger than the DS LEV. US-to-DS LEV circulation ratios as high as 3.74 and 5.06 for the fore and hind wings respectively were reported for DaF#1 (Table 6.5). The presence of the LEV in both half strokes shows that substantial forces are produced in both half strokes and that the US produces larger forces than the DS. This active US was responsible for weight support during speed-up as well as drag (negative thrust) generation to slow down during deceleration. The FWs dominated force production during speed up while the HWs were responsible for slowing the insect down.

Past work on forward free-flying butterflies [3] and dragonflies [22] have shown that use of aerodynamic mechanism can vary between flight phases in forward flight, that is, steady motion and rapid acceleration. Our findings add to the existing body of knowledge show that damselflies modulate kinematics and more importantly, flow features and aerodynamic mechanisms depending on the phase of flight by simple changes in wing kinematics.

Table 6.7. Percentage of the contribution of the DS and US to net force for different insects that use an inclined stroke plane during hover (*J*=0) and when there is body motion (*J*≠0).

insect	flight mode		DS force (%)	US force (%)	reference
cicada	forward		90	10	Liu et al. [42]
			80	20	Wan et al. [43]
	backward		50	50	Bode-Oke and Dong (under review)
damselfly	forward		75	25	Sato et al. [18]
			84	16	Bode-Oke et al. [19]
	takeoff		50	50	
	backward DF#1	acc.	41	59	current study
		dec.	21	79	
	backward DF#2	acc.	37	63	
		dec.	41	59	
dragonfly	backward		33	67	Bode-Oke et al. [4]
	forward		80	20	Azuma and Watanabe [33]
			67	33	Hefler et al. [34]
fruit fly	forward		61	39	Meng and Sun [44]
hawkmoth	forward		80	20	Willmott et al. [38]
	hovering		67	33	Aono and Liu [45]
butterfly	forward		75	25	Zheng et al. [46]
hoverfly	hovering		73	27	Mou et al. [47]
hummingbird	forward		74	26	Song et al. [48]
locust	forward		86	14	Young et al. [49]

Lastly, the backward flight phase was followed by an accelerating forward flight before transitioning into another flight mode (Figure 6.14). Our result showed that χ was significantly reduced to a horizontal posture ($\overline{\chi}$ was approximately 18º). In this configuration, the front end of the stroke plane which was tilted up in the backward flight phase was now tilted downward. As a result, the aerodynamic functions of the half strokes were reversed compared to the speed-up phase of backward flight. The DS generated vertical forces and the US horizontal forces to propel the insect forward.

6.6. References

[1] Sane, S.P. 2003 The aerodynamics of insect flight. *The journal of experimental Biology* **206**, 4191-4208.

[2] Wang, Z.J. 2005 Dissecting insect flight. *Annu. Rev. Fluid Mech.* **37**, 183-210.

[3] Srygley, R.B. & Thomas, A.L.R. 2002 Unconventional lift-generating mechanisms in free-flying butterflies. *Nature* **420**, 660. (doi:10.1038/nature01223 https://www.nature.com/articles/nature01223#supplementary-information).

[4] Bode-Oke, A.T., Zeyghami, S. & Dong, H. 2018 Flying in reverse: kinematics and aerodynamics of a dragonfly in backward free flight. *Journal of The Royal Society Interface* **15**. (doi:10.1098/rsif.2018.0102).

[5] Rüppell, G. 1989 Kinematic analysis of symmetrical flight manoeuvres of Odonata. *Journal of Experimental Biology* **144**, 13-42.

[6] Dudley, R. 2002 *The biomechanics of insect flight: form, function, evolution*, Princeton University Press.

[7] Yokoi, T. & Fujisaki, K. 2009 Hesitation behaviour of hoverflies Sphaerophoria spp. to avoid ambush by crab spiders. *Naturwissenschaften* **96**, 195-200.

[8] Sapir, N. & Dudley, R. 2012 Backward flight in hummingbirds employs unique kinematic adjustments and entails low metabolic cost. *The Journal of experimental biology* **215**, 3603-3611.

[9] Zeil, J. & Wittmann, D. 1989 Visually controlled station-keeping by hovering guard bees ofTrigona (Tetragonisca) angustula (Apidae, Meliponinae). *Journal of Comparative Physiology A* **165**, 711-718.

[10] Rüppell, G. 2015 Dragonfly flight: Small Red Eye Damselfly - Heavy Fighter. (https://youtu.be/_5HhXy3KD5k.

[11] Bomphrey, R.J., Taylor, G.K. & Thomas, A.L.R. 2009 Smoke visualization of free-flying bumblebees indicates independent leading-edge vortices on each wing pair. *Experiments in Fluids* **46**, 811-821. (doi:10.1007/s00348-009-0631-8).

[12] Nachtigall, W. 1998 Landing-and take-off flight behaviour of the potter wasp Odynerus reniformis at its nesting tube with and without a load (Hymenoptera: Eumenidae). *Entomologia Generalis* **22**, 177-198.

[13] Schneider, P. 1981 Flugmanöver der käfer. *Mitteilungen der Deutschen Gesellschaft für Allgemeine und Angewandte Entomologie* **3**, 259-263.

[14] Bomphrey, R.J., Nakata, T., Henningsson, P. & Lin, H.-T. 2016 Flight of the dragonflies and damselflies. *Philosophical Transactions of the Royal Society B: Biological Sciences* **371**. (doi:10.1098/rstb.2015.0389).

[15] Farina, W.M., Kramer, D. & Varjú, D. 1995 The response of the hovering hawk moth Macroglossum stellatarum to translatory pattern motion. *Journal of Comparative Physiology A* **176**, 551-562. (doi:10.1007/BF00196420).

[16] Koehler, C., Liang, Z., Gaston, Z., Wan, H. & Dong, H. 2012 3D reconstruction and analysis of wing deformation in free-flying dragonflies. *The Journal of experimental biology* **215**, 3018-3027.

[17] Mittal, R., Dong, H., Bozkurttas, M., Najjar, F., Vargas, A. & von Loebbecke, A. 2008 A versatile sharp interface immersed boundary method for incompressible flows with complex boundaries. *Journal of computational physics* **227**, 4825-4852.

[18] Sato, M. & Azuma, A. 1997 The flight performance of a damselfly Ceriagrion melanurum Selys. *Journal of Experimental Biology* **200**, 1765-1779.

[19] Bode-Oke, A., Zeyghami, S. & Dong, H. 2017 Aerodynamics and flow features of a damselfly in takeoff flight. *Bioinspiration & biomimetics* **12**, 056006.

[20] Haller, G. 2005 An objective definition of a vortex. *Journal of Fluid Mechanics* **525**, 1-26. (doi:10.1017/S0022112004002526).

[21] Bomphrey, R.J., Lawson, N.J., Taylor, G.K. & Thomas, A.L.R. 2006 Application of digital particle image velocimetry to insect aerodynamics: measurement of the leading-edge vortex and near wake of a Hawkmoth. *Experiments in Fluids* **40**, 546. (doi:10.1007/s00348-005-0094-5).

[22] Thomas, A.L., Taylor, G.K., Srygley, R.B., Nudds, R.L. & Bomphrey, R.J. 2004 Dragonfly flight: free-flight and tethered flow visualizations reveal a diverse array of unsteady lift-generating mechanisms, controlled primarily via angle of attack. *Journal of Experimental Biology* **207**, 4299-4323.

[23] Mukundarajan, H., Bardon, T.C., Kim, D.H. & Prakash, M. 2016 Surface tension dominates insect flight on fluid interfaces. *Journal of Experimental Biology* **219**, 752-766. (doi:10.1242/jeb.127829).

[24] Pfau, H. 1991 Contributions of functional morphology to the phylogenetic systematics of Odonata. *Advances in Odonatology* **5**, 109-141.

[25] Wakeling, J. & Ellington, C. 1997 Dragonfly flight. II. Velocities, accelerations and kinematics of flapping flight. *Journal of experimental biology* **200**, 557-582.

[26] Marden, J.H. 1987 Maximum lift production during takeoff in flying animals. *J. exp. Biol* **130**, 235-238.

[27] Lehmann, F.-O. 2009 Wing–wake interaction reduces power consumption in insect tandem wings. *Experiments in fluids* **46**, 765-775.

[28] Rüppell, G. & Hilfert, D. 1993 The flight of the relict dragonfly Epiophlebia superstes (Selys) in comparison with that of the modern Odonata (Anisozygoptera: Epiophlebiidae). *Odonatologica* **22**, 295-309.

[29] Pfau, H.K. 1986 Untersuchungen zur Konstruktion, Funktion und Evolution des Flugapparates der Libellen (Insecta, Odonata). *Tijdschrift voor entomologie.* **129**, 35-123.

[30] Caetano, J.V., de Visser, C.C., Remes, B.D., De Wagter, C., Van Kampen, E.-J. & Mulder, M. 2013 Controlled flight maneuvers of a Flapping Wing Micro Air Vehicle: a step towards the DelFly II Identification. In *AIAA Atmospheric Flight Mechanics (AFM) Conference* (p. 4843.

[31] Wakeling, J. & Ellington, C. 1997 Dragonfly flight. I. Gliding flight and steady-state aerodynamic forces. *Journal of Experimental Biology* **200**, 543-556.

[32] Ellington, C.P. 1999 The novel aerodynamics of insect flight: applications to micro-air vehicles. *Journal of Experimental Biology* **202**, 3439-3448.

[33] Azuma, A. & Watanabe, T. 1988 Flight performance of a dragonfly. *Journal of Experimental Biology* **137**, 221-252.

[34] Hefler, C., Noda, R., Shyy, W. & Qiu, H. 2017 Unsteady Vortex Interactions for Performance Enhancement of a Free Flying Dragonfly. In *ASME 2017 Fluids Engineering Division Summer Meeting* (pp. V01CT21A010-V001CT021A010, American Society of Mechanical Engineers.

[35] Willmott, A.P. & Ellington, C.P. 1997 The mechanics of flight in the hawkmoth Manduca sexta. II. Aerodynamic consequences of kinematic and morphological variation. *The Journal of Experimental Biology* **200**, 2723-2745.

[36] Crandell, K.E. & Tobalske, B.W. 2015 Kinematics and aerodynamics of avian upstrokes during slow flight. *The Journal of Experimental Biology* **218**, 2518-2527. (doi:10.1242/jeb.116228).

[37] Johansson, L.C., Engel, S., Kelber, A., Heerenbrink, M.K. & Hedenström, A. 2013 Multiple leading edge vortices of unexpected strength in freely flying hawkmoth. *Scientific Reports* **3**, 3264. (doi:10.1038/srep03264).

[38] Willmott, A.P., Ellington, C.P. & Thomas, A.L. 1997 Flow visualization and unsteady aerodynamics in the flight of the hawkmoth, Manduca sexta. *Philosophical Transactions of the Royal Society B: Biological Sciences* **352**, 303-316.

[39] Wang, J.K. & Sun, M. 2005 A computational study of the aerodynamics and forewing-hindwing interaction of a model dragonfly in forward flight. *Journal of Experimental Biology* **208**, 3785-3804. (doi:10.1242/jeb.01852).

[40] Azuma, A., Azuma, S., Watanabe, I. & Furuta, T. 1985 Flight mechanics of a dragonfly. *Journal of experimental biology* **116**, 79-107.

[41] Wang, Z.J. & Russell, D. 2007 Effect of forewing and hindwing interactions on aerodynamic forces and power in hovering dragonfly flight. *Physical review letters* **99**, 148101.

[42] Liu, G., Dong, H. & Li, C. 2016 Vortex dynamics and new lift enhancement mechanism of wing–body interaction in insect forward flight. *Journal of Fluid Mechanics* **795**, 634-651.

[43] Wan, H., Dong, H. & Gai, K. 2015 Computational investigation of cicada aerodynamics in forward flight. *Journal of The Royal Society Interface* **12**, 20141116.

[44] Meng, X. & Sun, M. 2016 Wing Kinematics, Aerodynamic Forces and Vortex-wake Structures in Fruit-flies in Forward Flight. *Journal of Bionic Engineering* **13**, 478-490. (doi:https://doi.org/10.1016/S1672-6529(16)60321-9).

[45] Aono, H. & Liu, H. 2006 Vortical Structure and Aerodynamics of Hawkmoth Hovering. *Journal of Biomechanical Science and Engineering* **1**, 234-245. (doi:10.1299/jbse.1.234).

[46] Zheng, L., Hedrick, T.L. & Mittal, R. 2013 Time-Varying Wing-Twist Improves Aerodynamic Efficiency of Forward Flight in Butterflies. *PLOS ONE* **8**, e53060. (doi:10.1371/journal.pone.0053060).

[47] Mou, X.L., Liu, Y.P. & Sun, M. 2011 Wing motion measurement and aerodynamics of hovering true hoverflies. *The Journal of Experimental Biology* **214**, 2832-2844. (doi:10.1242/jeb.054874).

[48] Song, J., Tobalske, B.W., Powers, D.R., Hedrick, T.L. & Luo, H. 2016 Three-dimensional simulation for fast forward flight of a calliope hummingbird. *Royal Society Open Science* **3**. (doi:10.1098/rsos.160230).
[49] Young, J., Walker, S.M., Bomphrey, R.J., Taylor, G.K. & Thomas, A.L.R. 2009 Details of Insect Wing Design and Deformation Enhance Aerodynamic Function and Flight Efficiency. *Science* **325**, 1549-1552. (doi:10.1126/science.1175928).

Chapter 7
Wing damage influence choice of wing kinematics in the backward flight of the dragonfly *(Erythemis simplicicollis)*

7.1. Abstract

Here, we investigated the effect of wing damage on the free backward flight of dragonflies. We performed substantial asymmetric incision of the wings both in the spanwise and chordwise direction and captured free flight kinematics with high-speed cameras. Our findings indicate that the choice of wing kinematics and the coordination between the wing pairs were affected. After wing damage, we observed an increase in flapping frequency for all but the forewing symmetric spanwise damage case which retained a similar flapping frequency as the intact wing case. There was also an increase in flapping amplitude and stroke plane tilt of the damaged wings. In contrast to the spanwise cuts, more significant increases in flapping amplitude occurred for the symmetric chordwise cuts on the forewings (20º). Surprisingly, accompanying this increase in forewing amplitude was a substantial reduction in hindwing flapping amplitude (40º). The phase relationship when the wings were damaged in the spanwise direction was maintained in the same range as the intact case (50º-70º). However, chordwise damaged changed the phase relationship between the wing pairs. The wings flapped approximately in phase, and then the FW led the motion, atypical of dragonfly flight. The change in phase relationship was responsible for the reduction in hindwing flapping amplitude because the forewings dictated that the number of chord lengths traveled between the wing pairs per stroke is approximately the same.

Keywords: wing damage, backward flight, active upstroke, phase relationship, dragonfly.

7.2. Introduction

Wing wear is common among flying taxa. Some forms of area loss are reversible such as seasonal wing feather molting in birds [1] while others are cumulative and irreversible, often resulting from external damage [2]. Non-repairable damage is a problem insects face, and the propensity of damage is linked to lifestyle choices, for instance, repeated collision with vegetation [3] and other species of the same kinds, intra-sexual competition[4], and mating [2]. Damage could potentially affect fecundity, mortality, predation success, foraging behavior [5, 6]. Flight performance may also be compromised not only as a result of the reduction in wing area but also the loss of sensing capabilities (due to loss of sensillae) and thus flight control [5, 7]. It is expected that the control challenges that impact insect in flight will affect impact micro-aerial vehicles.

Several studies have investigated the consequences of wing damage on flight performance with the majority having focused on two winged fliers such as flies or functionally four-winged fliers like hawkmoths and butterflies. Typically, damage in experimental studies involves symmetric or asymmetric spanwise or chordwise straight cuts. Some other studies have even varied the shape of the cut making jagged cuts and even poking holes to mimic natural wing wear [8]. However, not all types of damage have the same effect [9, 10]. To compensate for wing damage, insects rely on adjustments of both the wing and body kinematics. Past studies have reported ramifications such as increased flapping frequency, flapping amplitude, reduction in vertical acceleration, stoke plane angle adjustment [10-12].

Concerning four-winged fliers, most of the studies have been done on Odonates (dragonflies and damselflies) and Lepidopterans (Butterflies and moths). A recent work [2] on dragonflies showed that from samples collected in the field, 76.2 percent of the forewings and 78.6 percent of the hindwings were damaged. Most of the area loss was less than 10 percent of the wing area while severe damage could be as much as 75 percent of the wing area. Critical zones of wing damage were concentrated at the distal part of the wings toward to the trailing edge for both wing pairs and also around the proximal part of the hindwings (near the wing base) toward the trailing edge.

Hitherto, Combes et al. [5] showed that damage to the hindwings reduced the vertical acceleration during a drop-escape response, flight velocity, and predation success in the insectary. The amount of wing area loss was directly proportional to the reduction in vertical acceleration. The incisions made to the hindwings were symmetric (chordwise). Incising 30 percent of the hindwing led to a 30 percent decrease in vertical acceleration. Likewise, incising 50 percent of the area led to a 50 percent decrease in vertical acceleration, although at 50 percent the probability of arresting a fall in the drop escape response was lower. Kassner et al. [13] investigated how damselflies compensated for the loss of a fourth wing (hindwing). After completely removing the hindwings, damselflies could still fly albeit with kinematics adjustments. They observed an increase in flapping frequency, a reduction in the stroke plane relative to the body for the forewing on the same side as the ablated hindwing, as well as a reduction in flapping amplitude of only the hindwing involved in flight.

Spotting a butterfly out in the wild with broken wings is not uncommon. Thus, in a study on butterflies [7], the fully developed hindwings were removed entirely, reducing the total wing area by 49%. Nevertheless, the butterflies could still fly but lost their ability to zig-zag at high speed. This finding was evidenced by lower linear and turning acceleration, although their flight paths were not altered. Total forewing ablation precluded flight, however.

What is missing in the current studies, which is not possible in two-winged flight, is the investigation of the kinematics of the wing pairs and their coordination after wing damage. For butterflies, HW loss may potentially affect the aerodynamics, such as clap and peel, etc., which is dependent on the hindwings forming a seal [14], while for Odonates and other for four-winged fliers, the damage could affect the interaction between the wing pairs by influencing the phasing between wing pairs. In line with our previous on the aerodynamics of backward flight [15], here we investigated whether severe wing damage (both spanwise and chordwise) will preclude backward flight. Our laboratory observation indicated that flight can still be achieved after substantial incision of the wings. Our aim then was to investigate the changes in kinematics as well as coordination in fore and hindwing coordination.

7.3. Material and methods

7.3.1. Dragonflies, wing damage, high-speed video capture, and three-dimensional surface reconstruction.

The methods used in this study are identical to the methods outlined in previous studies [15, 16] except for wing incision. We captured dragonflies from a pond and transported to the lab for experiments. Shortly afterward, we placed the insects in a refrigerator to cool down and reduce muscle activity. Then, we dotted their wings for tracking purposes with a felt-tip marker. These marker points also served as the guidelines for incising the wings since we could not calculate the exact lost wing area *a priori*. We incised the wings using a pair of scissors, performing both symmetric and asymmetric cuts. Since the dragonflies could not be trained, we simply placed the dragonflies on a vertical paper platform to warm up. Our previous experience indicates that reverse flight is exhibited as an alternative to taking off and then turning around. Free flight was captured by three synchronized orthogonally arranged high-speed cameras recording at 1000 frames per second. Using a template based reconstruction technique [16], we reconstructed with the motion of the body and wings, which we used for both kinematics analysis and CFD simulations. The morphological parameters of the insects are documented in Table 7.1.

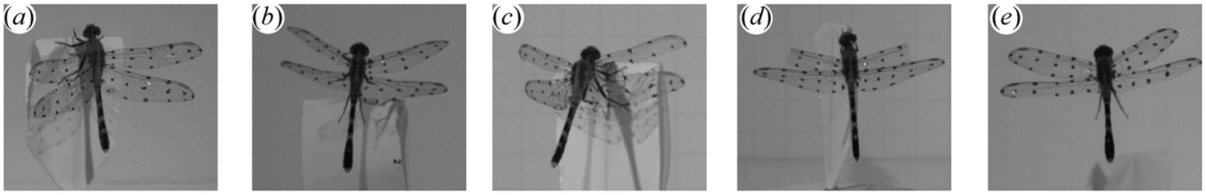

Figure 7.1. Examples of damage wings in the laboratory. (a) Intact wings (DF#1) (b) Asymmetric (left fore and hindwings) spanwise damage (DF#2) (c) Symmetric (left and right forewings) spanwise damage (DF#3). (d) Symmetric (left and right forewings) chordwise (DF#4) (e) Symmetric (left and right hindwings) spanwise damage (DF#5).

Table 7.1. Morphological parameters of the selected insects. CW-chordwise, SW-spanwise, sym-symmetric, asym-asymmetric. LF-left forewing, LH- left hindwing, RF- right forewing, RH –right hindwing

ID	damage type		damaged wing	area loss (%)	body weight (mg)	body length (mm)	FW length (mm)	FW chord (mm)	HW length (mm)	HW chord (mm)
DF#1	Intact	none	none	0	130	40	34	8	31	10
DF#2	SW	asym.	LF,LH	40	115	43	32	8	31	10
DF#3	CW	sym.	LF,RF	40	166	40	32	8	31	9
DF#4	SW	sym.	LF,RF	40	--	40	31	8	30	9
DF#5	SW	sym	LH,RH	40	83	40	30	8	29	9

7.3.2. Wing kinematics definitions

A coordinate system was fixed at the wing root, and the wing kinematics were measured relative to the mean stroke plane. The stroke plane was calculated based on the least square plane which passed through the centroid of the points comprising the wing base and wingtip and then averaged for all the complete wing beats. The Euler angles, flap (ϕ), deviation (θ), and pitch (ψ), define the rigid wing orientation relative to the stroke plane. Since the wing pitch changes along the span, we also defined a least-squares reference plane (see Figure 5 in [16]) which takes into account the deformation of whatever wing area is present be it intact or incised.

7.4. Results

7.4.1. Body kinematics

The displacements of all the flight sequences captured for this study are presented in Figure 7.2. All dragonflies were capable of flying backward over substantial distances, typically about two body lengths. The vertical displacement, however, varied greatly among individuals. Therefore, using load-lifting as the criterion to evaluate the effect of damage may be misleading since some damaged wing flight (DF#2) even outperformed intact wing flight. Nevertheless, it was clear that symmetric cuts (either chordwise or spanwise) to the forewing precluded substantial vertical displacement.

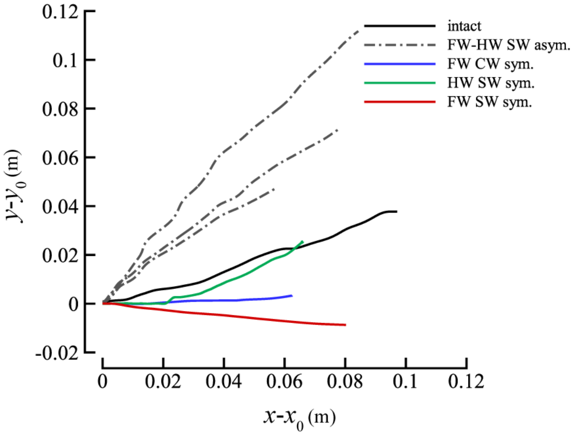

Figure 7.2. Body displacement for dragonflies with different types of damage.

7.4.2. Wing kinematics

The wing kinematics quantities of interest have been summarized in Table 7.2. The intact winged dragonfly (DF#1, Figure 7.1(a)) kinematics have been reported in previous work [15] and summarized here (Figure 7.3(a)). The kinematics of the left and right wings are not exactly symmetrical, although this is not uncommon in free flight [10]. The flapping amplitude (Φ) for all wing pairs was about 100º, with a steeply inclined stroke plane relative to body (approximately 40º). The flapping frequency (n_w) was 27 Hz, and the ipsilateral wings pairs beat out of phase about 60º, similar to the value reported for this species (*Erythemis simplicicollis*) in another work [17].

7.4.2.1. Stroke plane angle

The stroke plane was inclined relative to the body typical of Odonate flight. Among all flight sequences, the intact wing case had the least steep stroke plane (~40). All other flight sequences had values between 50º and 70º.

7.4.2.2. Flapping frequency

After wing damage, we observed an increase in n_w for all but the forewing symmetric spanwise damage case (Figure 7.1(c)), which retained a similar flapping frequency as the intact case. The asymmetric spanwise damaged dragonfly ((Figure 7.1(b))), had a slightly higher frequency, approximately 2-4 Hz. More obvious increases in frequency, however, occurred in symmetric cuts, specifically the forewing chordwise cuts (Figure 7.1(d)) and hindwing spanwise cuts (Figure 7.1(e)). The increase in frequency was 11 (40% increase) and 14 Hz (51% increase) for both cases, respectively.

7.4.2.3. Flapping amplitude

Wing damage also influenced the Φ. In most of the flight sequences, the hindwing amplitude was smaller than the forewings. For the asymmetric damage, Φ was larger on the damaged side, about 13° (FW) and 5° (HW). The dragonflies with symmetric spanwise cuts on either the FW or HW (DF #4 and 5), typically had a lower amplitude compared to the intact case. For the symmetric hindwing spanwise damage (DF#5), there was a reduction in Φ by about 17° (FW) and 30° (HW), when compared to the intact case.

In contrast to the spanwise cuts, increase in Φ was observed for symmetric chordwise cuts (DF#3). The increase in FW Φ was about 20° and was the largest increase in amplitude observed for all flight sequences. At the same time, the lowest hindwing amplitudes for all flight sequences was recorded for DF#3. There was a 40° reduction in Φ.

7.4.2.4. Fore and Hindwing Phasing

Typically, the HW led the FW in flight for both spanwise-damaged and intact wing flight. The average phase difference (φ) between the fore and hindwing pairs was within the range of 50-70°. The wings with chordwise damage exhibited a different trend, however.

Table 7.2. Wing kinematics parameters. n_w - flapping frequency, Φ -flapping amplitude, β_b -stroke plane relative to the body, φ-phase shift between fore and hindwings. *-denotes which wing is damaged. LF-left forewing, LH- left hindwing, RF-right forewing, RH –right hindwing, L-left wings, R-right wings.

ID	damage	n_w (Hz)	Φ (°)				β_b (°)				φ (°)	
			LF	RF	LH	RH	LF	RF	LH	RH	L	R
1	intact	27	100	98	96	97	41	42	41	41	63	56
2i	SW	29	105*	92	90*	86	54*	57	51*	49	62	66
2ii	SW	29	108*	97	91*	86	52*	54	50*	48	71	62
2iii	SW	31	97*	81	98*	91	57*	56	48*	57	76	77
3	CW	38	118*	122*	56	56	57*	55*	48	57	-23	-34
4	SW	27	65*	87*	92	71	69*	64*	57	60	41	56
5	SW	41	80	85	65*	67*	51	53	52*	53	53	59

For DF#3, φ was much smaller in magnitude but also of opposite sign, indicating that the FW led the HW slightly. The time history of the kinematics shown in Figure 7.3(b) shows that at the inception of flight the wings flap in phase, afterward the forewings lead slightly although φ does not exceed 1/8th of a flapping cycle.

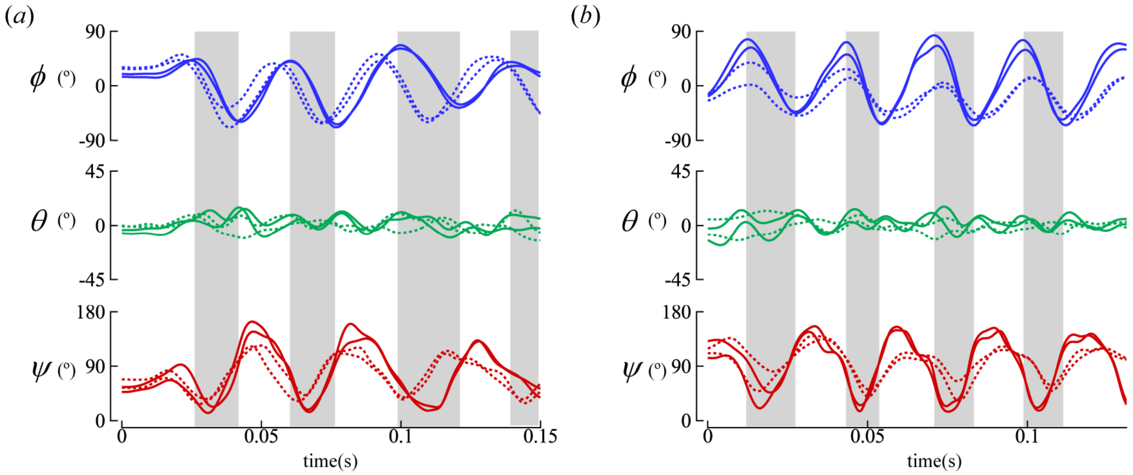

Figure 7.3. Wing kinematics. (a) intact wings (b) symmetric chord wise damage on the forewings. A picture of this dragonfly is shown in Figure 7.1(c). A visual representation of the tip trajectories is shown in Figure 7.4.

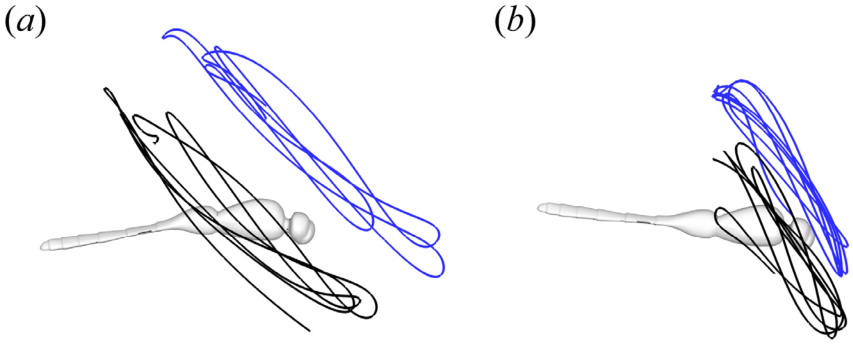

Figure 7.4. Tip trajectories. (a) intact wings (b) symmetric chordwise damage on the forewings.

7.5. Discussion and conclusion

In dragonfly flight in the wild, substantial wing damage is common over the lifetime of the insect. Our study of wing damage indicates that dragonflies can cope with severe damage of different kinds while still being able to perform exotic flight sequences like backward flight. Moreover, it is also known that with substantial damage, dragonflies can perform extreme maneuvers, such as chasing prey and arresting falls in drop escape responses [5]. Typically when damage is large (>10%), the wing response is active [10]. Thus we were confident that our observations were based on active response by the dragonflies.

Beyond the obvious aerodynamic consequences of a reduction in the second moment of area which affects the force production [10], or asymmetric torque and roll to the damaged side that is evident in asymmetric cuts [12], wing damage is likely to influence other flight characteristics. For dragonflies, we observed that that damage impacts the wing kinematics and the coordination between the fore and hindwings. Although classical models provide force and torque predictions [10], the coordination between wing pairs (such as phasing) still cannot be predicted by models.

In both forward and backward flight of intact winged dragonflies, it is well established that the hindwings lead the forewings [18, 19]. The phase shift ranges between 54–100° during straight forward, climbing flight, escape maneuvers, and turning flight at various speeds [20]. Previous work has shown that for *E. simplicicollis*, the phase difference is maintained in backward flight and turning flight [15, 17]. In hovering, however, dragonflies prefer counterstroking (180º out of phase between the wing pairs). Counterstroking has been shown to minimize aerodynamic power consumption [19].

Flapping out of phase reduces the fluctuations in force over a flapping cycle and reduces the oscillations of the body. Furthermore, the hindwings typically lead the forewings in flight to avoid the forewing downwash, which may reduce the effective angle of attack and attenuate the formation of a strong LEV. Flapping out of phase could also have wing-wing interaction benefits even in backward flight [15], whereby the trailing edge vortex of the FW can enhance the HW LEV. Typically, in-phase flapping is used when large forces are to be produced, such as during takeoff. The FW could potentially benefit from interaction due to the distortion of the forewings wakes by the hindwings via the "wall effect," which generates upwash or reflects the flow [20-22] although upwash is not as effective as downwash [23]. It is also well established that the hindwings of dragonflies generate larger forces than the forewings [15, 18].

Our results indicated that the phase relationship between the fore and hindwings for spanwise symmetric or asymmetric cuts is similar to that of an intact dragonfly. Our observation of the forward flight of dragonflies (during the video collection process) also confirms this. In contrast to the spanwise cuts, the symmetric chordwise damage to the forewings had the most impact on flight. We were not able to film any sequences where substantial backward flight was elicited when the hindwings were severed symmetrically, however. Under the condition of forewing chordwise damage, the rigid phase relationship typical of normal flight, and spanwise wing damage was no longer maintained. In-phase flapping or where the FW led slightly was appropriated.

To flap in phase or closely behind the forewings, the hindwings have to match the timing of wing reversal. In a sense, the forewing thus constrains the motion of the hindwings. Because of the reduction in chord lengths traveled, despite the increases in wing frequency, the wing tip speed of the hindwing is reduced, compared to the intact case. Thus, the contribution of the hindwings to large force production is sacrificed because the forewing dictates the hindwing motion. Interestingly, unlike the intact case, the mean position of the HW is shifted in front of the center of mass while FW mean position is shifted behind the center of mass so that the torques can cancel out and the flight can still be controlled (Figure 7.4(b)) since flapping out of phase is not a viable option.

There aerodynamic implications are distinct for different kinds of damage. Chordwise damage is detrimental because the distal part, which generates most of the flight forces, has been eliminated. Likewise, the translational velocity of the wing is reduced. Furthermore, the tip vortex of the FW is formed closer to the wing root. The tip vortex may continually interfere with the HW LEV and may even destroy it, especially if the FW leads. In contrast, spanwise damage may not be as detrimental because the trailing edge region of the wing does not generate large forces [24].

The positive benefits of wing-wing interaction may also be harnessed since vorticity can still shed from the trailing edge.

Lastly reduction in flapping amplitude of the wing during forewing chordwise damage reduces force production. Estimates from the flapping amplitude in this study indicate that HW tip only travels less than 3 chord lengths. LEV growth is a phenomenon dependent on the translational phase. Insects such as mosquitos that use very low flapping amplitude rely on rotational mechanisms for weight support. It is not clear if dragonflies rely on these mechanisms. In a future study, we will investigate the aerodynamics of wing damaged flight in detail.

7.6. References

[1] Achache, Y., Sapir, N. & Elimelech, Y. 2018 Hovering hummingbird wing aerodynamics during the annual cycle. II. Implications of wing feather moult. *Royal Society Open Science* **5**, 171766. (doi:doi:10.1098/rsos.171766).

[2] Rajabi, H., Schroeter, V., Eshghi, S. & Gorb, S.N. 2017 The probability of wing damage in the dragonfly Sympetrum vulgatum (Anisoptera: Libellulidae): a field study. *Biology Open* **6**, 1290-1293. (doi:10.1242/bio.027078).

[3] Foster, D.J. & Cartar, R.V. 2011 What causes wing wear in foraging bumble bees? *The Journal of Experimental Biology* **214**, 1896-1901. (doi:10.1242/jeb.051730).

[4] ALCOCK, J. 1996 Male size and survival: the effects of male combat and bird predation in Dawson's burrowing bees, Amegilladawsoni. *Ecological Entomology* **21**, 309-316. (doi:10.1046/j.1365-2311.1996.00007.x).

[5] Combes, S.A., Crall, J.D. & Mukherjee, S. 2010 Dynamics of animal movement in an ecological context: dragonfly wing damage reduces flight performance and predation success. *Biology Letters* **6**, 426-429. (doi:doi:10.1098/rsbl.2009.0915).

[6] Cartar, R.V. 1992 Morphological Senescence and Longevity: An Experiment Relating Wing Wear and Life Span in Foraging Wild Bumble Bees. *Journal of Animal Ecology* **61**, 225-231. (doi:10.2307/5525).

[7] Jantzen, B. & Eisner, T. 2008 Hindwings are unnecessary for flight but essential for execution of normal evasive flight in Lepidoptera. *Proceedings of the National Academy of Sciences* **105**, 16636-16640. (doi:10.1073/pnas.0807223105).

[8] Roberts, J.C. & Cartar, R.V. 2015 Shape of wing wear fails to affect load lifting in common eastern bumble bees (Bombus impatiens) with experimental wing wear. *Canadian Journal of Zoology* **93**, 531-537. (doi:10.1139/cjz-2014-0317).

[9] Hedenström, A., Ellington, C.P. & Wolf, T.J. 2001 Wing wear, aerodynamics and flight energetics in bumblebees (Bombus terrestris): an experimental study. *Functional Ecology* **15**, 417-422. (doi:10.1046/j.0269-8463.2001.00531.x).

[10] Fernández, M.J., Driver, M.E. & Hedrick, T.L. 2017 Asymmetry costs: effects of wing damage on hovering flight performance in the hawkmoth Manduca sexta. *The Journal of Experimental Biology* **220**, 3649-3656. (doi:10.1242/jeb.153494).

[11] Fernández, M.J., Springthorpe, D. & Hedrick, T.L. 2012 Neuromuscular and biomechanical compensation for wing asymmetry in insect hovering flight. *The Journal of Experimental Biology* **215**, 3631-3638. (doi:10.1242/jeb.073627).

[12] Muijres Florian, T., Iwasaki Nicole, A., Elzinga Michael, J., Melis Johan, M. & Dickinson Michael, H. 2017 Flies compensate for unilateral wing damage through modular adjustments of wing and body kinematics. *Interface Focus* **7**, 20160103. (doi:10.1098/rsfs.2016.0103).

[13] Kassner, Z., Dafni, E. & Ribak, G. 2016 Kinematic compensation for wing loss in flying damselflies. *Journal of Insect Physiology* **85**, 1-9. (doi:https://doi.org/10.1016/j.jinsphys.2015.11.009).

[14] Srygley, R.B. & Thomas, A.L.R. 2002 Unconventional lift-generating mechanisms in free-flying butterflies. *Nature* **420**, 660. (doi:10.1038/nature01223
https://www.nature.com/articles/nature01223#supplementary-information).

[15] Bode-Oke, A.T., Zeyghami, S. & Dong, H. 2018 Flying in reverse: kinematics and aerodynamics of a dragonfly in backward free flight. *Journal of The Royal Society Interface* **15**. (doi:10.1098/rsif.2018.0102).

[16] Koehler, C., Liang, Z., Gaston, Z., Wan, H. & Dong, H. 2012 3D reconstruction and analysis of wing deformation in free-flying dragonflies. *The Journal of experimental biology* **215**, 3018-3027.

[17] Chengyu, L. & Haibo, D. 2017 Wing kinematics measurement and aerodynamics of a dragonfly in turning flight. *Bioinspiration & Biomimetics* **12**, 026001.

[18] Hefler, C., Noda, R., Shyy, W. & Qiu, H. 2017 Unsteady Vortex Interactions for Performance Enhancement of a Free Flying Dragonfly. In *ASME 2017 Fluids Engineering Division Summer Meeting* (pp. V01CT21A010-V001CT021A010, American Society of Mechanical Engineers.

[19] Wang, Z.J. & Russell, D. 2007 Effect of forewing and hindwing interactions on aerodynamic forces and power in hovering dragonfly flight. *Physical review letters* **99**, 148101.

[20] Lehmann, F.-O. 2008 When wings touch wakes: understanding locomotor force control by wake–wing interference in insect wings. *Journal of Experimental Biology* **211**, 224-233.

[21] Rayner, J.M. 1991 On the aerodynamics of animal flight in ground effect. *Philosophical Transactions of the Royal Society of London B: Biological Sciences* **334**, 119-128.

[22] Bode-Oke, A., Zeyghami, S. & Dong, H. 2017 Aerodynamics and flow features of a damselfly in takeoff flight. *Bioinspiration & biomimetics* **12**, 056006.

[23] Maybury, W.J. & Lehmann, F.-O. 2004 The fluid dynamics of flight control by kinematic phase lag variation between two robotic insect wings. *Journal of Experimental Biology* **207**, 4707-4726. (doi:10.1242/jeb.01319).

[24] Li, C., Dong, H. & Zhao, K. 2018 A balance between aerodynamic and olfactory performance during flight in Drosophila. *Nature Communications* **9**, 3215. (doi:10.1038/s41467-018-05708-1).

Chapter 8
Conclusions

8.1. Summary of contributions.

By using an integrated approach combining high-speed photogrammetry of free-flying insects, high-fidelity 3-D surface reconstruction, and computational fluid dynamics, we sought to clarify how insects generate forces for flight. In particular, we were interested in understanding the role of the upstroke in flight when the insect in moving ($J \neq 0$). We hypothesized that upstroke effects would become evident if the upstroke can carry the weight of the insect. Our analysis indicated that a consequence of upstroke effects is a previously uncharacterized flight mode in the literature; backward flight or flight with negative advance ratio. Therefore, it was from the lens of flight with negative advance ratios that we investigated upstroke effects because the flight physics of the novel flight mode and the utility of the upstroke are intertwined, and thus can be unraveled simultaneously. Our work was split into two thrusts:

Thrust 1

a) Unraveling the flight mechanics of a new flight mode in the literature both in terms of body configuration and motion ($J<0$) by quantitatively analyzing the flight behavior, coordination between wing and body motion and comparing the findings to well-studied flight modes ($J \geq 0$).

b) Collecting flight data across different insects species (Lepidoptera, Hemiptera, and Odonata) which are diverse in morphology (spanning low to high aspect ratio fliers) and kinematics, flight performance, and techniques, to find similarities and juxtapose flight techniques when $J<0$.

Thrust 2

a) Uncovering how insects produce forces in the half-strokes (force asymmetry, upstroke effects) and how they orient and reorient those flight forces (force vectoring/helicopter model).

b) Identifying and quantifying the relevant flow features and aerodynamic mechanisms (vortex structures) and their correlation to force production.

c) Understanding the variation of flight force, aerodynamic mechanisms, and flight kinematics when both $J<0$ and body motions are unsteady (i.e., involving acceleration and deceleration), which has significance in nature for hesitation behaviors, obstacle avoidance, and transitioning from one flight mode to another.

d) Understanding the flight mechanics under damaged wing conditions.

The summary of each chapter addressing each item in the thrust is provided below.

In Chapter 3, we showed that the hypothesis that upstroke effects become evident when the upstroke has to provide weight support is valid. We also identified for the first time that backward flight was a consequence of upstroke effects. We found that alterations in kinematics and aerodynamic features which are different from hovering and forward flight characterize backward flight of dragonflies. Our study showed that backward flight is not merely a transient behavior but is sustainable for a relatively extended period, which may have implications for biology (prey capture or predator evasion) as well as micro-aerial vehicle design. To fly backward, dragonflies tilt their stroke plane toward their bodies, but the primary reorientation of the stroke plane and force vector is because of the steep body posture that was maintained. In addition to redirecting the force, we found that the force magnitude was significantly increased in the upstroke (when compared to forward flight). In contrast to forward flight, during which dragonflies generates little force in upstroke, the magnitude of the half-stroke-averaged force generated in upstroke during backward flight was 2-4 times the body weight. Also, we showed that a strong and stable leading edge vortex (LEV) in the upstoke was responsible for greater force production. We also identified that wing-wing interaction is beneficial. Given the right phasing, vorticity from the FW trailing edge enhanced the HW's LEV.

In Chapter 4, we sought to identify backward flight in a flyer with a simple actuation system (with reduced wing degrees of freedom). We showed that Cicadas which are heavy fliers elicit backward flight by changes in body posture to reorient both the stroke plane and the force vector in the global frame. We found that the steep body posture also influenced the wing aerodynamics by reversing the aerodynamic roles of the half strokes compared to forward flight in the global frame. The key difference here was that the orientation of aerodynamic force relative to the body, compared to other flight modes such as forward flight, takeoff, banked turns and so on, remained relatively fixed despite significantly different body orientations and motions. Thus, indicating that not only did postural changes occur but the helicopter model is sufficient to describe the flight of a simple flier in backward flight. An aerodynamically active upstroke signified by the presence of an LEV was identified, and the upstroke was principally responsible for weight support during backward flight. The LEV was present on the forewings which generated most of the flight forces in comparison to the smaller hindwings. The LEV's effect, together with the enhanced upstroke velocity increased the upstroke's force contribution from 10% of the net flight forces in forward flight to 50% in backward flight. Our results also clarified what the aerodynamics and kinematic adjustments might look like for other simple fliers with limited range of stroke plane motion relative to the body such as beetles which appropriate backward flight for both obstacle avoidance and interfacial flight, as well as micro-aerial vehicles which may use backward flight during free flight or takeoff from vertical surfaces

In chapter 5, we investigated the backward flight of another flier (a butterfly) with a simple actuation system, albeit with broad wings, load aspect ratio, high wing loading, and Reynolds number (*Re*). Our results indicate that backward flight is characterized by large body angles (>90º), with pitch-down and pitch-up motions in the downstroke and upstroke, respectively. Reminiscent of backward flight of other fliers, there was a reversal of the aerodynamic function of the half strokes in comparison to forward flight due to the body posture which reoriented the stroke plane. Novel lift production capabilities of the upstroke were observed, while the downstroke generated horizontal forces primarily. The upstroke dominated force production and was responsible for weight support. An LEV was formed in both half strokes. The LEV structure during the upstroke was consistent with a Class II LEV previously reported albeit during the downstroke of free-flying butterflies but different from the LEV structure identified in other chapters which were conical (CLASS III LEV). The upstroke was positively loaded, and the LEV (with the reversed sign of circulation) rested on the ventral surface of the wing which is different from the very rare positively loaded upstroke with the LEV (with the same sign of circulation) on the dorsal surface in forward flight. The combination of LEV and large upstroke effective velocity increased the upstroke's force contribution to the net forces from 32% in forward flight to 60% in backward flight of the net flight forces in forward flight. Likewise, upstroke contribution to vertical forces increased from 8% to 85%. The forewings also dominated force production, generating about 65% of the net forces. Just like the cicada, despite the variation of force orientation, leading to different flight trajectories and body oscillation the directions of the half stroke-average aerodynamic forces relative to the body were clumped together in a narrow range (<20º). We also discovered that the directions of the halfstroke-average forces in forward and backward flight relative to the body were consistent. The stroke plane relative to the body, and force vector was fixed, but the body angles were different indicating that that the helicopter model is being used by butterflies at least within the range of speeds -1 to 2m/s or advance ratios (*J*) of $-0.4 \leq J \leq 0.9$.

In chapter 6, we clarified the effect of unsteady body motion on the wing half stroke function and aerodynamics. We show that before the transition to forward flight, the backward flight of damselflies involves a speed-up (accelerating) and slow-down (deceleration) phase. During speed-up, an upright posture and high angle of attack in both half strokes were appropriated. The upright posture rotated the stroke plane in the inertial frame in comparison to forward flight, causing the reversal of the aerodynamic functions of the half strokes. An active upstroke signified by the presence of an LEV was the principal means of force production and weight support, while the downstroke produced backward forces. During slow-down, however, the body and stroke plane angles reduced, and a pronounced asymmetry in the half stroke angle of attack was observed. The upstroke angle of attack increased while the downstroke's reduced in comparison to the speed-up phase. Consequently, the upstroke remained aerodynamically active, though it assumed a dual function, generating both (i) weight support and (ii) negative horizontal forces (drag) to counteract the backward forces still being produced in the downstroke. If the downstroke angle of attack was low enough, the downstroke's force production diminished substantially, and the half stroke became aerodynamically inactive. Associated with the inactive downstroke was the switch from separated to attached flow. After the transition to accelerating forward flight, the body angle reduced and the aerodynamic roles of the half strokes reverted to their normal functions: downstroke lift, upstroke thrust. Our findings indicate that the half stroke kinematics and aerodynamics are different, and distinct in each flight phase, being characterized by adjustments mainly in body angle, stroke plane angle, and wing angle of attack. This chapter was also the only study in the dissertation to obtain forward and backward data from the same flight of the same insect.

Lastly, in chapter 7, we investigated the effect of wing damage on the free backward flight of dragonflies. We performed substantial asymmetric incision of the wings both in the spanwise and chordwise direction and captured free flight kinematics with high-speed cameras. Our findings indicate that the choice of wing kinematics and the coordination between the wing pairs were affected. After wing damage, we observed an increase in flapping frequency for all but the forewing symmetric spanwise damage case which retained a similar flapping frequency as the intact wing case. There was also an increase in flapping amplitude and stroke plane tilt of the damaged wings. In contrast to the spanwise cuts, more significant increases in flapping amplitude occurred for the symmetric chordwise cuts on the forewings (20º). Surprisingly, accompanying this increase in forewing amplitude was a substantial reduction in hindwing flapping amplitude (40º). The phase relationship when the wings were damaged in the spanwise direction was maintained in the same range as the intact case (50º-70º). However, chordwise damaged changed the phase relationship between the wing pairs. The wings flapped approximately in phase, and then the FW led the motion, atypical of dragonfly flight. The change in phase relationship was responsible for the reduction in hindwing flapping amplitude because the forewings dictated that the number of chord lengths traveled between the wing pairs per stroke is approximately the same.

The primary contributions of this dissertation are in the discovery and characterization of novel flight mode among vastly different species spanning the entire spectrum of Reynolds numbers of small to large-sized insects with varying complexity, quantitative measurement of flight kinematics, discovery of novel upstroke lift and associated unsteady aerodynamics, clarification of the facultative nature of wing half stroke function, elucidation of the importance of body aerodynamics on wing aerodynamics and finally extracting simple techniques to extend flight envelope for additional maneuverability.

8.2. Limitations and suggestions for future work.

Altogether, the work presented in this dissertation provides advancement of our understanding of insect flight mechanics and aerodynamics. Nevertheless, there is room for improvement and future work.

8.2.1. Limitations

We confirmed in all chapters that body reorientation is the key to backward flight and that this mechanism is widely shared in nature from insects to hummingbirds (convergent evolution). However, body reorientation in itself does not mean that the insect is using the helicopter model. An insect could change its body posture while also changing its stroke plane relative to the body drastically, for example, Odonates [1]. It was only in fliers with a restricted stroke plane relative to the body that the helicopter model was always valid. In particular, for cicadas, we demonstrated this fact in multiple flight modes such as backward, forward, climbing, and turning flights. For butterflies, we were restricted to investigating rectilinear flight modes; backward and forward flight. The helicopter model relies on body postural changes while the aerodynamic force vector is fixed relative to the body across different flight speeds. The work presented here focused on low-speed flight with speeds less than 2m/s. It is still not known what the upper limit of backward flight is for any species.

In forward flight, the helicopter model predicts that the body angle will reduce as flight speed increases (Figure 8.1). In backward flight, the helicopter model predicts that the body angle will continue to increase, such that in fast backward flight, the insect body will be upside down because parasite drag on the body is an issue at high speed [2]. However, only a few insects can fly upside down at low speeds in the forward direction [3, 4]. Morphological constraints and control challenges, thus, will restrict backward flight at high speeds and the helicopter model will break down.

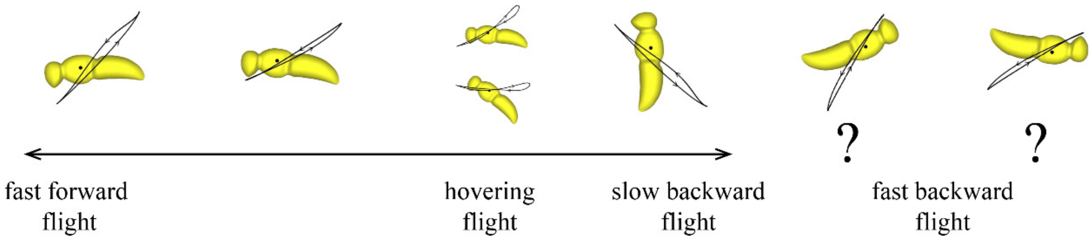

Figure 8.1. Limitations of the helicopter model. The arrows indicate the range of the rectilinear flight envelope that has now been studied for insects with this dissertation contributing to slow backward flight. The question marks in the fast backward flight indicate that although the helicopter model predicts the body configuration with high body angles in flight, it is still unknown whether backward flight can be sustained at high speeds, and if so what the mechanics and aerodynamics look like. The insect model was adapted from Meng and Sun [5].

One may also ask that if insects of different sizes and flight proficiencies can achieve backward flight, does this behavior scale with size? A survey of the literature indicates that small insects such as fruit flies and larger insects like cicadas and hawkmoth can perform backward flight. The hummingbird is the largest organism that can fly backward [6]. Thus, so far, backward flight is only utilized in *Re* ranging from 100-10000. As body size increases, the inertial costs of flight increases (wing to body mass ratio increases) and musculoskeletal limitations become very important. The reason larger organisms may not engage in backward flight is addressed below

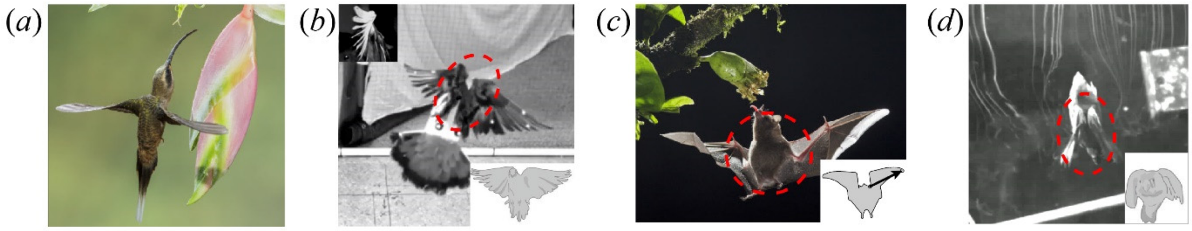

Figure 8.2. Upstroke type changes with scaling. (a) Hummingbird "insect-like" upstroke [7] involves substantial twist and no area reduction in the upstroke. The hummingbird upstroke can support 25% of the bodyweight (b) distally supinated 'tip-reversal' upstroke of a pigeon [8, 9] generates 50% of the net downstroke forces (c) tip-reversal upstroke of a nectar bat [7] can some weight support during hovering (d) flexed wing upstroke of a zebra finch [10] provides no weight support during forward flight. The red dashed-lined circles in (b)-(d) indicate that the wing area is reduced in the upstroke. The largest area reduction occurs for the zebra finch. Figures are adapted from the various citations listed above.

First, the upstroke type changes with scaling (Figure 8.2). Insects do not have musculature on the wings that restricts the upstroke motion. The wing is actuated from the hinge and deforms in response to the aerodynamic loading. The wings are highly supinated during the upstroke in backward flight. As body size increases, musculature and a skeletal system can be found on the wings as in the case of birds and bats and the ability to twist reduces. Hummingbirds can twist their wings, possessing an insect-like upstroke which helps them generate lift during hovering. In contrast, most birds have restricted musculature and thus cannot wholly supinate the wings. Except for the hummingbird upstroke, as body size increases, the upstroke switches from an insect-like upstroke to either a distally supinated tip reversal upstroke [8](Figure 8.2 (b,c)) or a flexed wing upstroke (Figure 8.2 (d)) [10]. There is also a wing area reduction that accompanies the upstroke, which reduces the upstroke force. During the flexed wing upstroke, the wing is simply tucked into the body, and no useful force is generated. During the tip reversal upstroke, there is not a completed reduction in wing area, and the wingtips are supinated. The tip reversal upstroke identified in some larger birds in forward flight generates thrust [10], although its magnitude cannot sustain body weight throughout the stroke. The inability to completely supinate the wing will lead to having to appropriate excessive body angles to effect upstroke lift without drag, and may not be viable for large birds. Wing area reduction is also not ideal because in backward flight, the upstroke carries the body weight.

Second, the ratio of the half stroke muscle size changes with scaling (Figure 8.3). Above the insect scale (*Re* ~100-10000), Sunbirds can perform short backward flight [11], while hummingbirds are the only birds that can fly backward continuously [6]. Hummingbirds possess insect-like kinematics [12, 13], and large upstroke muscles, the supracoracoideus [14, 15]. The upstroke muscle is half the size of the downstroke (pectoralis) (Figure 8.3(a)) for the hummingbird. For other birds with an aerodynamically limited upstroke, the upstroke muscle is very small one-fifth of the downstroke muscle, which is just sufficient flex the wings (Figure 8.3(b)). The small size of the upstroke muscles indicates that a large bird may not be able to cope with the inertial requirements as well as the aerodynamic loading required for backward flight because the reversal of the aerodynamic functions of the half stroke that accompanies backward flight necessitates developed upstroke muscles to carry the body weight.

Lastly, the visual system of an organism may also play a role in its ability to fly backward. If the organisms cannot see what is behind it, likely, prolonged reverse flight will not be appropriated.

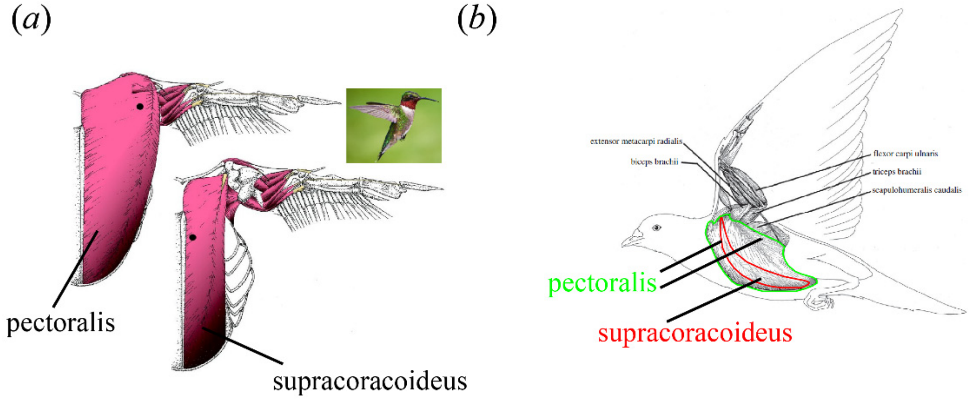

Figure 8.3. Half stroke muscle size changes with scaling. Pectoralis- downstroke muscle, supracoracoideus- upstroke muscle. (a) Hummingbird. Image modified from Mahalingam and Welch Jr. [15] (b) Pigeon. Image modified from Dial [16].

A major limitation in this work was that in the free flight of insects we studied, we did not have much control over the flight behavior, in that we could not select flight speeds and precise direction of flight. All we had control over was the initial placement of the insects on the takeoff platform. Wind tunnel studies may be useful here. That way, the kinematic changes with incremental flight speed can be observed, and the limits of the insects may be identified. Nevertheless, there are challenges associated with free flight studies in a wind tunnel [17, 18]. Nectar feeding insects such as hawkmoths, however, are ideal for this kind of studies because they can remain fixed at an artificial feeder and the incoming flow can simulate backward flight at various speeds. This way, the metabolic costs of flight can also be measured.

8.2.2. Suggestions for future work

In all the flights that we captured during the work for several insects, body postural adjustment was necessary for backward flight. Nevertheless, non-body adjustment based backward flight is possible and has been observed in the field. So far, this behavior has only been exhibited by extant Zygoptera [19] and Anisozygoptera [20]. These insects maintain a horizontal posture in backward flight. The techniques of this kind of flight are unknown and may provide significant insight into the wing kinematics and aerodynamics. It is also an avenue to juxtapose the pros and cons of the horizontal body versus steep body technique in backward flight.

The work presented here only focused on rectilinear flight modes. During the video capture process for this work, we also identified backward flight turns in both dragonflies, damselflies, and butterflies indicating that backward flight is not just restricted to rectilinear motions for insects. Currently, the mechanics and aerodynamics of this behavior is unknown and may provide further insights into the versatility of insects in flight, especially the role each half stroke plays in force and torque generation. It is interesting to note that backward turning flight has not been reported for hummingbirds. Understanding how backward flight contributes to various behavioral situations is still an open area of research both for hummingbirds [6] and insects.

The metabolic costs and power-speed relationships in insect backward flight is still unknown. Using CFD simulations, we were able to show that the aerodynamic power, this is the power needed to overcome air resistance, in forward and backward are in a similar range. However, we have no insights about metabolic costs. In the case of the hummingbird [6], the metabolic cost has been measured, but the aerodynamic power has not been quantified. It was reported that the metabolic cost of backward flight is similar to forward flight at an equivalent speed and is less expensive than hovering flight. As alluded to above, nectar-feeding insects are ideal for wind tunnel because they can remain fixed at an artificial feeder and the incoming flow can simulate backward flight at various speeds. The metabolic cost can be measured this way easily, the limit of backward flight can be known, and the power-speed relationship can be established. We still do not know whether the free flight speeds observed in our study are at the minimum sweet-spot or somewhere else in the power-speed curves.

A consistent theme in this dissertation was that upstroke lift is associated with high body angles. Our observations of dragonflies, cicadas, and butterflies indicate that upstroke lift is appropriated during such as steep climbing flight. In climbing flights, the body angles are not as steep as in backward flight but high enough for upstroke lift to kick in. In other Lepidoptera

(*Noctua pronuba),* performing a similar motion, a steep body posture with upstroke lift signified by an LEV was visualized [21]. These flight modes are worth studying and will further clarify the effect of the body on wing half stroke function.

Wing damage effects on wing aerodynamics is also an area worth exploring and the effect on the aerodynamics of four-winged fliers remain an active area of research. In this work, we were able to report the kinematics changes that occurred commensurate with either spanwise or chordwise damage. However, more work needs to be done on the aerodynamics. In free flight, generalizable results can only be obtained through a statistical analysis of a large number of flights

Lastly, as this work focused mainly on the kinematics and aerodynamics, insect flight control is also essential to translate the findings to design. The development of free flight computational simulation tools will enable us to isolate the effect of each kinematic parameter on flight dynamics, stability, and control.

8.3. References

[1] Wakeling, J. & Ellington, C. 1997 Dragonfly flight. II. Velocities, accelerations and kinematics of flapping flight. *Journal of experimental biology* **200**, 557-582.

[2] Dudley, R. 2002 *The biomechanics of insect flight: form, function, evolution*, Princeton University Press.

[3] Rüppell, G. 1989 Kinematic analysis of symmetrical flight manoeuvres of Odonata. *Journal of Experimental Biology* **144**, 13-42.

[4] Shumway, N., Gabryszuk, M. & Laurence, S.J. 2018 Flapping tandem-wing aerodynamics: dragonflies in steady forward flight. In *2018 AIAA Aerospace Sciences Meeting* (American Institute of Aeronautics and Astronautics.

[5] Meng, X.G. & Sun, M. 2016 Wing and body kinematics of forward flight in drone-flies. *Bioinspiration & Biomimetics* **11**, 056002. (doi:10.1088/1748-3190/11/5/056002).

[6] Sapir, N. & Dudley, R. 2012 Backward flight in hummingbirds employs unique kinematic adjustments and entails low metabolic cost. *The Journal of experimental biology* **215**, 3603-3611.

[7] Ingersoll, R., Haizmann, L. & Lentink, D. 2018 Biomechanics of hover performance in Neotropical hummingbirds versus bats. *Science Advances* **4**, eaat2980. (doi:10.1126/sciadv.aat2980).

[8] Ros, I.G., Bassman, L.C., Badger, M.A., Pierson, A.N. & Biewener, A.A. 2011 Pigeons steer like helicopters and generate down- and upstroke lift during low speed turns. *Proceedings of the National Academy of Sciences* **108**, 19990-19995. (doi:10.1073/pnas.1107519108).

[9] Crandell, K.E. & Tobalske, B.W. 2011 Aerodynamics of tip-reversal upstroke in a revolving pigeon wing. *The Journal of Experimental Biology* **214**, 1867-1873. (doi:10.1242/jeb.051342).

[10] Crandell, K.E. & Tobalske, B.W. 2015 Kinematics and aerodynamics of avian upstrokes during slow flight. *The Journal of experimental biology* **218**, 2518-2527.

[11] Ng'weno, F. 1990 Sunbird flying backwards? *East Africa Nat. Hist. Bull.* **20**, 27-28.

[12] Warrick, D.R., Tobalske, B.W. & Powers, D.R. 2005 Aerodynamics of the hovering hummingbird. *Nature* **435**, 1094-1097. (doi:10.1038/nature03647).

[13] Warrick, D.R., Tobalske, B.W. & Powers, D.R. 2009 Lift production in the hovering hummingbird. *Proceedings of the Royal Society of London B: Biological Sciences* **276**, 3747-3752. (doi:10.1098/rspb.2009.1003).

[14] Warrick, D., Hedrick, T., Fernández, M.J., Tobalske, B. & Biewener, A. 2012 Hummingbird flight. *Current Biology* **22**, R472-R477. (doi:https://doi.org/10.1016/j.cub.2012.04.057).

[15] Mahalingam, S. & Welch, K.C. 2013 Neuromuscular control of hovering wingbeat kinematics in response to distinct flight challenges in the ruby-throated hummingbird, Archilochus colubris. *The Journal of Experimental Biology* **216**, 4161-4171. (doi:10.1242/jeb.089383).

[16] Dial, K.P. 1992 Activity patterns of the wing muscles of the pigeon (Columba livia) during different modes of flight. *Journal of Experimental Zoology* **262**, 357-373. (doi:10.1002/jez.1402620402).

[17] Bomphrey, R.J., Lawson, N.J., Harding, N.J., Taylor, G.K. & Thomas, A.L.R. 2005 The aerodynamics of Manduca sexta: digital particle image velocimetry analysis of the leading-edge vortex. *Journal of Experimental Biology* **208**, 1079-1094. (doi:10.1242/jeb.01471).

[18] Thomas, A.L., Taylor, G.K., Srygley, R.B., Nudds, R.L. & Bomphrey, R.J. 2004 Dragonfly flight: free-flight and tethered flow visualizations reveal a diverse array of unsteady lift-generating mechanisms, controlled primarily via angle of attack. *Journal of Experimental Biology* **207**, 4299-4323.
[19] Rüppell, G. 2015 Dragonfly flight: Small Red Eye Damselfly - Heavy Fighter. (https://youtu.be/_5HhXy3KD5k.
[20] Rüppell, G. & Hilfert, D. 1993 The flight of the relict dragonfly Epiophlebia superstes (Selys) in comparison with that of the modern Odonata (Anisozygoptera: Epiophlebiidae). *Odonatologica* **22**, 295-309.
[21] Bomphrey, R.J., Srygley, R.B., Taylor, G.K. & Thomas, A.L.R. 2002 Visualizing the Flow around Insect Wings. *Physics of Fluids* **14**, S4-S4. (doi:10.1063/1.4739193).